UNIVERSITY OF CALIFORNIA
RIVERSIDE

Real-time Battery Control Method for Microgrid Energy Management

A Thesis submitted in partial satisfaction
of the requirements for the degree of

Master of Science

in

Electrical Engineering

by

Yun Xue

December 2015

Thesis Committee:

Dr. Alfredo Martinez-Morales, Co-Chairperson
Dr. Matthew Barth, Co-Chairperson
Dr. Sadrul Ula
Dr. Nanpeng Yu

The Thesis of Yun Xue is approved:

_____

_____

_____
Committee Co-Chairperson

_____
Committee Co-Chairperson

University of California, Riverside

Acknowledgements

I would like to express my sincere gratitude and appreciation to my research advisor Dr. Alfredo Martinez-Morales for his invaluable guidance, support and encouragement throughout my entire master program. I would also like to thank Dr. Sadrul Ula and Mr. Michael Todd. Without their guidance and instructions I cannot finish my research other than this thesis.

I would also like to thank Prof. Matthew Barth and Prof. Nanpeng Yu for serving on my committee and offering valuable advices for my thesis.

I would like to offer my special thanks to the labmates at CE-CERT (Yujie Cao, Ryan Chen, Kevin Harvard and Ye Li). With their help and understanding I can accomplish my thesis better.

At the end, I would thank my family for their endless love, support and encouragement. Additionally, I would like to express my special thanks to my husband. Without my “driver”, I cannot go to CE-CERT every day.

Dedicated to my beloved husband
Kaifan Xu
and my beloved mother and father
Wenying Liu and Jinhe Xue
and my beloved parents-in-law
Yuping Zhang and Zhuliang Xu

ABSTRACT OF THE THESIS

Real-time Battery Control Method for Microgrid Energy Management

by

Yun Xue

Master of Science, Graduate Program in Electrical Engineering
University of California, Riverside, December 2015
Dr. Alfredo. Martinez-Morales, Co-Chairperson
Dr. Matthew Barth, Co-Chairperson

Renewable energy has been playing an increasingly important role worldwide recently. For 2012 and 2013, renewables contributed 19% to energy consumption and 22% to electricity generation [1]. In 2014, solar energy represented 36% of new generating capacity in the U.S., second only to natural gas [2]. Due to the intermittent nature of renewable sources, energy storage systems have been integrated into the architecture of Microgrid systems to make them more efficient and robust. Within a Microgrid system, the battery energy storage system (BESS) can be used to reduce the electricity cost by delivering energy during the On-Peak rate period and storing energy (i.e. charging) during the Off-Peak rate period. This thesis proposes a real-time battery control method to reduce the electrical bill in an energy intensive environment, and more effectively utilize a BESS within Microgrid testbed system at the College of Engineering Center for Environmental

Research and Technology (CE-CERT). The monthly electrical bill is based on the rate schedule time-of-use (TOU) for Large General and Industrial Service in the city of Riverside. Each month, this rate schedule has both demand charge (kW) and energy consumption (kWh) charge for three different rate periods: On-Peak, Mid-Peak, and Off-Peak. The real-time control method considers both rates for different rate periods separately. The main parts of the control method are the control algorithms, which comprise two model predictive control (MPC) algorithms, for the On-Peak rate period. The first algorithm is called the constant threshold MPC (CT-MPC) algorithm, and it is implemented in the system with the relatively stable solar generation and building load profiles in the winter season. This control algorithm can maintain the On-Peak demand below the constant threshold during the entire On-Peak rate period. The second one is called the adjusting demand threshold MPC (ADT-MPC) algorithm. The ADT-MPC algorithm fits a system with unpredictable solar generation and building load profiles. During the On-Peak rate period, by applying the ADT-MPC algorithm, the On-Peak threshold can be adjusted to optimized values. Both algorithms can maintain a low level of energy import from the external grid (i.e. Riverside Public Utilities grid) during the On-Peak rate period. For the other two rate periods, the Off-Peak and Mid-Peak control algorithms are also developed. With the real-time battery control method, the BESS continuously maintains the lowest demand and energy consumption for the entire day.

Table of Contents

List of Tables

List of Figures

Chapter 1 Introduction to Microgrid

Microgrid definition by the Microgrid Exchange Group:

> *"A Microgrid is a group of interconnected loads and distributed energy resources within clearly defined electrical boundaries that acts as a single controllable entity with respect to the grid. A Microgrid can connect and disconnect from the grid to enable it to operate in both grid-connected or island-mode."* [3]

Based on the above definition, a Microgrid should have the ability to generate and distribute energy within its internal architecture, as well as being able to control different load components as a single intelligent network entity. Three basic components should be included in a Microgrid based on CIGRÉ C6.22 Definition Qualifiers: (1) generators, (2) storage devices, and (3) controlled loads.

1.1 Generators: Renewable Energy Resources (RES)

An electric generator converts thermal, mechanical or other form of energy to electrical energy to drive in an external circuit (load). Generators can use conventional energy like fossil fuels or renewable energy such as sunlight, wind, tides and nuclear energy.

Crude oil, coal and natural gas are three main conventional energy resources around the world. Due to their finite nature and detrimental impacts on the environment, renewable energy resources are promising as an alternative and sustainable forms of energy, for meeting society's future energy needs. In 1981, the United Nations held a conference called "The United Nations Conference on New and Renewable Sources of Energy". The conference raised the international attention on the exploration and utilization of renewable sources. Renewable energy is generally defined as energy that comes from resources that are naturally replenished on a human timescale [4].

Photovoltaic (PV) modules generate electricity directly from sunlight via the photovoltaic effect that occurs in semiconductors. Due to the semiconductor structure, the electrons are forced in one direction creating a flow of electrical current. Solar cells are not 100% efficient because some of the light spectrum is reflected, some (infrared) of it is too weak to create electricity and some (ultraviolet) creates heat energy instead of electricity. The energy crisis in the 1970s trigged the beginning of major interest in using solar cells to produce electricity in homes and businesses, but prohibitive prices (nearly 30 times higher than the current price) made large-scale applications impractical and economically unfeasible. Research and development in the years to follow made PV devices more efficient and financially viable, and a trend of increasing performance and decreasing cost has continued to the present. [5]

From the Solar Energy Industries Association (SEIA) and Greentech Media(GTM) research “U.S. Solar Market Insight: Q3 2014”, since the third quarter of 2010, the average price of a PV panel has dropped by 63%. By the end of 2014, the U.S. should have over 20 GW of cumulative solar electric capacity, roughly the same amount that is expected to be installed just from 2015 – 2016 [6].

1.2 Electrical Energy Storage (EES)

Based on the review of progress in electrical energy storage system [7], EES refers to a process of converting electrical energy from a power network into a form that can be stored for converting back to electrical energy when needed.

There are two main reasons for the importance of using EES in Microgrid architecture. First, the consumption of electricity is not uniformly distributed. In the mid-night and early morning the electricity load is much lower than during working hours, which means electricity can be stored during Off-Peak time and delivered during On-Peak rate period to achieve a higher electricity cost saving, stability and reliability of the Microgrid. Especially under a time-of-use (TOU) rate schedule in buildings, the controlled charging and discharging ESS allows for reducing the building load demand significantly. Both energy charge and demand charge can be drastically lowered. Second, one significant characteristic of renewable energy such as solar and wind energy is their

intermittency and variability. Energy storage systems are critically important to address and compensate for the intermittency and variability of renewable source.

From a review of energy storage technologies [8], six critical technologies can be used to effectively store electrical energy.

a) Pumped Hydro Storage (PHS): water is pumped from a lower reservoir to an upper reservoir during low electricity consumption or high renewable energy generation, and reserve the process to activate the turbines to generate electricity when demand is high. Energy is stored as gravitational potential energy with water reservoirs.

b) Compressed Air Energy Storage (CAES): air is compressed and stored under pressure in an underground storage carven during low power demand or high energy generation. During high electricity usage time, compressed air is heated and expanded in an expansion turbine driving a generator to produce electricity. Energy is stored as compressed (highly pressured) air.

c) Battery Energy Storage System (BESS): battery banks are charged during the low electricity consumption period (such as midnight for office buildings) or high renewable energy generation time period and discharged during high electricity needs time. Energy is stored as electrochemical energy in batteries and flow batteries.

d) Hydrogen-based Energy Storage System (HESS): hydrogen is produced by electrolysis and stored during low power demand or high renewable energy

generation. During high power demand, the hydrogen is re-electrified by fuel cells to produce electricity. Energy is stored as chemical energy in fuel cells.

e) Flywheel Energy Storage System (FESS): the flywheel is accelerated by electric motor as charging process during low power demand or high renewable energy generation and decelerated to activate electric generation as discharge during high power demand. Energy is stored as kinetic energy in flywheels.

f) Superconducting magnetic energy storage (SMES): the superconducting coil is charged by generating magnetic field through the flow of direct current (DC) in itself and discharged by transforming magnetic energy to electric energy. Energy is stored as magnetic field in inductors.

g) Supercapacitor energy storage system (SESS): the supercapacitor also called ultracapacitor or electric double-layer capacitor, is charged by applying a voltage to it and causing both electrodes in the capacitor to generate electrical double-layers to store electric energy and discharged by releasing positive and negative ions to the electrolyte. There is no chemical reaction among charging or discharging process so little energy will be lose. Energy is stored as an electric field in capacitors.

1.3 Inverter

A power inverter, or inverter, is an electronic device or circuitry that changes direct current (DC) to alternating current (AC) [9].

To a Microgrid system with power supplied by solar PV and from a BESS, at least two inverters are needed. One inverter is for the PV modules. The second is for the battery energy storage system.

For the PV modules, the inverter is needed for two main reasons. First and the basic reason is to convert the direct current (DC) output to alternative current (AC). Second, the relationship between the power generated by solar modules and solar irradiance, temperature and resistance is non-linear and complex. The power generated by PV arrays delivered from the modules is very sensitive to the point of operation, the inverter uses maximum power point tracking (MPPT) method to obtain the maximum power from PV modules [10]. The PV inverter can be turned on or off to manipulate solar generation into the grid, which makes the solar inverter as a controlled device in the system.

For the BESS, the inverter is needed for three reasons. First, like the PV inverter, the battery inverter converts DC input from batteries to AC output to the grid when batteries are discharged. The charger controller transfers AC input from the grid to DC output when batteries are charged. Second, the AC output from the inverter is synchronized with the utility system. Frequency and each phase of three phases are synchronized with the grid [11]. Third, the power to charge or discharge the batteries can be changed to any value, which makes the BESS a controllable load source to the grid.

1.4 Controlled Devices in a Microgrid System

As discussed in Section 1.3, inverters in a Microgrid system can be part of controlled devices. The PV inverter can control (modulate) the generation within the Microgrid. The battery inverter can control the power to charge or discharge the BESS. Air conditioners and air handles (AH) are the common building load that can be controlled by different smart controllers. Due to these controllable devices in Microgrid, different control methods can be designed to optimize the generation from renewable energy and management of energy storage system.

Figure 1-1 shows a controlled experiment on the Sustainable Integrated Grid Initiative (SIGI) Project at the College of Engineering Center for Environment Research & Technology (CE-CERT). This test was carried by controlling the air handles (AH) loads, the solar inverter and the BESS connected to the building (shown as CAEE building). The experiment was conducted on 9/19/14.

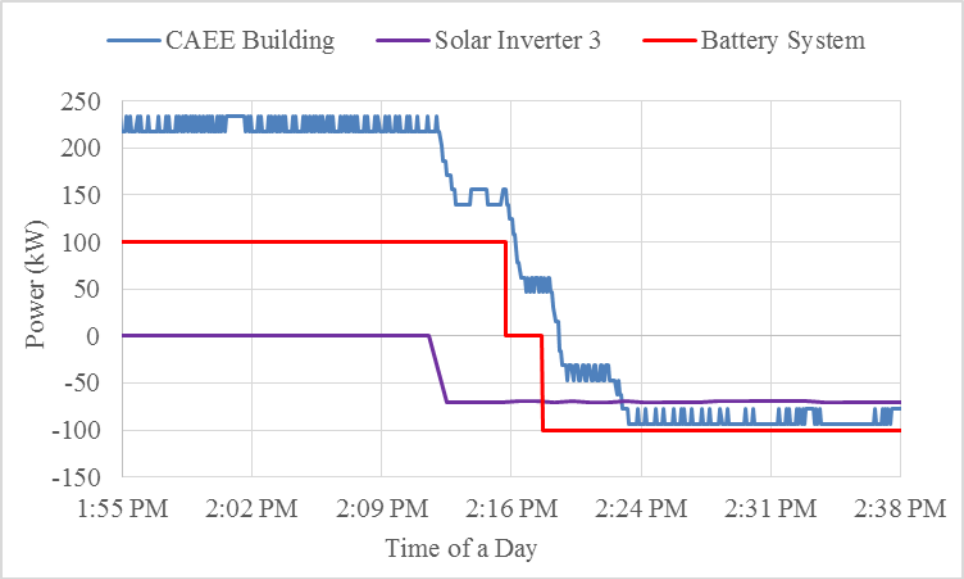

Figure 1-1 Controlled Devices Operation in Microgrid

In Figure 1-1, it can be observed that from 1:55 PM to 2:12 PM, the normal building load was about 225 kW, the solar inverter was off, and the batteries were charging at a rate of 100kW. Then, the PV inverter was turned on (2:13 PM) to let the PV panels deliver power to the grid. The building load started to decrease down to 150 kW. Around 2:16 PM the battery inverter was shut down and the net load became 50kW. At 2:18 PM, the battery inverter switched to discharge mode, discharging the batteries at a rate of 100kW. The building instantaneous net load dropped to -50 kW. As the last control action, some of the AHs were turned off in the building, further decreasing the net load to about -90 kW. Figure 1-1 shows that by implementing series of controlling actions in the SIGI's Microgrid testbed system, the building net load decreased from 225 kW down to -90 kW, indicating

that not only the net load could be reduced without impacting the activities of the building facility, but the Microgrid system was able to deliver power to the external grid.

1.5 Conclusion

In this chapter, three basic components --- generators, energy storage systems and controlled devices in the Microgrid are discussed. Due to the intermittent characteristics of renewable energy (such as solar and wind generation) integrated into a Microgrid as the generator, energy storage systems become important to make the Microgrid more reliable and efficient of energy utilization. Inverters and charger controllers are indispensable for any Microgrid to bring different electric instruments into unity by transforming the electric current from AC to DC or DC to AC.

How to utilize the BESS to achieve the optimum electricity usage efficiency is a key topic for any Microgrid. In the following chapters, a real-time control algorithm for the operation of the BESS is developed and tested in the Microgrid testbed of SIGI Project located at CE-CERT. A detailed Microgrid structure with the three basic components of the SIGI is discussed in Chapter 2.

Chapter 2 Overview of the Sustainable Integrated Grid Initiative (SIGI) Project in CE-CERT

The Sustainable Integrated Grid Initiative (SIGI) project integrates photovoltaic, energy storage and a local utility for electrical transportation to implement a testbed for a smart grid system. The system will provide the University with renewable energy while serving as a platform to learn about how new technologies could be applied in the real world.

There are four primary components in the testbed: four megawatts (MW) of UCR integrated solar PV; two megawatts-hours (MWH) of battery energy storage; several level two electric vehicle charging stations and one level three fast charging station; an electric trolley route servicing the general UCR region [12]. The overall structure of the SIGI project is shown in Figure 2-1.

2.1 Structure and Layout of the Project

2.1.1 The Overall Structure of the SIGI Project

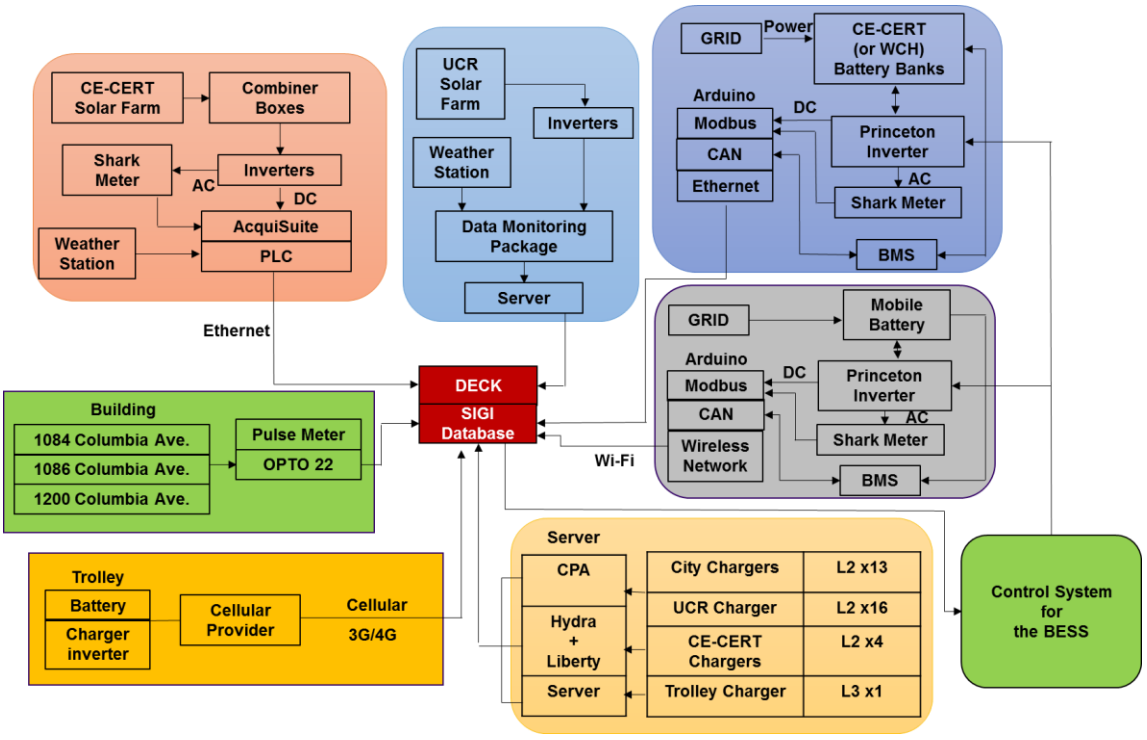

Figure 2-1 The Overall Structure of the SIGI Project

1) Solar Farm

There are two solar farms in the system: one 3.5 MW PV system located at UCR west campus, another 0.5 MW PV system located at CE-CERT. The generation from PV modules goes to the local (the city of Riverside) power company's distribution grid through inverters connected to the buildings. The weather stations collect data such as temperature, solar irradiance, wind direction, etc. All the data from PV modules and weather stations is

collected by data monitoring package. In CE-CERT, the Obvius AcquiSuite [13] package is used as the solar data monitoring system.

2) Stationary Battery Banks

There are two stationary battery storage systems installed at UCR – one MWh system at the Winton Chung Hall (WCH) building of Bourns College of Engineering (BCOE) and a 0.5 MWh system at CE-CERT. The battery banks are charged from the grid when appropriate and deliver power back to the grid as needed. A Princeton inverter (model: GTIB-100) [14] works as a battery inverter; it converts DC to AC when the battery banks are discharged and the charger controller transfers AC to DC when the battery banks are charged. A Shark meter (model: Shark 100) [15] is a data-metering device that can measure different types of AC data. Arduino [16] is a microcontroller which provides different communication interfaces and sends data from the Princeton inverter and the Shark meter to the next data-logging component. An Orion Battery Management system (BMS) [17] is also included in the system. The BMS protects and manages individual battery health to ensure that the battery packs work safety and continuously.

3) Mobile Battery Banks

A trailer mounted 0.5 MWh battery energy storage system has also been assembled at CE-CERT. This system is roughly the same as the stationary battery banks component at CE-CERT, except for the communication methods between data-logging devices. The

advantage of the mobile battery banks is its mobility that they can be plugged or unplugged into various buildings grids to contribute towards different building load requirements.

4) Building Load Components

At CE-CERT, there are three different buildings with industrial electrical metering; the 1084 building (B1084) has 100 kW PV panels, the1200 building (B1200) has 100 kW PV panels and 500 kWh battery storage and the 1086 building (B1086) has 200 kW PV panels. The Pulse meter [18] is a net-metering system that can measure the electricity usage (net load). For B1086, the building consumption is less than the solar generation for most of the day time. On a sunny day, the mobile battery banks may be charged from B1086 and deliver power to B1084 or B1200 if suitable plug points are available.

5) Electric Trolley

One of the diesel trolley of UCR was converted to an electric trolley as part of the SIGI project. It will receive energy from either the solar PV or the stationary BESS, and service the general UCR region. The battery status in the trolley will be sent through a cellular provider to the data-logging system.

6) Server and EV Charger System

Several Level 2 chargers are located at the UCR campus and CE-CERT. One level 3 charger for trolley is under construction at CE-CERT. The battery status and charging process are recorded from each charger and sent to a different server for later data analysis.

7) Data-logging System

The solar data is sent and saved to the web-based software called Deck [19] for checking and monitoring solar data and displaying live solar data. The SIGI database is designed to display and restore the entire system data including solar generation, battery storage system and EV chargers.

8) Control System for the BESS Component

The control system is designed to reduce the electricity cost by smartly controlling the stationary and mobile BESS on a daily basis. The control system receives the system real-time information from the SIGI database, and sends charging or discharging power value to the Princeton inverter to control the BESS.

2.1.2 The Detailed Microgrid Structural Layout at CE-CERT

All the work reported in this thesis was performed at the CE-CERT facilities. The detailed structure of the solar and the stationary BESS shown in Figure 2-1 is discussed in this section.

1. Solar PV System

As shown in Figure 2-2, there are 14 combiner boxes in the 500 kW PV system. The output from multiple PV modules is connected in series to make a string, and a number of strings are combined to produce a single DC output. The combiner boxes are used to minimize wiring costs and losses.

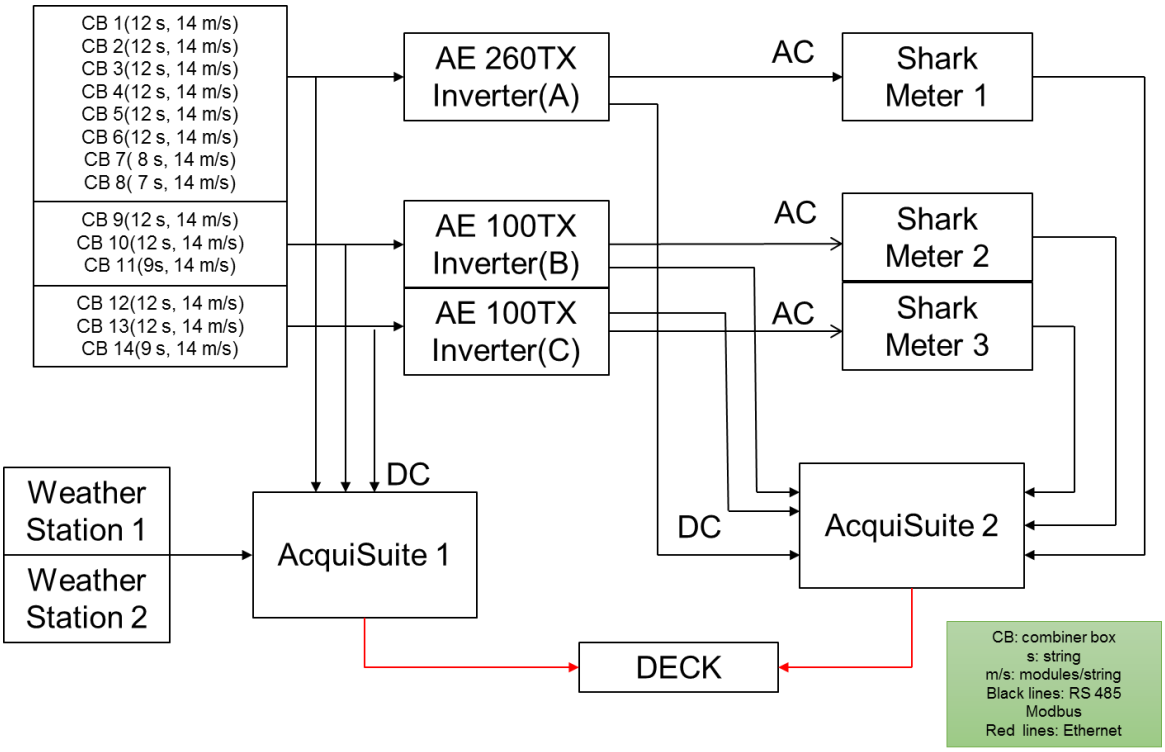

Figure 2-2 The AcquiSuite System

In this system, there are 10 combiner boxes which combine 12 PV strings individually; there are 2 combiner boxes which combine 9 PV strings, and there is 1 combiner box which combines 8 PV strings and 1 combiner box which combines 7 PV strings. Each PV string contains 14 PV modules in series. The DC generated by PV modules goes to solar inverters before being connected to the building AC grid. There are 3 inverters in the system; two of them are 100 kW inverters and one is 260 kW inverter. The 100 kW and 260 kW means that the inverter can continuously output 100 kW and 260 kW power respectively [20][21]. The inverter converts DC into usable AC. The power from the inverters is used directly by the buildings and excess power may be sent back to the

utility for later use by the buildings. The Shark Meter is a metering device; it monitors AC data from inverters and transmits the AC data to the next data-monitoring device AcquiSuite. The two AcquiSuites in the system acquire data from different devices and sensors. The AcquiSuite sends these data to a web-based software DECK to let users check different solar information or weather data.

2. Stationary Battery System

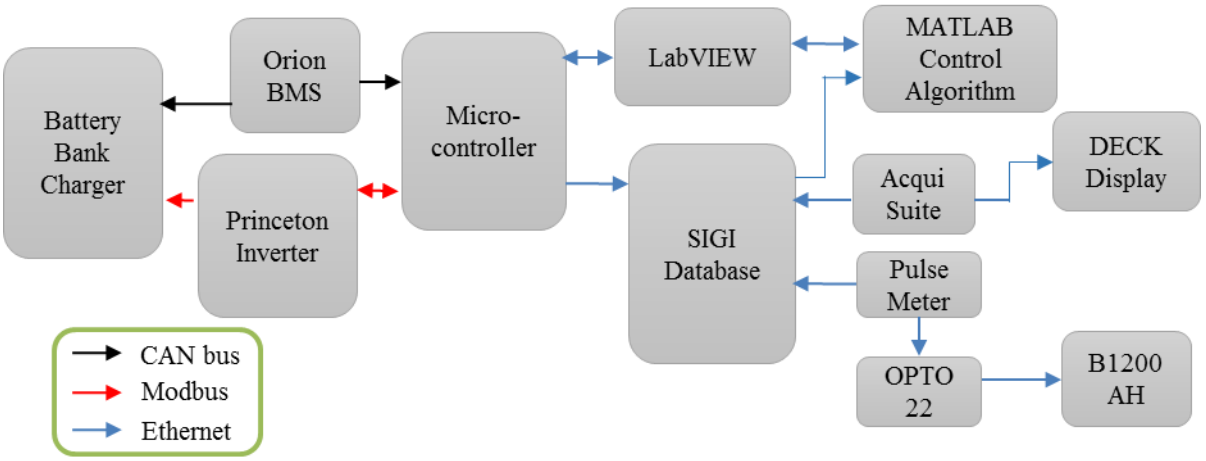

Figure 2-3 The Stationary Battery Energy Storage System Schematic

The main objective of this thesis is the optimal battery operation in the SIGI Microgrid testbed based on the rate of Schedule time-of-use (TOU) for Large General and Industrial Service rate in the city of Riverside. The stationary battery system schematic is shown in Figure 2-3. The Orion BMS is a battery management system that balances current and voltage for each individual battery cell to meet the requirements of protecting and managing the battery. The Princeton inverter converts DC to AC when discharges the

battery banks from the grid. Another important function for the inverter is controlling the charging or discharging rate for the BESS. The battery charger converts AC to DC when charges the battery banks. Arduino shield is a board that can be plugged on the Arduino Printed Circuit Board (PCB) to extend its capabilities. In the system, the shield is used to apply different communication interfaces, such as Modbus and controller area network (CAN) bus, between different devices. The Arduino is a data transmission microcontroller which can transfer various information through the shield. LabVIEW (short for Laboratory Virtual Instrument Engineering Workbench) is a system-design platform and development environment for a visual programming language from National Instruments [22]. The LabVIEW software works as the entire system controller which sends the charging/ discharging power value to the BESS. MATLAB (short for matrix laboratory) is a multi-paradigm numerical computing environment and fourth-generation programming language [23]. MATLAB works as an optimization controller to calculate the optimal power rate based on real time and historical data under real-time control algorithm. Detailed control algorithm is discussed in Chapter 3, 4 and 5. The Pulse Meter measures the net load and sends the net load information to the OPTO 22 system and SIGI database. The OPTO 22 [24] is a building smart microcontroller device that can turn on or off the air conditioners and air handlers in the building based on a certain control strategy, for example, when the net load is larger than a scheduled

threshold the air handlers/conditions is turned off one by one. The SIGI database collects data from different system components to let users check or manipulate these data for analysis and control.

2.2 Communication Between Different Components

2.2.1 Communication Between Solar Related Components

As shown in Figure 2-3, most communication is based on Modbus & RS-485 network. The communication between DECK and AcquiSuite is through Ethernet.

Communication on a Modbus network is initiated by a “Master” with a “Query” to a “Slave”. The “Slave” which is constantly monitoring the network for “Queries” will recognize only the “Queries” addressed to it and will respond either by performing an action (setting a value for example) or by returning a “response” [25]. Only the Master can initiate a query. Each Modbus Device must have a unique address. The Modbus protocol defines the format for the master’s query and the slave’s response. A simplified system’s Modbus communication is shown in Figure 2-4.

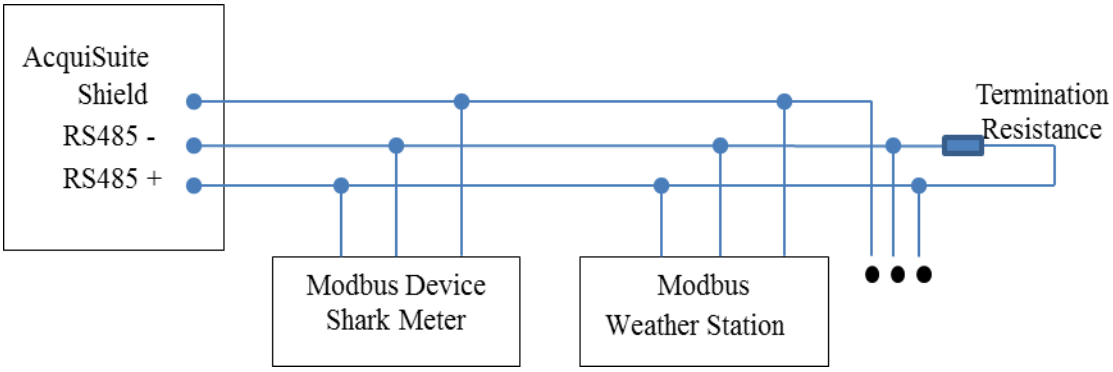

Figure 2-4 Modbus Communication

2.2.2 Communication Between Stationary BESS Related Components

1. CAN bus Communication

The CAN bus is the abbreviated form of controller area network. It is a vehicle bus standard designed to allow microcontrollers and devices to communicate with each other in applications without a host computer. CAN is a multi-master serial bus standard for connecting Electronic Control Units [ECUs] also known as nodes. CAN is a message broadcast system. Two or more nodes are required on the CAN network to communicate [26]. Unlike a traditional network such as USB or Ethernet, CAN does not send point-to-point data under the supervision of a central bus master; instead, many short messages like temperature are broadcast to the entire network, which provides for data consistency in every node of the system [27].

There are two CAN bus interfaces located in the Orion BMS. One is connected to the battery bank charger; the other is connected to the Arduino Shield. The BMS collects multiple types of data from the battery, such as cell voltages, current (Amperage), temperatures, total pack voltage and etc. from sensors in the BMS units. Then it calculates the state of charge (SOC), state of health (SOH), internal resistance and other important battery parameters [28]. Then through CAN network, the Arduino retrieves SOC, battery charge rate, pack current and voltage and etc. and sends them to the SIGI

database for further research. In this thesis, SOC of the battery banks and battery charge rate need to be collected for the calculation under MATLAB control algorithm.

2. Modbus Communication

The main mechanism of Modbus communication has been discussed in Section 2.2.1. Figure 2-3 shows that the Modbus communication occurs amongst the Princeton inverter, the battery bank charger and the Arduino Shield. The Princeton inverter has a meter which measures DC information, and the Shark meter in the inverter measures AC information, such as voltage, current and the charge rate. The Arduino transmits power or kW information to the Princeton inverter to control the battery banks and also receives power from the inverter for checking the live battery status. It also completes any further calculations for the optimal battery operation.

3. Ethernet Communication

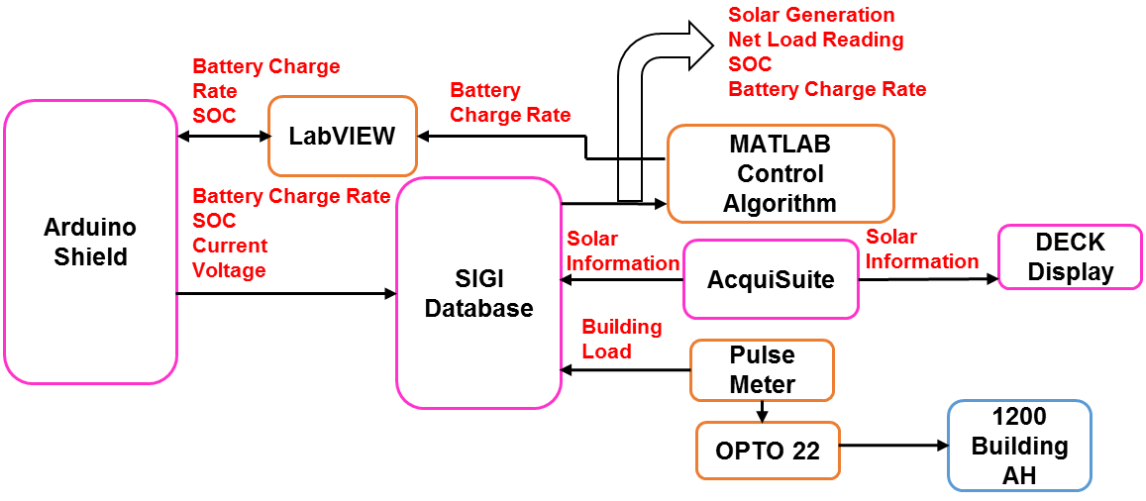

Figure 2-5 Data Flow of the Stationary Battery Energy Management System

Ethernet communication provides fast and remote management between different devices. A detailed data transmission is shown in Figure 2-5.

The real-time battery control operation integrates various data into a coherent system. LabVIEW works as a control center as shown in Figure 2-5, and it communicates with various components through Ethernet. In LabVIEW, there are two kinds of control method: one is Schedule Control, the other is Real-Time Control. In Schedule Control, a default table is built where a day is separated into 96 intervals with 15-minutes per interval and each time interval has a preset power value. Time interval of 15 minutes is chosen as the power companies use a rolling 15-minute average to charge for various types of peak demand. The LabVIEW automatically runs in 24 hours in a day with different preset power values sent to the Arduino. The tables are built as Tables 1 and 2.

Rate Period	Time	Power (kW)
Off-Peak	12:00 AM – 6:30 AM	-30
	6:30 AM – 8:00 AM	0
Mid-Peak	8:00 AM – 4:45 PM	0
	4:45 PM – 5:00 PM	60
On-Peak	5:00 PM – 7:00 PM	60
	7:00 PM – 9:00 PM	40
Off-Peak	9:00 PM – 9:15 PM	40
	9:15 PM – 10:15 PM	0
	10:15 PM – 12:00 PM	-30

Table 1 Winter Time[1] Schedule

[1] Based on the TOU electricity rate schedule, winter time are the months of January, February, March, April, May, October, November and December.

Rate Period	Time	Power (kW)
Off-Peak	12:00 AM – 3:45 AM	-35
	3:45 AM – 8:00 AM	-30
Mid-Peak	8:00 AM – 11:45 PM	0
	11:45 PM – 12:00 PM	40
On-Peak	12:00 PM – 6:00 PM	40
Mid-Peak	6:00 PM – 6:15 PM	40
	6:15 PM – 11:00 PM	0
Off-Peak	11:00 PM – 11:15 PM	0
	11:15 PM – 12:00 PM	-35

Table 2 Summer Time[2] Schedule

For the winter schedule, the On-Peak rate period is from 5:00 PM to 9:00 PM, and the Mid-Peak rate period is from 8:00 AM to 5:00 PM; the rest is the Off-Peak rate period. While for the summer schedule, Off-Peak is from 11:00 PM to 8:00 AM and On-Peak starts at noon and lasts till 6:00 PM; the rest is the Mid-Peak rate period. In Tables 1 and 2, the negative values mean that the battery is in charge mode and the positive values mean that the battery is in discharge mode. Tables 1 and 2 show that the batteries are charged during the Off-Peak rate period and discharged during the On-Peak rate period. Battery power delivery over the 6 hours On-Peak rate period in summer makes the battery discharge to 34% SOC, which requires more charging procedure to occur during the Off-Peak rate period. As electricity demand charges are calculated based on 15 minutes moving average, to be on the safe side, the battery banks are programmed to start discharging 15 minutes prior to On-Peak start point and 15 minutes later than ending time.

[2] Based on the TOU rate schedule, summer time are the months of June, July, August and September.

In real-time control algorithm, LabVIEW directly receives power from MATLAB control algorithm other than the Tables 1 and 2. MATLAB retrieves the real-time solar generation, SOC, Pulse Meter net load reading from SIGI database to implement the optimization function. Through Ethernet network, the SIGI database gathers all of the important information from the BESS, the solar PV generation and the building load usage. From the battery operations side, battery charge rate, SOC, battery current and voltage values are collected; from the solar PV side, SIGI database acquires various solar information through the Shark meters located in the solar inverters; for the building, the real-time building load is measured by Pulse Meter and is sent to the database.

Through the Ethernet communication, the AcquiSuite sends various solar data to DECK for displaying and storing solar data. The OPTO 22 system can maintain the building load in certain threshold by controlling some of the AHs in the B1200.

2.3 Conclusion

In this chapter, detailed structure of the SIGI Microgrid architecture and the communication between different components in the Microgrid system are fully discussed. The entire SIGI Microgrid can be divided into 8 different components as follows: the solar farm, the stationary BESS, the mobile BESS, the electrical loads of buildings, the electric trolley, the server and charger component, the data-logging component and the control system for the BESS. The control system for the Microgrid at

CE-CERT is the main focus of this thesis. A complete dataflow involving various instruments and components related to the control system is shown in Figure 2-5. A detailed MPC control algorithm in MATLAB is discussed in Chapter 3.

Chapter 3 MPC Method

3.1 Introduction to MPC

Model Predictive Control (MPC) is an advanced method of process control that has been in use in the process industries such as chemical plants and oil refineries since 1980s. In recent years, it has also been used in power system balancing model [29]. The term MPC does not designate a specific control strategy but rather an ample range of control methods which make explicit use of a model of the process to obtain the control signal by minimizing an objective function [30]. Due to the dynamic nature of real system, decision making should occur at each time step to adapt to the most updated situation. MPC algorithm consists of an optimization problem at each time instants which can be feed to the dynamic model.

3.1.1 MPC Model

MPC algorithm consists of three parts: system model, predictive model and optimization problem.

- System model

Most dynamic model can be described as:

$$x(k+1) = g\big(x(k), u(k)\big), x(0) = x_0 \tag{3-1}$$

$$y(k) = f(x(k), u(k)) \tag{3-2}$$

$x(k)$ is the state of the model, and it changes with time from initial state x_0. (3-1) describes the evolution of the model state from initial time. The future state $x(k+1)$ is affected by the input $u(k)$ and its past and current states $x(k)$. $y(k)$ is the output of the system. Both $g(x,u)$ and $f(x,u)$ can be nonlinear or linear which depends on the real system model.

- Prediction model

  A model which describes the input to output behavior of the process, is needed. Mechanistic models derived from conservation laws can be used. Usually, however in practice simply data-driven linear models are used. ” [31]

- Optimization problem

$$\min COST(\boldsymbol{u}(\boldsymbol{k}), \boldsymbol{x}(\boldsymbol{k})) \tag{3-3}$$

$$\text{subject to } u(k) \leq u_i ; i = k, k+1, \dots\dots, N+k-1;$$

$$x(k) \leq x_i ; i = k, k+1, \dots\dots, N+k-1;$$

$$y(k) \in Y_i ; i = k, k+1, \dots\dots, N+k-1;$$

$$\textit{where } k = 0,1, \dots\dots, L-1;$$

In the MPC model, the optimization function is calculated repeatedly from initial time, say $k = 0$ to $k = L-1$. At each time *k*, the goal is to find the optimized solution for (3-3) within a control horizon *N* and only apply the first index of the optimized solution. In both constraints and optimization function, future control inputs and future

plant responses are predicted using a system model and optimized. There are several ways to solve the optimization function according to different optimization function. If the function is linear or convex, convex optimization can be utilized; if it's non-convex, neural network algorithm can be used. In the thesis, convex optimization is discussed in Section 3.1.3.

3.1.2 The MPC Principles

MPC models have a prediction horizon *M* and a control horizon *L*, which always has $L \leq M$. The detailed MPC principles is applied as follows [32]:

(i) At time *k*, retrieve the system current information and solve an optimal control problem for (3-3) over a fixed future interval, applying the current and future constraints.

(ii) Apply only the first index in the optimal control sequence.

(iii) Go to next time $k+1$ and acquire the system most updated information for this current time which is $k+1$.

(iv) Repeat the fixed horizon optimization at time $k+1$ over the future interval $[k+1, k+L]$, the starting state is x_{k+1}.

(v) Repeat for M times, say $k = 1, \ldots\ldots, M$.

After finishing the above steps, the output vector can be expressed by

$$\boldsymbol{u^{OPT}} \triangleq [u_1^{OPT} u_2^{OPT} \ldots\ldots u_M^{OPT}]^T \tag{3-4}$$

3.1.3 Convex Optimization

A standard convex optimization problem is one of the forms “

$$\begin{aligned} &\text{minimize } f_0(x) \\ &\text{subject to } f_i(x) \le 0, i = 1, \dots \dots, m \\ &\qquad h_j(x) = c_j, j = 1, \dots \dots, p, x \in C \end{aligned} \tag{3-5}$$

where the functions $f_0, \dots \dots, f_m: \mathbf{R}^n \to \mathbf{R}$ are convex, i.e., satisfy

$$f_i(\alpha x + \beta y) \le \alpha f_i(x) + \beta f_i(y)$$

For all $x, y \in \mathbf{R}^n$ and all $x, y \in \mathbf{R}$ with $\alpha + \beta = 1, \alpha \ge 0, \beta \ge 0$.

And $h_j(x) = c_j$ are affine, i.e., for any $x_1, x_2 \in C$ and $\theta \in \mathbf{R}$, $\theta x_1 + (1-\theta)x_2 \in C$. In other words, *C* contains the linear combination of any two points in *C*. To be more general, a point $x \in C$ of the form $\theta_1 x_1 + \theta_2 x_2 + \cdots + \theta_k x_k$, where $\theta_1 + \cdots + \theta_k = 1$, is an affine combination of the points $x_1, \dots, x_k$.

The inequalities $f_i(x) \le b_i$ are called inequality constraints and the equations $h_i(x) = c_i$ are called the equality constraints.

The set of points for which the objective and all constraint functions are defined,

$$D = \bigcap_{i=0}^{m} \mathbf{dom}\, f_i \cap \bigcap_{j=1}^{p} \mathbf{dom}\, h_i,$$

is called the domain of the optimization problem (3-5). A point $x \in D$ is feasible if it satisfies the constraints $f_i(x) \le 0, i = 1, \dots \dots, m$ and $h_j(x) = c_j, j = 1, \dots \dots, p$. The problem (3-5) is feasible if there exists at least one feasible point, and infeasible

otherwise. The set of all feasible points is called the feasible set or the constraints set.

The optimal value p^* of the problem (3-5) is defined as

$p^* = \inf \{f_0(x) \mid f_i(x) \leq 0, i = 1, \dots\dots, m, h_j(x) = 0, j = 1, \dots\dots, p\}$." (Boyd, 2004)[33]

For the MPC problem, (3-4) can be described as $\boldsymbol{u^{OPT}} \triangleq [p_0^*, p_1^*, \dots\dots, p_{L-1}^*]^T$.

For a linear programming problem, the objective and constraint functions are linear:

$$\begin{aligned} &\text{minimize } c^T x \\ &\text{subject to } a_i^T x \leq b_i, i = 1, \dots\dots, m. \end{aligned} \tag{3-6}$$

From (3-6), $f_i(x) \triangleq a_i^T x, f_0(x) \triangleq c^T x$, which always have

$$f_i(\alpha x + \beta y) = a_i^T(\alpha x + \beta y) = \alpha \cdot a_i^T x + \beta \cdot a_i^T y$$

$$= \alpha f_i(x) + \beta f_i(y)$$

and $f_0(\alpha x + \beta y) = \alpha f_0(x) + \beta f_0(y)$. So linear functions are all convex and linear programing problem is the convex optimization problem.

3.2 Introduction to the Model of the Real System's MPC Algorithm

As discussed in Section 2.1.1, one 500kWh battery storage management system and one 100kW PV inverter were installed for B1200. Based on the real time solar generation and building usage, the battery is implemented to manage different demand for Off-Peak, Mid-Peak and On-Peak demand respectively and the building electricity usage for On-Peak and Mid-Peak time periods.

For the controlling system, MPC algorithm is applied for controlling for the On-Peak rate period. As the experiments operated in B1200 for both summer and winter time, MPC can control the battery properly and decrease the electricity bill for several months. Especially for TOU building, with the help of battery management system, the electricity bill can be decreased for thousands of dollars.

3.2.1 The Battery System Model

The 500 kWh battery packs are from the Winton Global Energy Limited, and the type of batteries is WB-LYP1000AHC. From the company's official site [34], the battery's cycle of life can be found, which is when depth of discharge (DOD) is 80%, the cycles are more than 5000 times and when DOD is 70%, the cycles are more than 7000 times. To maintain the longest lifetime of the WCH battery, the battery packs are used the capacity between 40% SOC and 90% SOC at usual occasion, and the minimal SOC which can be used is 20%. When it reaches 20% SOC, the system will be shut down automatically to keep the stability of the whole system.

To test the charging and discharging efficiency of the battery packs, several experiments have been done. Two experiments are selected shown in Figure 3-2 and 3-3 in different time period. For Figure 3-2, the experiment was done on a winter period day; the battery was discharged at 60 kW from 4:45 PM to 7:00 PM and then discharged at 40kW. And for Figure 3-3, the experiment was done on a summer period day; the battery was

discharged at 40 kW from 11:45 AM to 6:15 PM. In these two figures, the blue line is the actual SOC collected by the sensor, and the red line is the simulated SOC calculated by (3-7). The step decrease trend of the red line is due to the precision of data acquisition system. The minimal is 1% SOC.

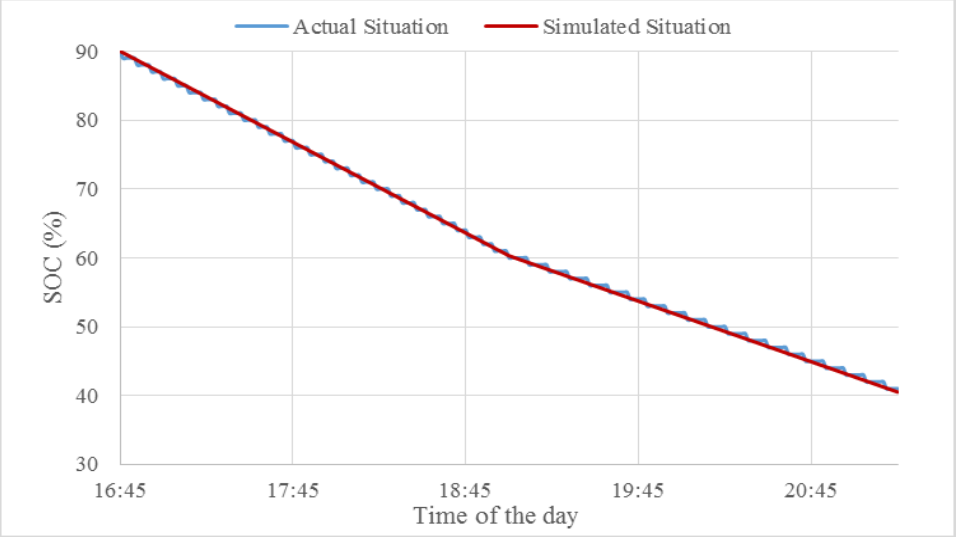

Figure 3-1 Discharging Efficiency Experiment for Winter Time

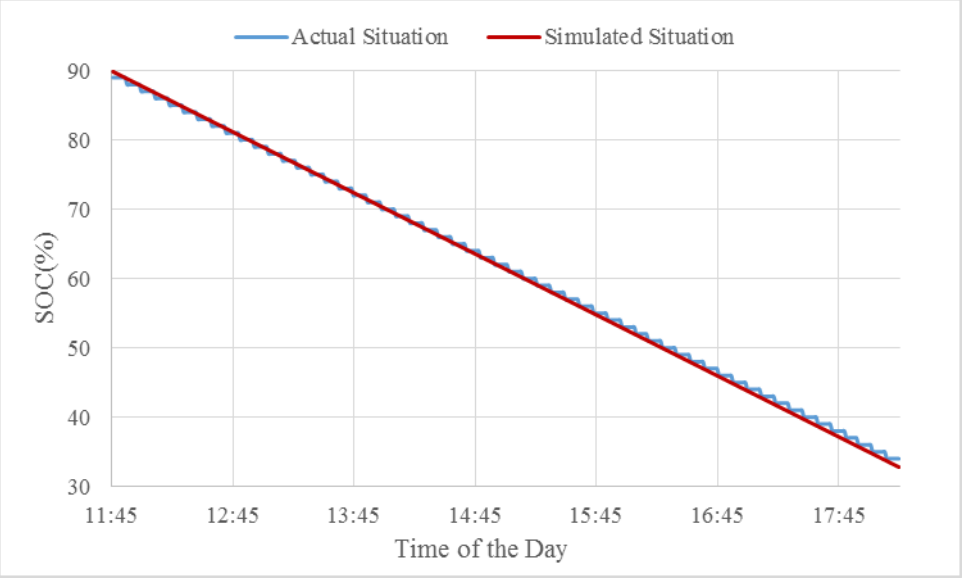

Figure 3-2 Discharging Efficiency Experiment for Summer Time

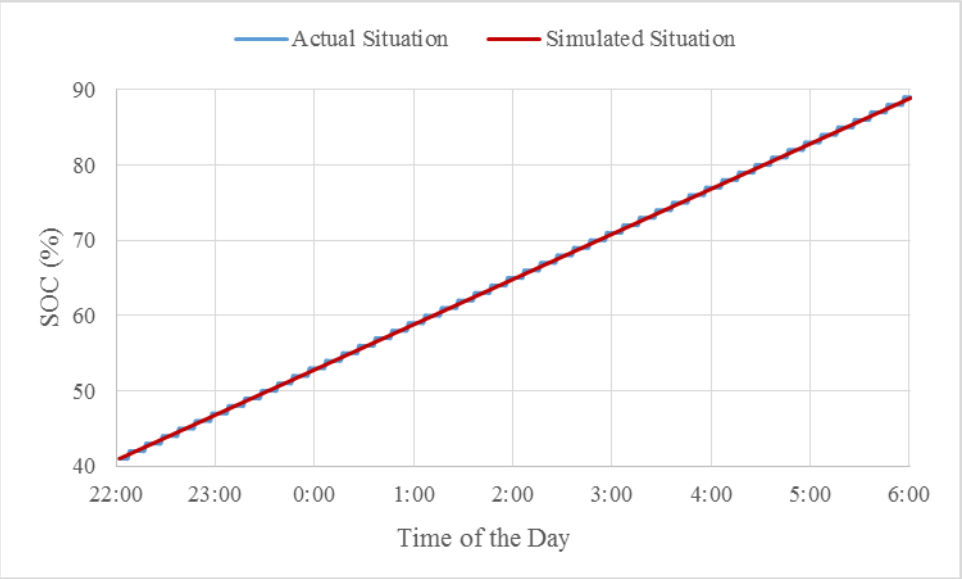

Figure 3-3 Charging Efficiency Experiment

From the above three figures, it is clear to see that the discharging or charging process is an approximately linear process. And the charging efficiency α is 1 and the discharging efficiency β is 1.1 which is determined by large amount of experiments.

$$bc(k+1) = bc(k) - \epsilon \cdot p(k) \cdot \Delta t \tag{3-7}$$

where $k = 0,1, \dots \dots, L$ and $k = 0$ represents for the initial time of the control strategy. $bc(k)$ represents for the battery capacity at time k and $bc(0)$ is the battery capacity at initial time; ϵ is the battery charging/discharging efficiency; $p(k)$ is the charging or discharging power of the battery system, $p(k) = \begin{cases} p(k)_{discharge}, & p(k) > 0, \epsilon = \beta \\ p(k)_{charge}, & p(k) < 0, \epsilon = \alpha \end{cases}$; Δt represents for the time interval of each time k.

$$\mathbf{bc}_{L\times 1} = \mathbf{bc_0}_{L\times 1} - \epsilon \cdot \mathrm{A}_{L\times L} \cdot \mathbf{p}_{L\times 1} \tag{3-8}$$

where $\mathbf{bc}_{L\times 1} \triangleq \begin{bmatrix} bc(1) \\ bc(2) \\ ... \\ bc(L) \end{bmatrix}_{L\times 1}$ is the battery capacity vector; $\mathbf{bc_0}_{L\times 1} \triangleq \begin{bmatrix} bc(0) \\ bc(0) \\ ... \\ bc(0) \end{bmatrix}_{L\times 1}$ is the battery capacity initial vector; $\mathbf{A}_{L\times L} \triangleq \begin{bmatrix} 1 & 0 & ... & 0 \\ 1 & 1 & 0 & ... \\ ... & ... & ... & ... \\ 1 & 1 & ... & 1 \end{bmatrix}_{L\times L}$ is a lower triangular matrix; $\mathbf{p}_{L\times 1} \triangleq \begin{bmatrix} p(1) \\ p(2) \\ ... \\ p(L) \end{bmatrix}_{L\times 1}$ is the battery operation vector: at time k, how much power the battery will be discharged or charged.

To be more specific, when it is a discharging process:

$$bc(1) = bc(0) - \beta \cdot p(1)_{discharge} \cdot \Delta t$$

$$bc(2) = bc(1) - \beta \cdot p(2)_{discharge} \cdot \Delta t$$

$$= \left(bc(0) - \beta \cdot p(1)_{discharge} \cdot \Delta t\right) - \beta \cdot p(2)_{discharge}$$

$$= bc(0) - \beta \cdot p(1)_{discharge} \cdot \Delta t - \beta \cdot p(2)_{discharge} \cdot \Delta t$$

……

$$bc(L) = bc(L-1) - \beta \cdot p(L-1)_{discharge} \cdot \Delta t$$

$$= bc(0) - \beta \cdot p(1)_{discharge} \cdot \Delta t - \cdots - \beta \cdot p(L-1)_{discharge} \cdot \Delta t$$

$$\begin{bmatrix} bc(1) \\ bc(2) \\ ... \\ bc(L) \end{bmatrix}_{L\times 1} = \begin{bmatrix} bc(0) \\ bc(0) \\ ... \\ bc(0) \end{bmatrix}_{L\times 1} - \beta \cdot \begin{bmatrix} 1 & 0 & ... & 0 \\ 1 & 1 & 0 & ... \\ ... & ... & ... & ... \\ 1 & 1 & ... & 1 \end{bmatrix}_{L\times L} \cdot \begin{bmatrix} p_{discharge}(1) \\ p_{discharge}(2) \\ ... \\ p_{discharge}(L) \end{bmatrix}_{L\times 1} \quad (3\text{-}9)$$

$\mathbf{p_{dis}} \triangleq \begin{bmatrix} p_{discharge}(1) \\ p_{discharge}(2) \\ ... \\ p_{discharge}(L) \end{bmatrix}_{L\times 1}$ is the battery discharging power vector, which is the same as (3-4).

3.2.2 Predictive Model

1. Solar Generation Predictive Model

The solar generation prediction model is designed in two different methods: one is the System Advisor Model (SAM) and the other is based on several months of historical solar data.

1) SAM solar generation production

SAM is developed by the National Renewable Energy Laboratory (NREL) and it makes performance predictions and cost of energy estimates for grid-connected power projects [35]. The thesis focuses on the performance predictions part, which is the solar production in this thesis.

In SAM's interface, users can select different system information based on the real system. The key parameters are location and resource, PV modules, inverter type, the system size and the losses of different equipment. The location and resource determines the weather historical information which includes solar and wind resource. There are four

databases for solar resource: National Solar Resource Database (NSRDB), Solar and Wind Energy Resource Assessment Programme (SWERA), The ASHRAE International Weather for Energy Calculations Version 1.1 (IWEC) and the Canadian Weather for Energy Calculations (CWEC) [36]. In this thesis, NSRDB is selected for simulation and the time horizon for historical weather information is from year 1991 to 2005.

Location and Resource		Riverside, CA
Module		Zhongli Talesun TP 660P-240
Inverter	A	PVP 260 kW 480V
	B/C	PVP 100kW 480V
Array	A	14 modules per string 87 strings in parallel
	B/C	14 modules per string 33 strings in parallel

Table 3 System Detailed Information

Deratement Factor	Value
Module Age	1.00
Array Soiling	0.93
Module Nameplate Tolerance	1.00
Module Mismatch	0.97
DC Wiring Loss	0.97
Shading	0.995
Total	0.865

Table 4 DC System Deratement Factors [37]

According to the real Microgrid system of this thesis, the detailed information is listed in Table 3 and Table 4, monthly solar production can be predicted by SAM. In Figure 3-4 and Figure 3-5, actual solar generation includes two years' solar production, which is from January to June, it's for the year 2015 and the rest is for the year 2014 (the most updated solar generation when the thesis is done).

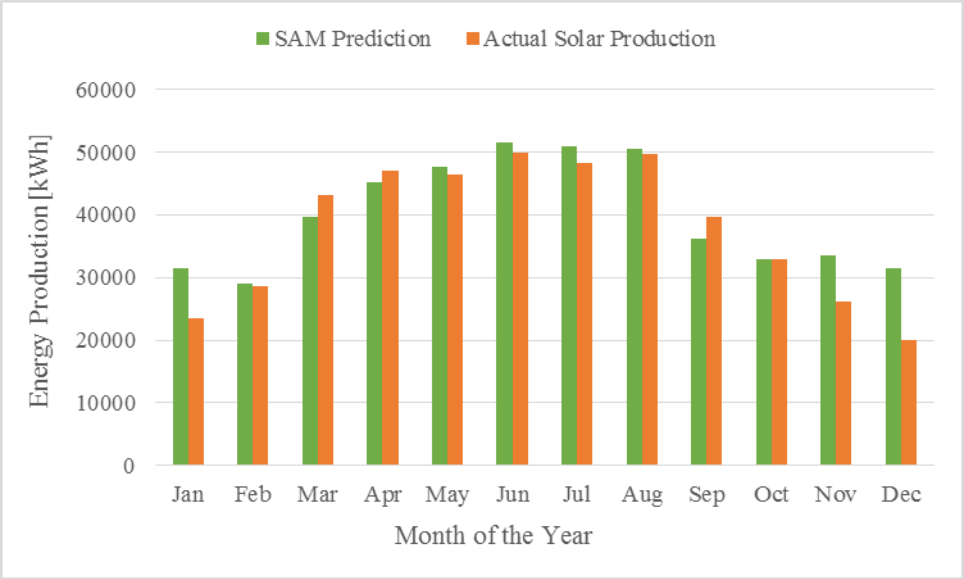

Figure 3-4 SAM Solar Generation Prediction vs. Actual Solar Generation for a 260 kW Inverter

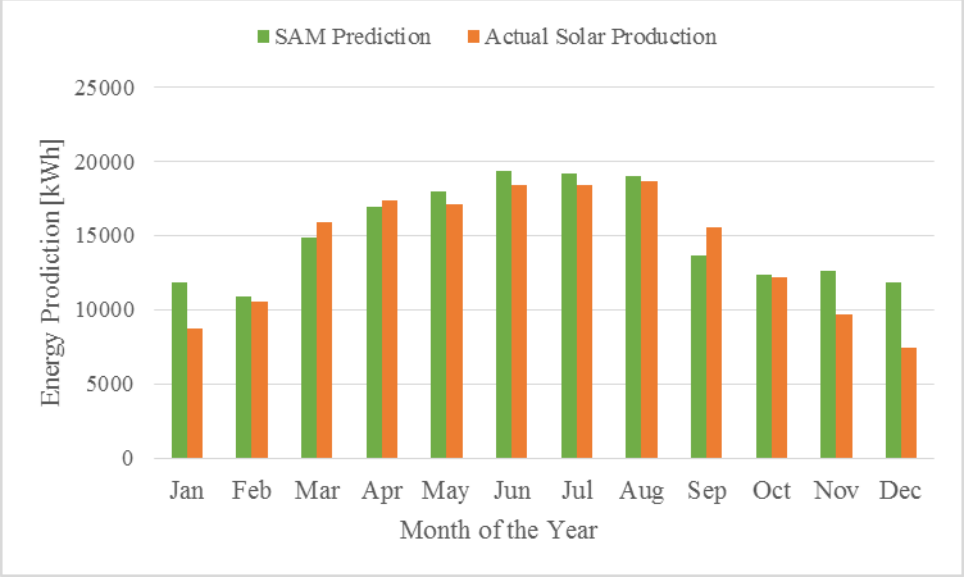

Figure 3-5 SAM Solar Generation Prediction vs. Actual Solar Generation for a 100 kW Inverter

Figures 3-4 and 3-5 show that the SAM's solar generation prediction can approximately provide the overall solar generation trend for the whole year with higher solar generation in the Summer time and lower solar generation in the Winter months.

Overall, the highest solar generation happens in the months when the days are long and sunny with the cooler ambient temperature (i.e. month of June). For most months, the deviation between SAM and actual generation is less than 15%. For the months of November, December and January, the deviation was higher than 20%, and can be mainly attributed to unpredictable weather events during these months.

Figure 3-6 shows the actual generation of the 260 kW inverter in the project for the months of November, December and January. All the solar generation data is from the DECK Monitoring system. The left side of Figure 3-6 represents the actual daily solar production versus the generation of one sunny day during the related month. The right side shows the related sunny day's solar profile. From Figure 3-6 (a), the highest daily solar production in November was in 11/03/2014 which was 1160 kWh. From 3-6 (b), it is clear to see that the day was a sunny and clear day. Comparison between the daily solar generation and the generation from 11/03, most days in November were cloudy and generation in these days was much smaller than 1160 kWh. A similar situation can be observed for the months of December and January 2015, where weather fluctuates significantly throughout these months.

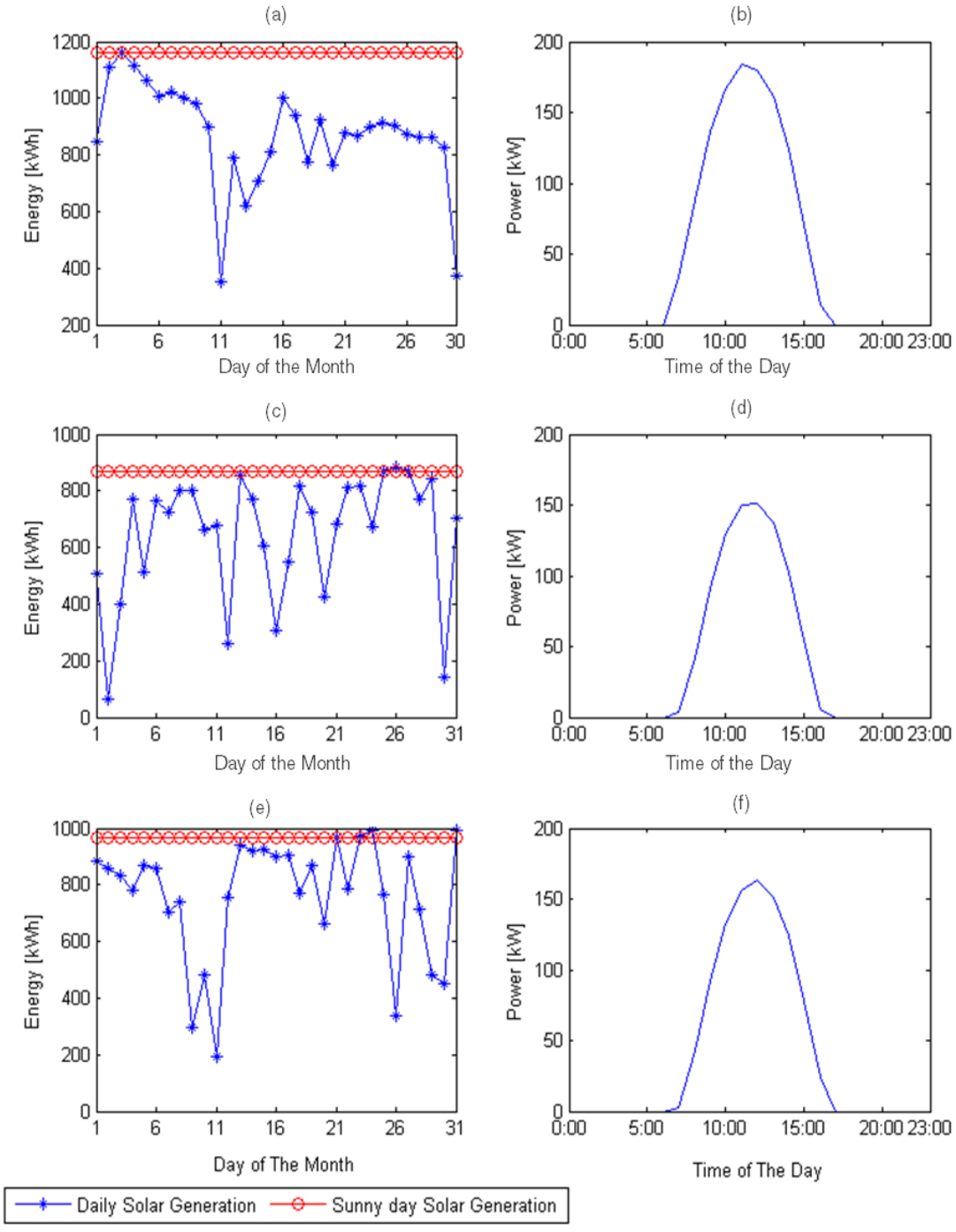

Figure 3-6 Daily Solar Generation vs. A Sunny Day Solar Generation for 260 kW Inverter. (a) November 2014; (b) 11/03/2014; (c) December 2014; (d) 12/25/2014; (e) January 2015 (f) 01/21/2015

From Figure 3-6 (e), it can be observed that on a sunny and clear day (01/21/2015), solar production was 966 kWh, while about half of the days in the month were cloudy. Figure 3-4 shows that the largest gap between the SAM solar generation prediction and actual solar generation is in the month of December. From Figures 3-6 (c) and 3-6 (d), the reasons can be concluded as follows: 1) The normal sunny day's solar generation for this month was 868 kWh, while most days of this month the generation was smaller than 12/25, which means most of the days weather conditions were cloudy or rainy; 2) From Figure 3-7, with comparison of the year 1991 to 2005, the average solar radiation was smaller than the average of these years which was the range for SAM's weather database.

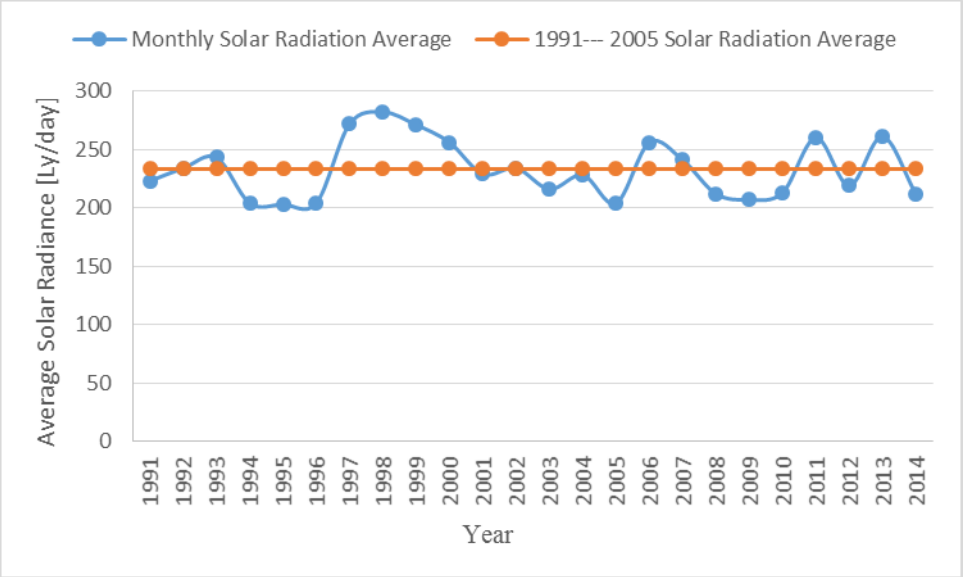

Figure 3-7 24 Years Monthly Solar Radiation vs. 15 Years Average Solar Radiation for December

Figure 3-7 and Figure 3-8 show the recent years' monthly solar radiation for December and January information. All the data is based on the weather station 044 U.C.

Riverside in California Irrigation Management Information System (CIMIS). The unit for solar radiation $1\ Ly/day = 0.484853\ Watt/m^2$. In November, the average for 1991 – 2005 is $253.33\ Ly/day$ and the in 2014 the average is $212\ Ly/day$. So the solar generation prediction from SAM is not accurate as the same situation.

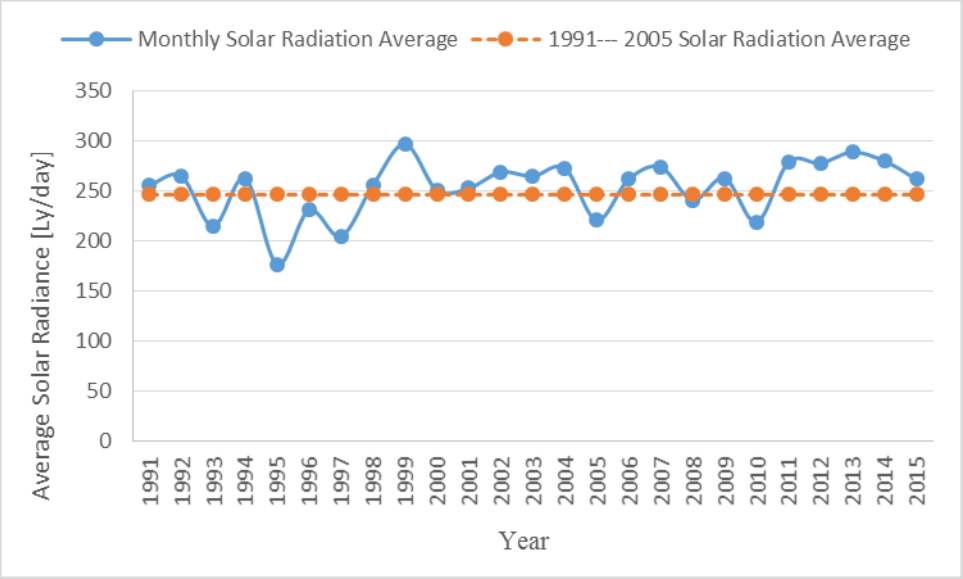

Figure 3-8 25 Years Monthly Solar Radiation vs. 15 Years Average Solar Radiation for January

From Figure 3-8, the radiation difference between 15 years average and year of 2015 is small while the prediction is not as accurate as expected. Meanwhile, the minimal time interval unit for SAM solar predication is 1 hour. So in real scenario of Microgrid real-time controller, SAM solar generation prediction is not dependable.

2) Historical Data of Solar Generation

A comprehensive database was built for the SIGI Project for storing and monitoring the entire system. The detailed communication and parameters used for the controller the

database collecting has been discussed in Section 2.2.2. Users can download diversity of data like solar information, battery management information and OPTO 22 Reading (net metering) from the database.

The predictive solar generation model is chosen by averaging the historical solar information in the thesis.

$$\widehat{\mathbf{Ps}}_{M\times 1} = \frac{1}{n}\cdot\sum_{i=1}^{n}(\mathbf{Ps}_{M\times 1})_i$$

where n represents for the amount of data samples chosen; *M* represents for the amount of time intervals in the solar generation model. The principles for real time solar generation prediction are as follows: for any real time data Ps_k, if $\widehat{\mathbf{Ps}}(k)/Ps_k \geq 1.25$, $\widehat{\mathbf{Ps}}_k = \frac{Ps_k}{\widehat{\mathbf{Ps}}(k)}\cdot\widehat{\mathbf{Ps}}$; else $\widehat{\mathbf{Ps}}_k = \widehat{\mathbf{Ps}}$.

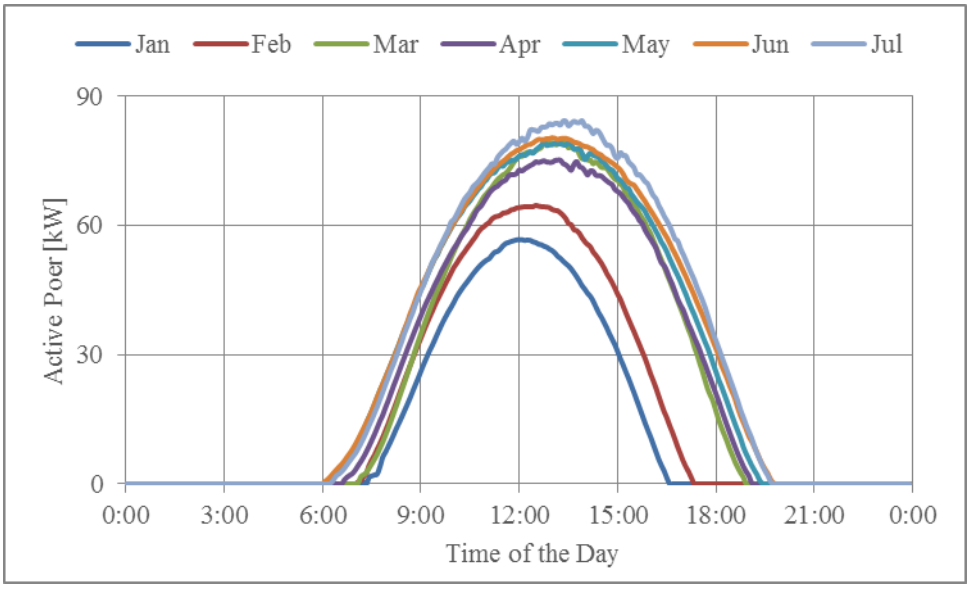

Figure 3-9 Average Solar Generation in Different Months

Figure 3-9 is the solar average generation in different months of Year 2015; the solar generation curves are shifted by day time saving on March 8th of this year and solar motion. It is clear to see that the solar generation increases with more sunshine duration. The average solar generation profile can be used as the solar prediction model for each month.

2. Building Load Prediction Model

The B1200 load prediction model, is the same algorithm used for the solar generation prediction model, in which the model averages the historical building load data.

$$\widehat{\mathbf{Pl}}_{M\times 1} = \frac{1}{n}\cdot\sum_{i=1}^{n}(\mathbf{Pl}_{M\times 1})_i$$

The principles for real time load prediction are as following: for any real time data Pl_k, if $Pl_k / \widehat{\mathbf{Pl}}(k) \geq 1.25$,

$$\widehat{\mathbf{Pl}}_k(k:k+\Delta T) = \frac{\widehat{\mathbf{Pl}}(k)}{Pl_k}\cdot\widehat{\mathbf{Pl}}(k:k+\Delta T)$$

$$\widehat{\mathbf{Pl}}_k(k+\Delta T:M) = \widehat{\mathbf{Pl}}(k+\Delta T:M);$$

else $\widehat{\mathbf{Pl}}_k = \widehat{\mathbf{Pl}}$.

The above algorithm shows that when the actual load is larger than the average load only a small portion of the prediction model needs to be changed. In B1200, the unpredicted load always lasts less than 2 hours. Therefore, a value of $\Delta T = 2$ hours is used by the building load predictive model.

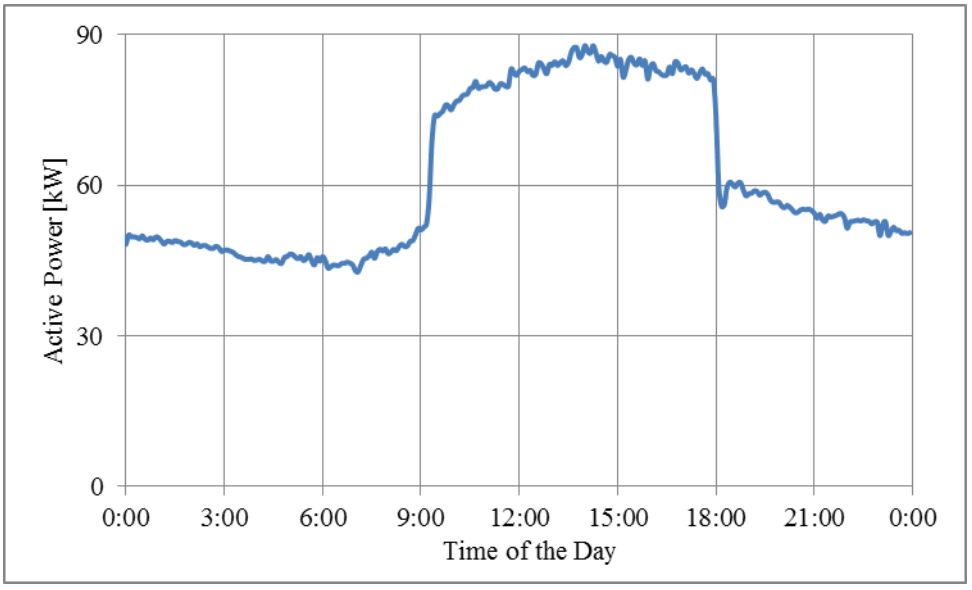

Figure 3-10 Building Load Profile for B1200

Figure 3-10 shows the average workday building load for B1200, and it is also the load prediction model in the thesis.

3.2.3 Optimization Model

The optimization is performed with regards to the electricity cost and it will always keep the cost as little as possible. The cost includes two parts: electricity energy cost which is the kWh cost and demand cost which is the kW cost. In the chapter, demand needs to be maintained below certain kW. At time slot *k*:

$$\text{minimize } (\mathbf{price}^{T}_{L\times 1})_k \cdot (\mathbf{pex}_{L\times 1})_k \cdot \Delta t \tag{3-10}$$

$$\text{subject to: } (\mathbf{bc}_{L\times 1})_k = (\mathbf{bc_0}_{L\times 1})_k - \beta \cdot \Delta \mathrm{t} \cdot \mathrm{A} \cdot (\mathbf{pd}_{L\times 1})_k \tag{3-11}$$

$$0 \le (\mathbf{pd}_{L\times 1})_k \le pda_k \cdot ONE \tag{3-12}$$

$$ONE \cdot bc_{\min} \le (\mathbf{bc}_{L\times 1})_k \le bc_{\max} \cdot ONE \tag{3-13}$$

$$(\mathbf{pex}_{L\times 1})_k = (\widehat{\mathbf{Pl}}_{L\times 1})_k - (\widehat{\mathbf{Ps}}_{L\times 1})_k + (\mathbf{pd}_{L\times 1})_k \tag{3-14}$$

$$0 \le (\mathbf{pex}_{L\times 1})_k \le onDemand \cdot ONE \tag{3-15}$$

where:

$(\mathbf{price}_{L\times 1})_k$ is the electricity price for time period $k : k+L-1$;

$(\mathbf{pex}_{L\times 1})_k$ represents the power from external grid/utility to the building;

$(\mathbf{bc}_{L\times 1})_k$ represents the battery capacity and $(\mathbf{bc_0}_{L\times 1})_k$ represents for the battery capacity at time k;

$(\mathbf{pd}_{L\times 1})_k$ represents the battery discharging power vector;

pda_k represents the average discharging power at time *k*, which is

$$pda_k = \frac{(bc_0)_k - disRate \cdot bcmax}{Remaining\ Time} \tag{3-16}$$

disRate is the minimal SOC(%) allowed to reach. In the thesis, $disRate_{min} = 0.2$ and as discussed before when the SOC reaches 20% the BMS will stop discharge. *disRate* will change during the operation time from 40% to 20%. Remaining time means the remaining control horizon time.

$$pdamax_k = \frac{(bc_0)_k - 0.2 \cdot bcmax}{Remaining\ Time} \tag{3-17}$$

So, the other average discharging power $pdamax_k$ is calculated by (3-17) to make sure during the control horizon, battery capacity can be remained at a SOC larger than 20%.

$(\widehat{\mathbf{Pl}}_{L\times 1})_k$ and $(\widehat{\mathbf{Ps}}_{L\times 1})_k$ represent the prediction for the building load and solar generation for time period $k : k+L-1$, where $\widehat{Pl}(1)_k$ and $\widehat{Ps}(1)_k$ is the building load and solar

generation at time k; Δt represents the interval's length which is 5 minutes in the system; $ONE = \begin{bmatrix} 1 \\ \vdots \\ 1 \end{bmatrix}_{L\times 1}$; bc_{min} and bc_{max} is the minimum and maximum capacity of the battery packs, respectively, where $bc_{min} = 100\ kWh$ and $bc_{max} = 450\ kWh$; *onPeakini* is the constant value of the initial On-Peak demand.

Formulas (3-11) to (3-13) represent the battery constraints. Formula (3-11) is the battery discharging process model constraint which has been discussed in Section 3.2.1. Formula (3-12) is the maximum battery discharging power constraint which sometimes can also be considered as the inverter size constraint. In this thesis, $\max_{k=1,..,M}\{pdmax_k, pd_k\} = 100\,\text{kW}$ which is the inverter size for the project, and *pda* is the average discharging power according to the remaining time and remaining battery capacity which can be seen as a tracking profile of future battery information. Formula (3-13) is the battery capacity constraint which always keeps battery capacity within a certain range to achieve the maximum lifetime of battery packs. Formula (3-14) is the power supply constraint that the power provided to the building should be the same as the building's consumption. Formula (3-15) is the demand maintaining constraint; the optimization will always keep the demand below *onPeakini*.

The battery discharging power vector $(\mathbf{pd}_{L\times 1})_k$ can be solved by the above optimization problem. For each k, $\boldsymbol{pd}_k$ is a $L \times 1$ battery discharging power vector for the next L time slots, for which the optimized battery operation should be $\boldsymbol{pd}_k$.

As mentioned above, under RPU's TOU rate schedule, there are three rate periods: Off-Peak, Mid-Peak, On-Peak. The electricity cost in the Off-Peak time is the lowest while in the On-Peak time is the highest. Unlike other works and research in energy management of Microgrid systems, the BESS is charged or discharged depending on the renewable energy generation within each rate period. In this thesis, the control algorithm is designed to always charge the battery bank during Off-Peak time and discharging during On-Peak rate period. During control implementation, the time interval period is chosen to be 5 minutes. The time interval period is chosen based on limitations posed by the net metering system are the quick operation of the battery system and a large variation of power in a very short time cause an imprecise reading of the actual net load. Considering the average solar generation and building load profile in Section 3.2.2, the B1200 needs the largest electricity consumption during On-Peak rate period which is always higher than solar generation in summer. In the winter half of the On-Peak rate periods are during the night time without sunshine. Additionally, the frequent cycling process of charging and discharging harms the Princeton inverter's electronics. During this time, using the extra solar production to supplement the battery is mostly unrealistic.

3.2.4 MPC Model

According to the battery system model, the predictive model of solar generation and building load, and the optimization model of electricity cost, the actual system MPC principles about the system can be built as follows:

i. For each On-Peak rate period in a single day, the time intervals can be divided into *M*, where $M = hour \times 12 + 6$, *hour* is the hours of On-Peak time: in summer, $hour = 6$ (from 12:00 to 18:00) and in winter $hour = 4$ (17:00 to 21:00). The duration for each interval is 5 minutes; within 1 hour, there are 12 intervals. The control algorithm runs 15 minutes before the On-Peak starting time and 15 minutes past the ending point. This will add six more intervals to the On-Peak rate period.

ii. Set time horizon to 1 hour, which is $L = 12$ and fetch the prediction model for solar generation and building load, $\widehat{\mathbf{Ps}}_{(M+L)\times 1}$ and $\widehat{\mathbf{Pl}}_{(M+L)\times 1}$ respectively. Additionally, fetch the electricity price $\mathbf{price}_{(M+L)\times 1}$ and set $disRate = 0.4$.

iii. At initial time, set time interval $i = 0$.

iv. At time *i=k*, fetch real time solar generation Ps_k, building load Pl_k, battery capacity bc_k and battery operation power bp_k of the battery system; additionally, the electricity price $\mathbf{price}(k : k + L - 1)$ needs to be retrieved and the prediction information $(\widehat{\mathbf{Ps}}(k : k + L - 1))_k$ and $(\widehat{\mathbf{Pl}}(k : k + L - 1))_k$ are updated.

v. Calculate the average discharging power and average maximum discharging power from (3-16) and (3-17): $a_k = \frac{bc_k - disRate \cdot bmax}{M-k+1}$; $pdamax_k = \frac{bc_k - 0.2 \cdot bmax}{M-k+1}$ when $pda_k \leq 0, set\ disRate = 0.35(0.3; 0.25; 0.2)$, recalculate pda_k untill $pda_k > 0$. Update *disRate*.

vi. Calculate optimization problem (3-10) with constraints (3-11) to (3-15).

vii. Obtain the result $(\mathbf{pd}_{L\times 1})_k$ and only use the first index of $(\mathbf{pd}_{L\times 1})_k$ to be the battery discharging operation: $\mathbf{p}_{discharge}(i) = (\mathbf{pd}_{L\times 1})_k(1)$

viii. Set $i = k+1$; then go back to step iv until $i = M$.

The prediction horizon should be *L* slots more than the overall control operation horizon because at time $i = M$, the prediction model at this time should be $(\widehat{\mathbf{Ps}}(M : M+L-1))_k$ and $(\widehat{\mathbf{Pl}}(M : M+L-1))_k$ to achieve the final MPC result at this time. At the end, the battery operation can be solved as

$$\mathbf{p}_{discharge} = \begin{bmatrix} (\mathbf{pd}_{L\times 1})_1(1) \\ (\mathbf{pd}_{L\times 1})_2(1) \\ \vdots \\ (\mathbf{pd}_{L\times 1})_M(1) \end{bmatrix} \quad (3\text{-}18)$$

3.3 Constant Threshold MPC (CT-MPC) Algorithm

As previously mentioned, the MPC algorithm will maintain the On-Peak demand to be within a certain range value. In the thesis, the method for keeping a stable On-Peak threshold is called constant threshold MPC (CT-MPC) algorithm.

In the actual system, due to the unpredictable nature of solar generation and building load, there are times when the constraints of the optimization cannot be met. In particular, there are two practical scenarios where this is the case: (1) when the building load is significantly large such that $Pl_k - Ps_k - pda > onPeakini$ and (2) when the solar generation is large enough that $Ps_k > Pl_k$. In both of these two scenarios, optimization from (3-10) to (3-15) cannot give any meaningful results. Therefore, it is required that the basic MPC principles are revised from step vi: to account for scenarios (1) and (2). The revision requires that, instead of calculating the optimization problem, a straightforward operation is implemented, depending on which scenarios is being handled.

For scenario (1), because of the high building load and low solar generation, the action of maintaining the demand below *onPeakini* should be the priority, and $p_{th} = Pl_k - Ps_k - onPeakini$ is calculated. If $p_{th} > pdmax_k$, the need to maintain the battery capacity above 20% SOC over the On-Peak rate period is also considered; so that $\mathbf{p}_{discharge}(k) = pdmax_k$. At this situation, a new On-Peak demand will occur and the new *onPeakini* changes to $onPeakini = Pl_k - Ps_k - pdmax_k$; else $\mathbf{p}_{discharge}(k) = p_{th}$.

For scenario (2), it was first considered that charging for the most part was not allowed during the On-Peak rate time for the actual system. To be more adequate and flexible, the action of allowing charging process to take place is added to the operation of the system: $Ps_k > Pl_k + 10$ and $soc < 90$, $p_{charge} = -(Ps_k - Pl_k - 5)$. In the actual system,

the calculation of battery operation occurs at the starting point of every five minutes; the optimization always occurs at 11:45, 11:50, ……., 18:10 in the summer time and at 16:45, 16:50, ……, 21:10 in the winter time and lasts for 5 minutes. For the charging process, one extreme situation that could happen is when at the starting point of an interval, scenario (2) is satisfied but for the remaining 5 minutes is not. For these cases 10 kW is added to the constraint and 5 kW is subtracted in the charging power. This procedure ensures that the charging process will not jeopardize the On-Peak discharging process.

The detailed procedure of the actual system during On-Peak battery operation is shown as a flowchart in Figure 3-11.

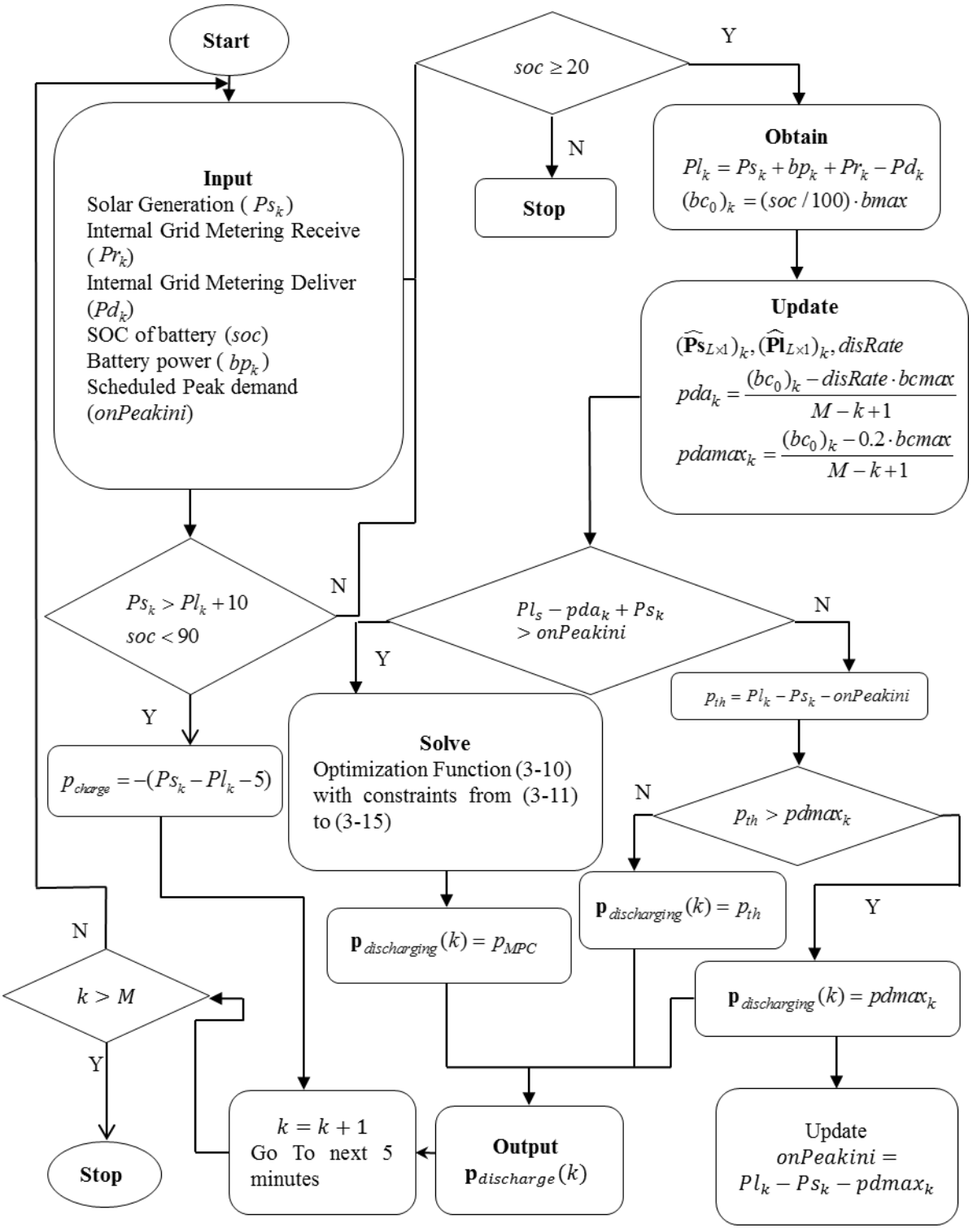

Figure 3-11 CT-MPC Algorithm Flowchart for the Microgrid

3.4 Simulation of CT-MPC Algorithm

In this section, the results from the MATLAB simulation and plots for the CT-MPC algorithm are discussed. All the data for solar generation and building load is based on the real-world measured data of the system stored in SIGI's database for the winter time. Different scenarios about different solar generation and building load forecast are discussed in this section.

3.4.1 Scenario 1: Ideal Forecast for Both Solar Generation and Building Load

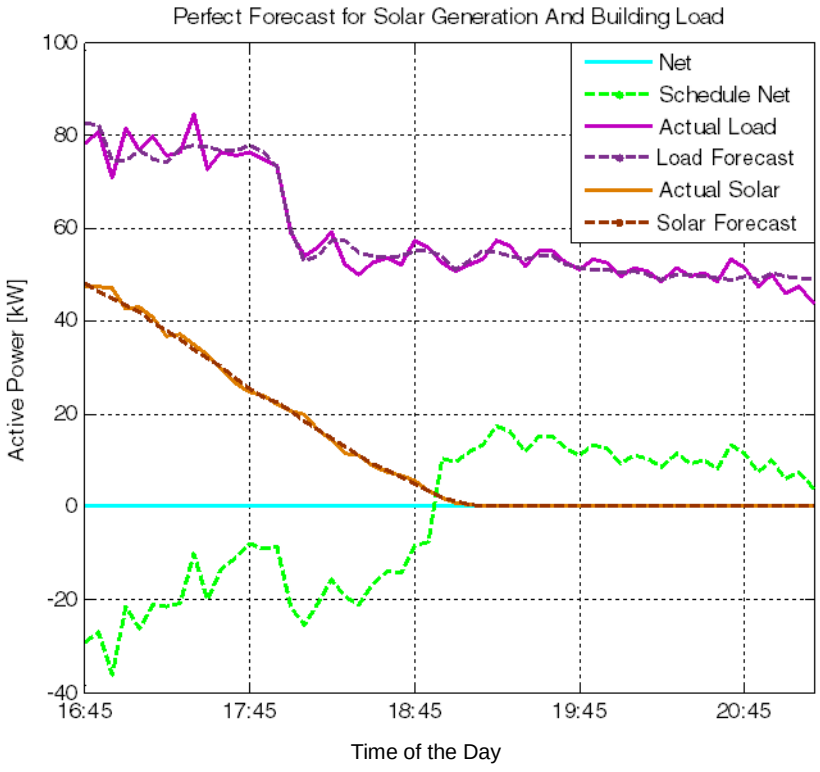

Figure 3-12 Net Load Demonstration in MPC/Schedule Operation Under Ideal Forecast Scenario

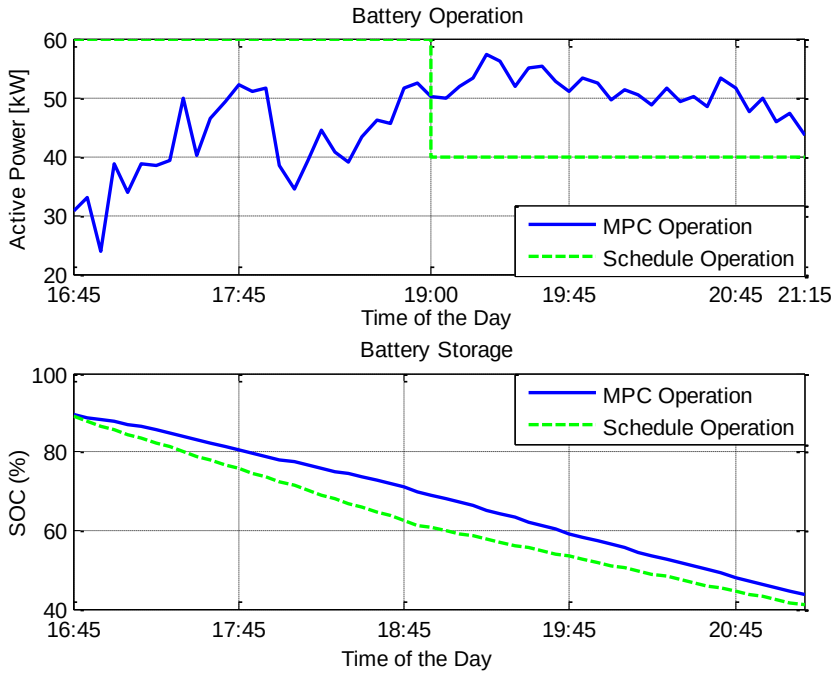

Figure 3-13 Battery Operation and Storage in MPC/Schedule Operation Under Ideal Forecast

Figures 3-12 and 3-13 show the simulation of the net load and battery operation and the SOC of the battery banks under ideal forecast. The ideal forecast can be demonstrated as:

$$\widehat{\mathbf{Pl}} = \mathbf{Pl} \cdot (1 + E_{Pl}\mathbf{R}_{Pl})$$

$$\widehat{\mathbf{Ps}} = \mathbf{Ps} \cdot (1 + E_{Ps}\mathbf{R}_{Ps})$$

$\mathbf{R}_{Pl}, \mathbf{R}_{Ps}$ are random vectors subject to uniform distribution and E_{Pl}, E_{Ps} denote the forecast error percentage of the building load and solar generation prediction. ($E_{Pl} = E_{Ps} = 5\%$), and $onPeakini = 20$ kW. The MPC Operation uses the algorithm discussed in Section 3.3 and the Schedule Operation is based on Table 1. In this scenario, the time horizon is 1 hour; the operation horizon is 4.5 hours; and the prediction horizon is 5.5 hours: $L = 12, M = 12 \times 4 + 6 = 54$.

As shown in Figure 3-12, the deviations are chosen as 5% between actual load and forecast load, actual solar generation and solar generation forecast. The negative net under the Schedule Operation indicates that the power provided by the Microgrid system is larger than the actual power needed by the system. The surplus energy is sent to the external grid under a very low electricity rate. In Figure 3-12, the blue line represents the net load using the MPC algorithm discussed in Section 3.3. Under this control algorithm, MPC operation can keep the energy coming from the external grid close to zero by managing the battery storage and solar generation and is able to keep the maximum net load below *onPeakini*. Because there is no-real-time information collected for the Schedule Control, the battery continuously discharges at a certain power value for the first two hours and the system sends a significant amount energy back to the external grid. In the following two hours, due to a decreasing solar generation the energy from external grid to the Microgrid increases.

Figure 3-13 is the simulated battery performance. From the Battery Operation graph, in MPC Operation, the battery is operated according to the real time building load and solar generation. In the first two hours, because of a higher solar generation the battery is discharged at a relative low level and for the next two hours battery is discharged a little bit higher. The battery storage decreases from 90% SOC to 43.7% under MPC Operation and down to 40.87% SOC under Schedule Operation. From the above two graphs, it is

clear that in Schedule Operation, the efficiency of utilizing the battery is much lower than MPC Operation. Although both of the two operations can maintain the On-Peak demand below *onPeakini* in this scenario, the On-Peak demand under MPC Operation is much smaller than one under Schedule Operation.

3.4.2 Scenario 2: Matched Solar Generation Forecast, Mismatched Building Load Forecast

Figures 3-14 and 3-15 are the simulation for a sunny day. In this scenario, time horizon is 1 hour; operation horizon is 4.5 hours; and prediction horizon is 5.5 hours: $L = 12, M = 12 \times 4 + 6 = 54$. $onPeakini = 20\,\text{kW}$.

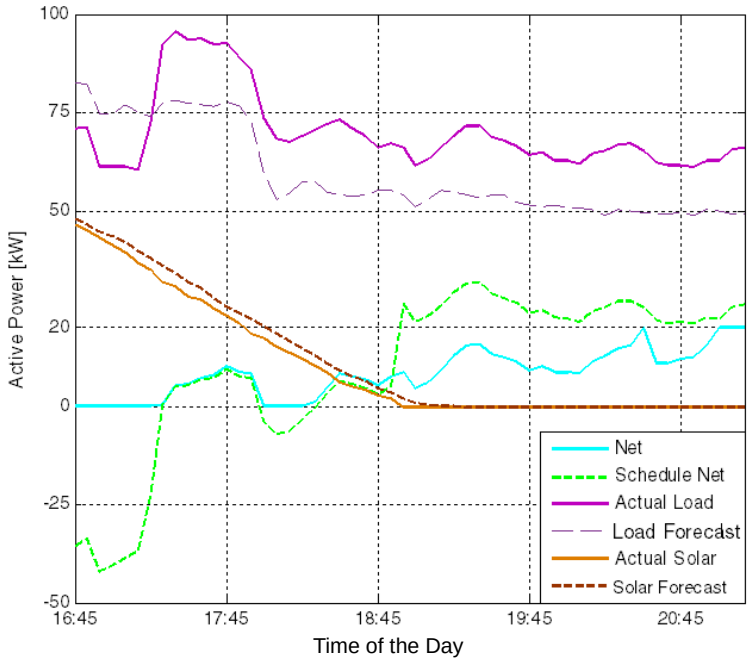

Figure 3-14 Net Load Demonstration in MPC/Schedule Operation Based on the Data of 4/1/15

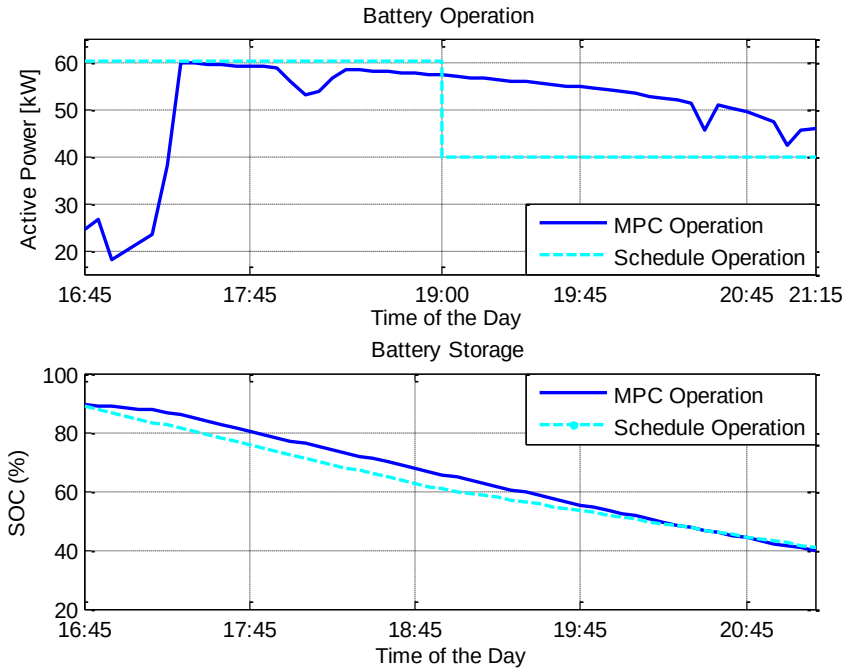

Figure 3-15 Battery Operation and Storage in MPC/Schedule Operation Based on the Data of 4/1/15

Figure 3-14 is a summary of actual and predicted solar generation and building load profiles during On-Peak hours on April 4th 2015. From this graph, the solar generation and building load forecasts are calculated as described in Section 3.2.2. As the figure shows, the actual solar generation during the On-Peak rate period is smaller than the solar forecast. The deviation between these two data sets is small with the actual building load being larger than the forecast load for most time of the period. For this type of situation, the net load under MPC Operation can be maintained below *onPeakini* but under the Schedule Operation, the On-Peak demand can reach up to 31.59 kW.

Figure 3-15 shows the simulation for the battery storage system. Under MPC Operation, the battery packs are discharged based on the real time solar generation,

building load and the remaining battery capacity and eventually go down to 40% SOC. With the help of the battery storage system and CT-MPC control algorithm, the energy consumption and On-Peak demand are all controlled within a satisfactory range.

3.4.3 Scenario 3: Matched Building Load Forecast, Mismatched Solar Generation Forecast

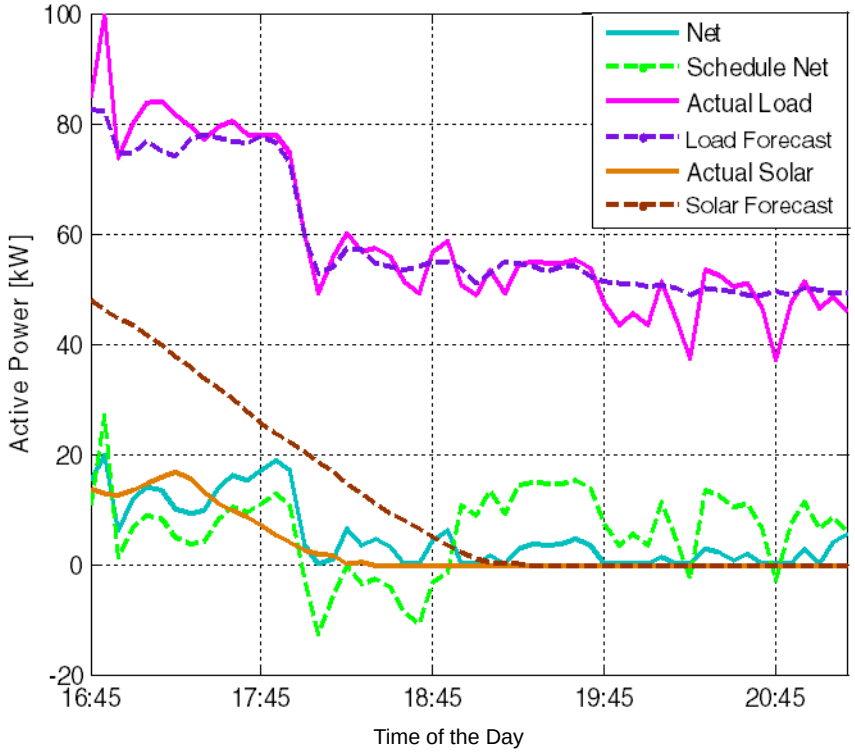

Figure 3-16 Net Load Demonstration in MPC/Schedule Operation Based on the Data of 4/21/15

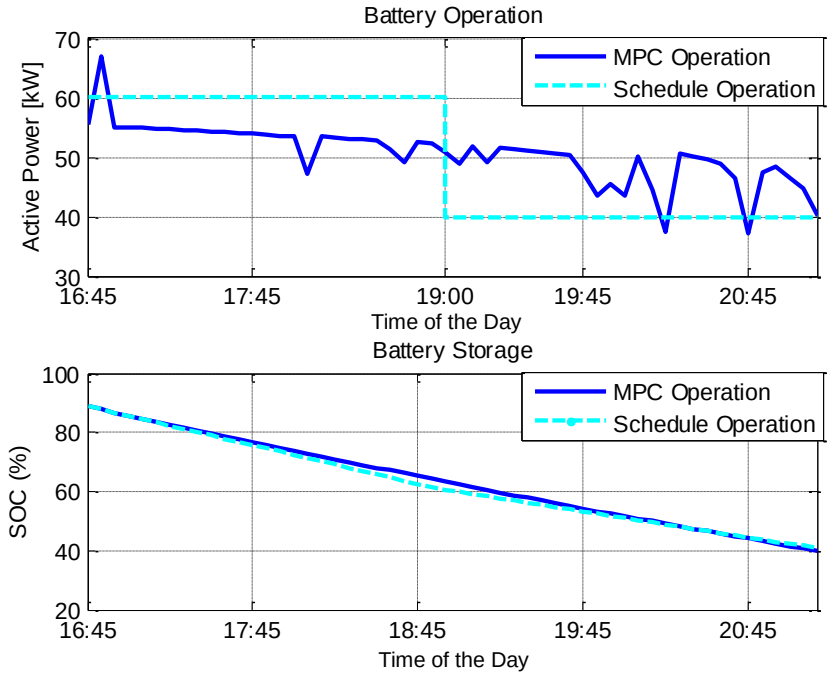

Figure 3-17 Battery Operation and Storage in MPC/Schedule Operation Based on the Data of 4/21/15

Figures 3-16 and 3-17 show the simulation for a cloudy/rainy day in which the solar generation is much smaller than the solar generation forecast. In this scenario, the time horizon is 1 hour; the operation horizon is 4.5 hours; and the prediction horizon is 5.5 hours: $L = 12, M = 12 \times 4 + 6 = 54$; $onPeakini = 20\,\text{kW}$. The prediction profiles for the solar generation and building load are the same as Scenario 2.

In Figure 3-16, the deviation between actual building load and the building load forecast is small, except for the first 10 minutes, and is taken to be a matched forecast for building load for this time period. Additionally the graph shows that the net load under MPC Operation is near zero during the last two hours. Because during the last two hours of this period, there is no solar generation; this scenario can be regarded as Scenario 1

(discussed above). During the first two hours, due to the uncertainty of solar generation, the building energy consumption cannot be maintained at zero. Since the CT-MPC algorithm prediction information is updated at each time slot *k*, the On-Peak demand can still be kept under *onPeakini*. The CT-MPC algorithm retrieves the Microgrid information each time slot and it can react to abnormal situations quickly. So, at about 16:50 a high load occurs, the MPC algorithm determines that a higher battery discharge is needed to let the net decrease while under Schedule Control, without the system real time information, a new On-Peak Demand 26.97 kW is reached.

Figure 3-17 shows the simulation of the BESS information under CT-MPC and Schedule Operation. This figure clearly shows that a higher discharging value takes place at about 16:50, as response to maintain the On-Peak demand lower than *onPeakini*. At the end of the On-Peak rate period, the SOC is maintained in 40% and battery energy is distributed properly within the entire On-Peak rate period under MPC Operation.

3.4.4 Scenario 4: Mismatched Forecast for Both Solar Generation and Building Load

Scenario 4 combines the building load profile in Scenario 2 and the solar generation data in Scenario 3 with the prediction profiles of solar generation and building load. The time horizon and *onPeakini* are the same as of Scenario 2 and 3.

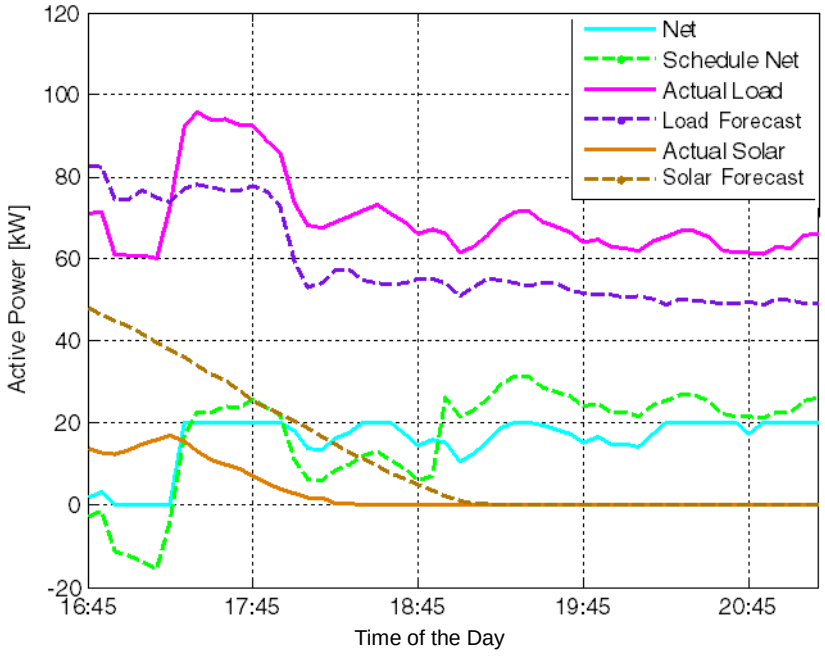

Figure 3-18 Net Load Demonstration in MPC/Schedule Operation Under Mismatched Prediction

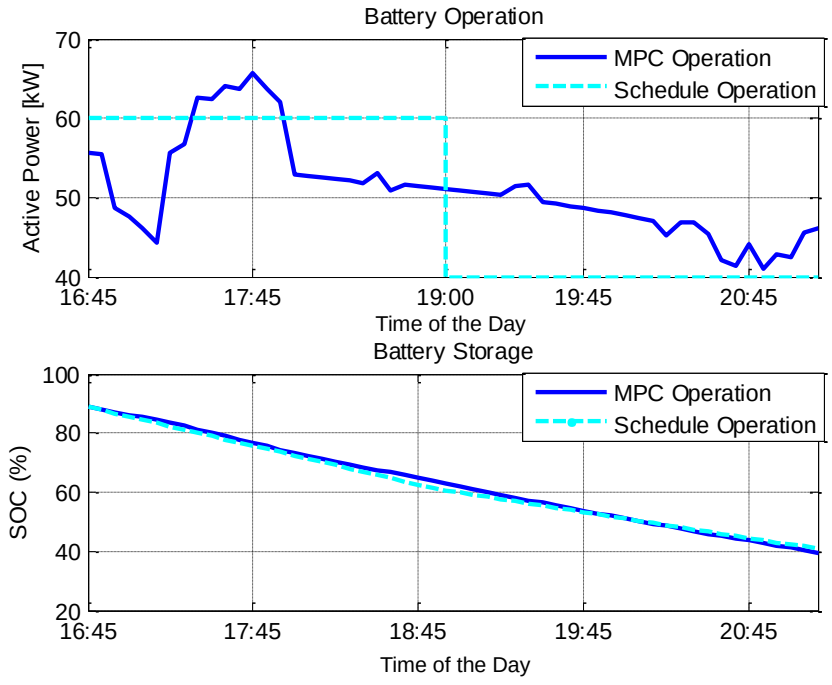

Figure 3-19 Battery Operation and Storage in MPC/Schedule Operation Under Mismatched Prediction

From Figure 3-18, it is clear to see that the difference between the actual data and the prediction data is large and deviates significantly. The On-Peak demand under MPC Operation is still below *onPeakini* but On-Peak demand under Schedule Operation reaches 31.59 kW. The net under MPC Operation is tightly kept near 20 kW during the entire On-Peak rate period, to avoid higher On-Peak demand.

From Figure 3-19, at the end of the On-Peak rate period the SOC decreases to 39.6% under MPC Operation which is still in the controllable battery storage (the safety SOC is 20%). With a higher building load and lower solar generation in winter time, the CT-MPC control algorithm can still work properly to achieve the user's goal of maintaining a low kW demand and kWh electricity usage. It can achieve the highest utilization efficiency of the BESS during the entire On-Peak rate period.

3.5 CT-MPC Control Algorithm Experiments Using the SIGI Microgrid as a Testbed System

To test and demonstrate the effectiveness of the CT-MPC algorithm in controlling the battery energy storage, the CT-MPC control algorithm was ran on B1200 during the months of April and May (2015). During this two-month period, the CT-MPC algorithm was validated, and demonstrated that the BESS is able to maintain an optimized level of energy consumption (kWh) and On-Peak demand (kW) during winter rate period. The graphs below show a variety of experiments carried out over different days, each under a

different set of experimental conditions (scenarios). The actual solar generation and the net load data in these graphs are based on the measured actual experimental values during daily operation of B1200. The time horizon and *onPeakini* are the same as those defined for the simulation scenarios $L = 12$ kW, $M = 12 \times 4 + 6 = 54$ $onPeakini = 20$ kW.

3.5.1 Single Day Experiments Under Different Scenarios

Figures 3-20 to 3-25 are different experiments selected for representing different scenarios. Figures 3-20 and 21, Figures 3-22 and 23, Figures 3-24 and 25 solar generation and building load are in Scenario 1, Scenario 2, and Scenario 3, respectively (as described in the previous sections above).

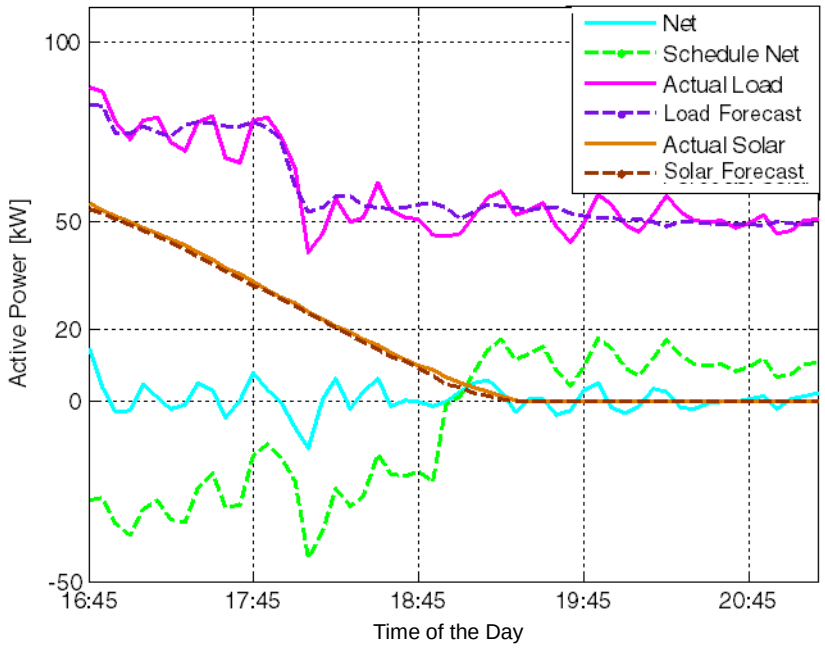

Figure 3-20 Solar Generation and Building Load in Scenario 1 Experiment on 5/14/15

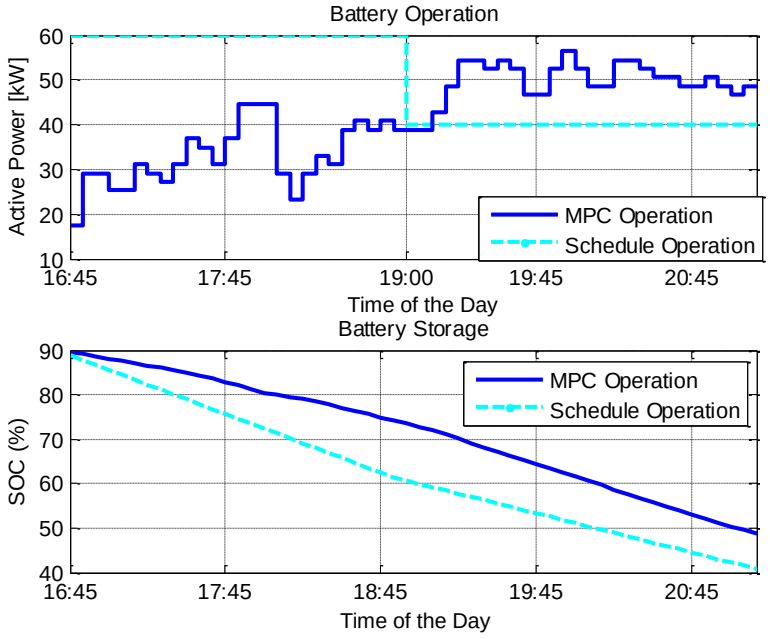

Figure 3-21 Battery Operation and Storage in Scenario 1 Experiment

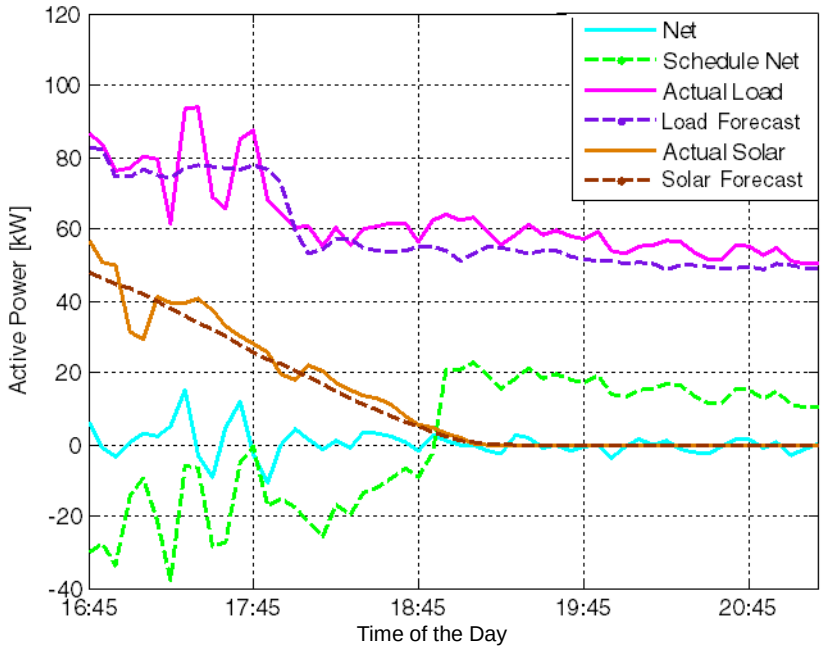

Figure 3-22 Solar Generation and Building Load in Scenario 2 Experiment on 4/29

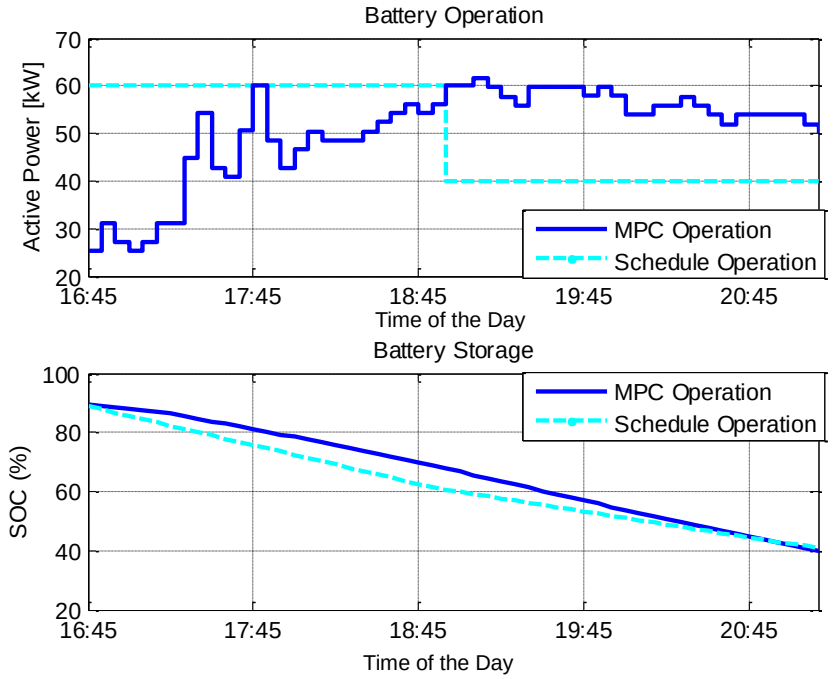

Figure 3-23 Battery Operation and Storage in Scenario 2 Experiment

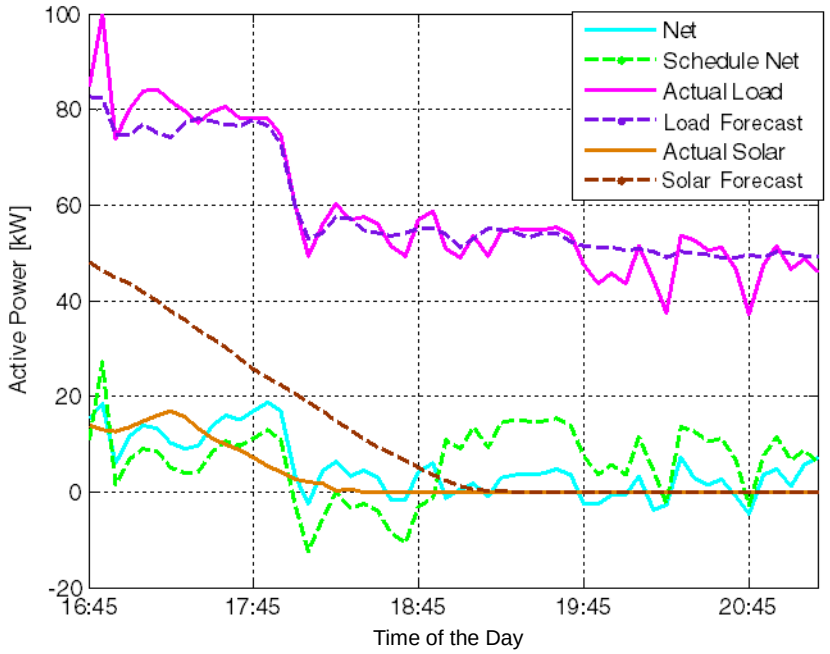

Figure 3-24 Solar Generation and Building Load in Scenario 3 Experiment

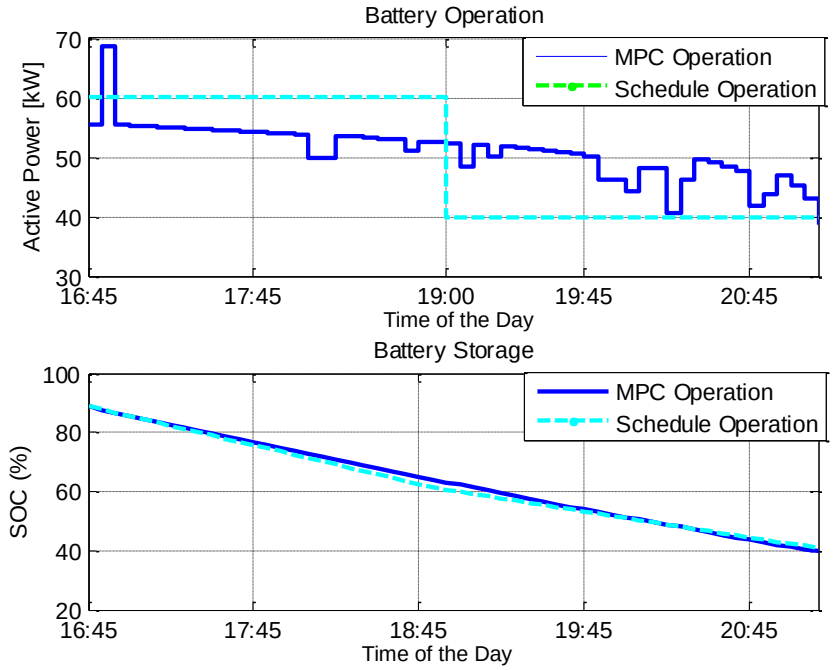

Figure 3-25 Battery Operation and Storage in Scenario 3 Experiment

During the two-month period in which the experiments were performed, it is not possible to have the experimental conditions for testing the CT-MPC control algorithm for Scenario 4.

Compared to the simulation results, the net load under CT-MPC Operation is sometimes below 0 kW. This can be explained by two facts: (1) the CT-MPC algorithm operates at the initial time of every interval and the control operation is kept constant for a 5 minute- intervals; and, (2) the frequency of solar generation collected by the database, is 1 data value per minute, while the frequency of the net metering data is 20 data values per minute. The X-axis unit for Figures 3-20 to 3-25 above is 1 data value per 5 minutes. To handle this difference in data values per minute, different data types from the database

are all processed to 1 data value per 5 minutes by averaging the values. Therefore a negative value for the net load under MPC Operation is possible to occur.

In Figure 3-20, it is clear to see that the net load was tightly controlled below *onPeakini* and most of the time it was around a zero net load value, which shows that no power needs to be supplied from the external grid. Alternately, under Schedule Operation, the net load is always below 0 kW during the first two hours and around 20 kW during the last two hours. Although the Schedule Control can also maintain the On-Peak demand below *onPeakini*, a significant amount of energy produced by the SIGI Microgrid was unnecessarily injected into the external grid. In Figure 3-21, the observed step-like trend of battery operation, is the result of the 5-minute time intervals that kept operation constant at a certain value. At the end of the On-Peak rate period, the remaining SOC under MPC Operation is 48.6%. In Scenario 1, the MPC Operation can maximize the utilization of the battery capacity to achieve the minimum electricity consumption (kWh) and the On-Peak demand (kW).

In Figure 3-22, the actual building load is a little bit higher than the load forecast. The net load under MPC Operation is maintained below *onPeakini* while the On-Peak demand under Schedule Operation reaches a value of 21.4 kW. Similar to the situation show in Figure 3-20, under Schedule Operation the first two hours of operation, the SIGI Microgrid sent all surplus energy to the external grid, but the next two following hours, as

less battery storage capacity was left much more energy was bought from the external grid to meet the Microgrid electricity needs. In Figure 3-23, both of the two operation methods used the same battery storage, but clearly less external energy was used under MPC Operation than Schedule Operation.

In Figures 3-24 and 3-25, due to low solar generation in the first two hours, less energy was sent back to the external grid under Schedule Operation. Because of the lack of real time information about the system high demand can easily occur under Schedule Operation. The demand for Schedule Operation reached 24.6 kW. While under MPC Operation, with the real time solar generation and building load the algorithm can always make the best decision for each time interval. The net load was tightly maintained below *onPeakini* and the energy consumption from the external grid was as small as possible. With the same amount of battery energy capacity used under these two methods, CT-MPC Operation can save much more money than Schedule Operation.

3.5.2 One-Week Long Experiments

Figures 3-26 to 3-29 show the performance of the net load under the CT-MPC control algorithm. The performance is shown over the length of a full-week. In the CT-MPC operation, the prediction method for solar generation and building load is based on the content in Section 3.2.2 and the time horizon for each MPC optimization problem

is 1 hour; the control time horizon is 4.5 hours; and the prediction horizon is 5.5 hours: $L = 12, M = 12 \times 4 + 6 = 54$. The constant On-Peak demand is $onPeakini = 20\,\text{kW}$.

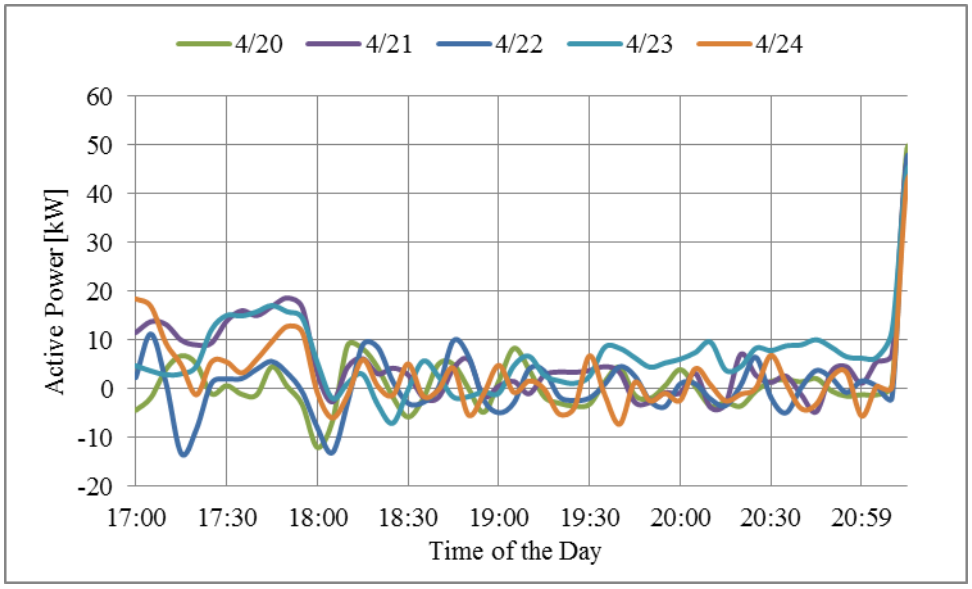

Figure 3-26 April Week 4 Net Load Under MPC Algorithm

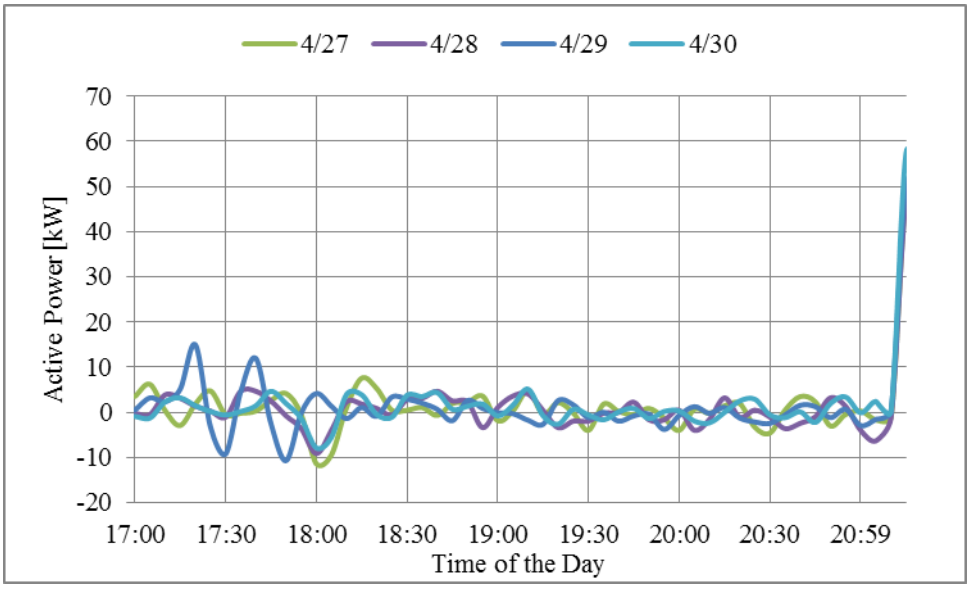

Figure 3-27 April Week 5 Net Load Under MPC Algorithm

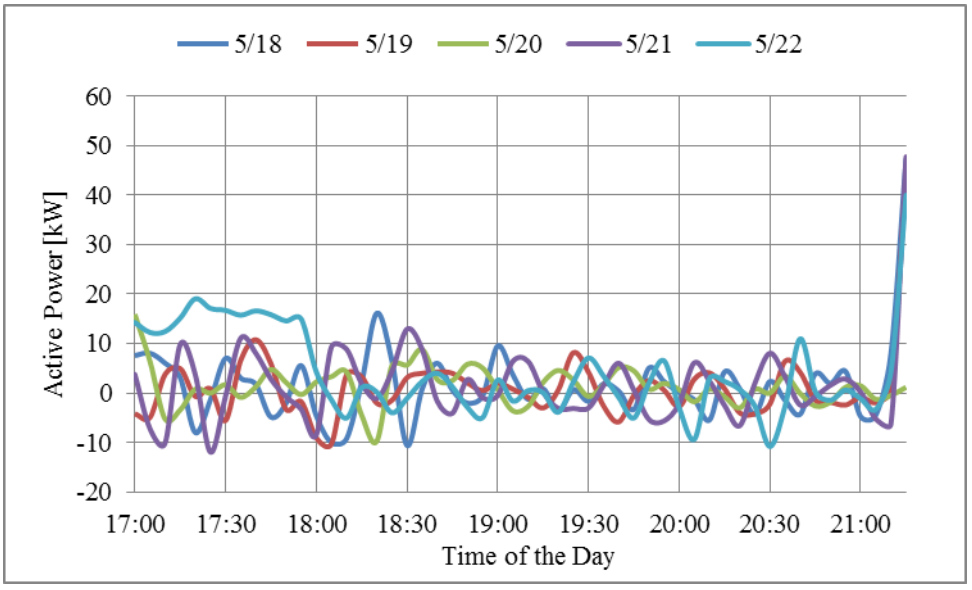

Figure 3-28 May Week 3 Net Load Under MPC Algorithm

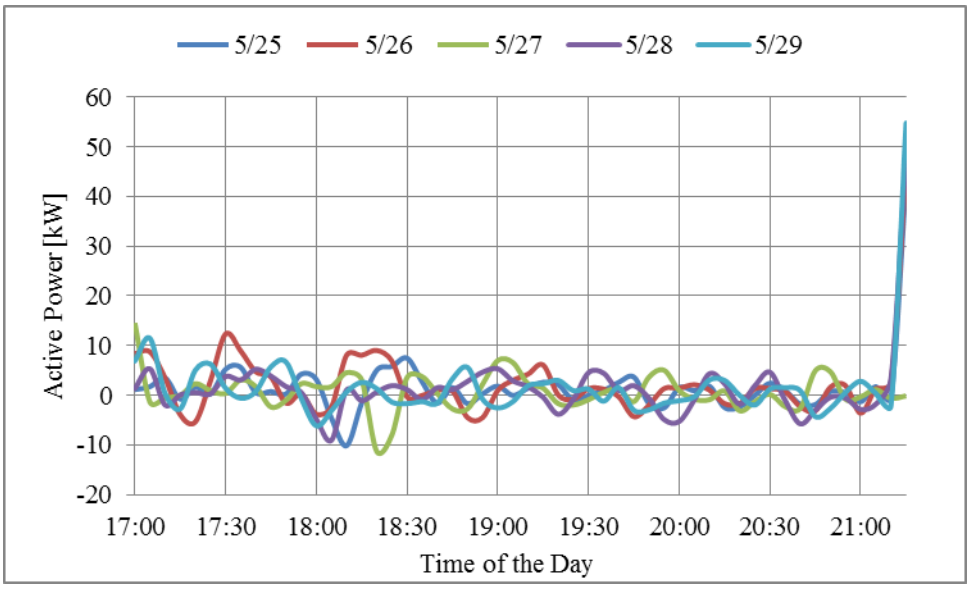

Figure 3-29 May Week 4 Net Load Under MPC Algorithm

The four figures represent four independent weeks of battery operation in April and May. All days shown in the graph are workdays from Monday to Friday and the On-Peak rate period is from 17:00 to 21:00. From Figure 3-26 to Figure 3-29, the net load for these

days was tightly kept below *onPeakini* and most days the net is near zero. At 21:15 each day, battery stopped discharging so the net load increased to a high level. With continuously experiments for different days, it is validated that the MPC control algorithm proposed by the thesis can control the battery system efficiently to maintain certain On-Peak demand and the lowest electricity consumption in winter time.

3.6 Conclusion

After several simulations and experiments, the CT-MPC control algorithm discussed in this chapter can meet the needs of demand load peak shaving (On-Peak electricity money saving). It is clear to see that even if the starting forecast model for solar generation or building load is not accurate the continuous updating of the prediction after each 5-minute time interval, allow the CT-MPC Operation to work in satisfactory manner. The forecast model accuracy will not affect the result of MPC algorithm too much so the simplicity of developing and solving the forecast model decreases.

In the winter time, the characteristics of solar generation and building load are relatively stable for most of the days therefore the forecast model can adjust well. Additionally, there are only 4 hours of the On-Peak rate periods so the 250 kWh battery storage (40% --- 90% SOC) is capable to maintain a relatively low On-Peak demand even with Schedule Operation for most of the days. The CT-MPC algorithm proposed can make the largest efficiency of utilization of battery storage system. While during the

summer tine from June 1st to August 31st, the On-Peak rate period is from 12:00 to 18:00. The overall On-Peak time horizon increases to 6 hours and the uncertainty of the solar generation and the building load becomes much larger than the winter time. So a novel revised ADT-MPC algorithm has been developed and is discussed in Chapter 4.

Chapter 4 Adjusting Demand Threshold MPC Algorithm (ADT - MPC Algorithm)

Since B1200 is a research laboratory building, there are many experiments conducted with unpredictable equipment loads during working hours. During the winter time solar generation gradually decreases through the On-Peak rate periods (5 PM – 9 PM) as the sun sets and eventually goes to zero in the last two hours. The influence of inconsistent solar generation during winter On-Peak rate periods is reduced relative to summer On-Peak rate periods (12 AM – 6 PM) conditions. The forecast horizon of solar generation covers the entire On-Peak rate period in the summer time which clearly increases the uncertainty of the solar generation prediction. In this chapter, the same forecast method as discussed in Section 3.2.2 is used, but the *onPeakini* will not be constant during the On-Peak rate period. The *onPeakini* will adjust to a more appropriate value to compensate for high load or low solar generation conditions.

4.1 The Principles of Adjusting Demand Threshold MPC Algorithm

In the winter CT-MPC algorithm, the prediction horizon for each optimization step is 1 hour due to the On-Peak time solar generation and building load performance having a relatively stable pattern. The algorithm does not require much forecast information. The only future operation constraints are pda_k and $pdmax_k$. The summer time prediction

pattern is not as stable as winter time; the algorithm is more dependent on system forecast information. During the more variable summer On-Peak, the forecast model should contain all the information within the On-Peak rate periods and the forecast horizon increases to 6.5 hours.

According to the basic MPC principles discussed in Section 3.1.2, the prediction horizon extends beyond the actual control horizon. For example, if the control horizon is *M* and operation prediction horizon is *L*, when time interval $i = M$, the forecast window should be from $M+1 : M+L-1$. As *L* increases, the forecast accuracy decreases. Since the control horizon is *M*, it is redundant to take all the prediction till $M+L-1$ into consideration to obtain the best solution for the current time. For example, the *M* + 1 time is beyond the On-Peak rate period, in time interval *i* = *M*, the BMS should only consider the current time system information to get the optimum solution. To consider the whole control horizon, the descending forecast horizon should be included.

In the summer time, from Equation (3-16) $pda_1 = \frac{bmax \cdot (0.9 - 0.4)}{6.5} \approx 38.46$ kW provides an initialization value. The B1200 has the largest summer On-Peak building load. As the CT-MPC algorithm illustrated in Figure 3-9, the worst situation will happen when $Pl_k - pda_k - Ps_k < onPeakini$ is always satisfied and pda_k decreases over time. In this situation the battery capacity should be kept above 40% SOC, resulting in the On-Peak demand threshold increasing to a new level.

The new ADT-MPC algorithm should consider both the descending prediction horizon and the adjusting peak demand. The adjusting demand is based on the change of SOC which is the deviation between actual change and predicted change. In this thesis, it is called tracking ΔSOC.

As discussed before in Chapter 3, at time slot $i = k$, only the first index at each optimization result vector will be used. To implement ΔSOC, the $\Delta \mathbf{pd}_k$ vector is used to record the predicted discharging power at time slot $k + 1$:

$$\Delta \mathbf{pd} = \begin{bmatrix} 0 & \Delta pd^1 & \ldots & \Delta pd^{k-1} \end{bmatrix}^{\mathbf{T}}_{k\times 1}$$

$$\text{which has } \Delta \mathbf{pd}(1) = 0,\ \Delta \mathbf{pd}(2) = \Delta pd^1,\ \cdots \Delta \mathbf{pd}(k) = \Delta pd^{k-1}$$

If the optimization problem (3-10) with constraints from (3-11) to (3-15) can be solved,

$flag = flag + 1$ $flag$ means the continuously successful optimization times

$$\Delta pd(k) = \mathbf{pd}_k(2);$$

$$\mathbf{pd}_{discharging}(k) = \mathbf{pd}_k(1);$$

Else,

$$node = 1;$$
$$flag = 0;$$

$$\mathbf{pd}_{discharge}(k) = Pl_k - Ps_k - onPeak;$$

$$\Delta pd^k = \widehat{\mathbf{Pl}}_k(2) - \widehat{\mathbf{Ps}}_k(2) - onPeak \text{ or } \Delta pd^k = pda_k \text{ or } \Delta pd^k = pdamax_k;$$

$$\Delta SOC(k) = [\mathbf{pd}_k(1) - \Delta \mathrm{pd}^{k-1}] \times \frac{\Delta t}{bmax/100}$$

$$\Delta SOC_k = \sum_{i=t}^{k} \Delta SOC(i) = \begin{bmatrix} 1 & \cdots & 1 \end{bmatrix}_{(k-t+1)\times 1} \cdot (\mathbf{pd}_{discharge}(t:k) - \Delta \mathbf{pd}(t:k)) \times \frac{\Delta t}{bmax/100} \tag{4-1}$$

$$\text{when } (\Delta \mathrm{SOC_k} \leq \varepsilon \;\&\&\; \text{node} == 1) \text{ or } \Delta \mathrm{SOC} \leq -5 \tag{4-2}$$

$$onPeak = \max(\max(pex), onPeakini) - \left[\frac{\Delta SOC/100 \times bmax}{k-t+1}\right] \tag{4-3}$$

The term *pex* in Formula (4-3) refers to the historical net load vector in a month. Under TOU electricity rate demand is charged for one-time peak 15 minute demand during the whole month. When a higher load happens in previous days the best control algorithm should keep other days' net load below the peak load. For example, after three days of operation, $\max(pex)$ should be the peak net load in these three days. Then reset $\Delta SOC = 0$.

The detailed principles are shown as follows:

i. For each On-Peak rate period of a day, time intervals can be divided into *M*, where $M = hour \times 12 + 6$, *hour* is the hours of On-Peak time: in summer, $hour = 6$ which is from 12:00 to 18:00; the time slot for each interval is 5 minutes; within 1 hour, there are 12 time slots. The control algorithm runs 15 minutes before the On-Peak starting point and 15 minutes beyond the actual ending point resulting in 6 more time intervals.

ii. At initial time, set time interval $i=0$. Also get the prediction model for solar generation and building load, $\widehat{\mathbf{Ps}}_{M\times 1}$ and $\widehat{\mathbf{Pl}}_{M\times 1}$ respectively; get electricity price $\mathbf{price}_{M\times 1}$. Set $disRate = 0.4$ $\Delta SOC = 0$ and *onPeak* = *onPeakini*.

iii. At time *i*=*k*, set optimization operation horizon $L_{des} = M - k + 1$. Retrieve real time solar generation Ps_k, building load Pl_k, battery capacity bc_k and battery operation power bp_k of the battery system; and meanwhile get the electricity price $\mathbf{price}(k:M)$ and update prediction information $(\widehat{\mathbf{Ps}}(k:M))_k$ and $(\widehat{\mathbf{Pl}}(k:k+M))_k$.

iv. Calculate the average discharging power from (3-16): $pda_k = \frac{bc_k - disRate \cdot bmax}{M-k+1}$ and maximum average discharging power from (3-17): $pdamax_k = \frac{bc_k - 0.2 \cdot bmax}{M-k+1}$; when $pda_k \le 0, set\ disRate = 0.35(0.3; 0.25; 0.2)$, recalculate pda_k until $pda_k > 0$. If pda_k or $pdamax_k$ is larger than 100 kW, set them equal to 100 kW. Update *disRate*.

v. If solar generation is large enough where $Ps_k > Pl_k$, $\Delta\mathbf{pd}(k) = pda_k$ and $\mathbf{pd}_{discharging}(k) = \begin{cases} Pl_k + 5 - Ps_k \text{ (charging process)}, & Ps_k > Pl_k + 5 \ and \ SOC < 90 \\ 0 \quad , \text{ else} \end{cases}$; else go to next step.

vi. Calculate optimization problem (3-10) with constraints (3-11) to (3-15) and obtain the result $(\mathbf{pd}_{L\times 1})_k$. Now $\mathbf{pd}_{discharge}(k) = \mathbf{pd}_k(1)$ and $\Delta\mathbf{pd}(k) = \mathbf{pd}_k(2)$. Set $flag = flag + 1$. If no result from optimization problem when the constraints cannot be satisfied in this time period, now set $flag = 0;\ node = 1$,

$\mathbf{pd}_{discharge}(k) = \begin{cases} \min(Pl_k - Ps_k - \max(pex), 100), & \Delta SOC \geq 0 \\ \min(Pl_k - Ps_k - onPeak), 100), & \Delta SOC < 0 \end{cases}$ to keep the maximum discharging power less than the inverter size; at this time, also need to check $\mathbf{pd}_{discharge}(k) \geq 0$, if not, $\mathbf{pd}_{discharge}(k) = \begin{cases} 0 & , \quad SOC < 20 \\ Pl_k - Ps_k, & Pl_k - Ps_k < pda \\ pda & , \quad else \end{cases}$.

$\Delta pd_{temp} = \begin{cases} \min(\widehat{\mathbf{Pl}}_k(2) - \widehat{\mathbf{Ps}}_k(2) - onPeak, 100), & \Delta SOC \leq 0 \\ \min(\widehat{\mathbf{Pl}}_k(2) - \widehat{\mathbf{Ps}}_k(2) - \max(pex), 100), & \Delta SOC > 0 \end{cases}$, in these two situations, $\Delta\mathbf{pd}(k) = \begin{cases} pdamax_k & , \mathbf{pd}_{discharge}(k) > pdamax_k \\ pda & , \quad \Delta pd_{temp} > pda \\ \Delta pd_{temp} & , \quad else \end{cases}$; if $\Delta\mathbf{pd}(k) < 0$,set $\Delta\mathbf{pd}(k) = pda$.

vii. Calculate ΔSOC_k by (4-1).

viii. If $flag > 12$, set

$$onPeak = \max(onPeakini, \max(pex)) \tag{4-4}$$

and reset $flag = 0$. This step shows that if MPC can be successfully solved over an hour, On-Peak threshold value should be chosen as the previous maximum net load or *onPeakini*; then the future *onPeak* should be increased upon (4-4) rather than the previous caculated *onPeak* value.

ix. If (4-2) is satisfied, calculate new On-Peak demand threshold by (4-3), record $t = k$ and reset $\Delta SOC = 0$; else go to x.

x. Set $i = k + 1,\ node = 0$; then go back to step iv until $i = M$.

xi. For each new day in the month: check new maximum net load and set $onPeakini = \max(onPeakini, \max(pex))$. Then go back to ii.

4.2 Simulation of ADT - MPC Algorithm Under Different Scenarios

In this section, the influence of different parameters chosen in ADT – MPC algorithm will be discussed. Different values of ε and *onPeakini* in ADT-MPC principles and the algorithm's sensitivity to forecast model is elaborated and simulated in this section.

4.2.1 Scenario 1: Different Actual Building Load or Solar Generation Profile

Simulations under different actual load and solar generation profile are discussed in this section.

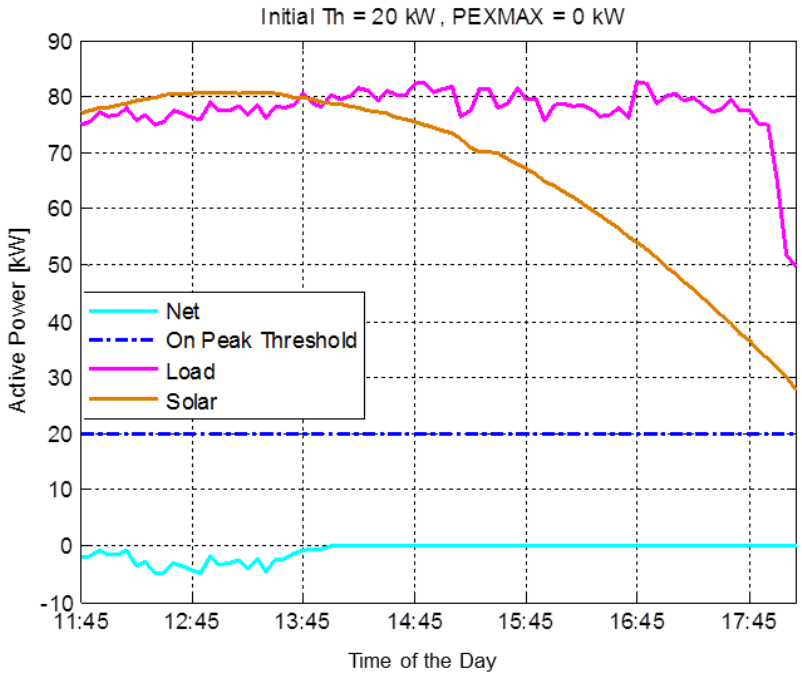

Figure 4-1 Net Load Simulation Under Ideal Forecast

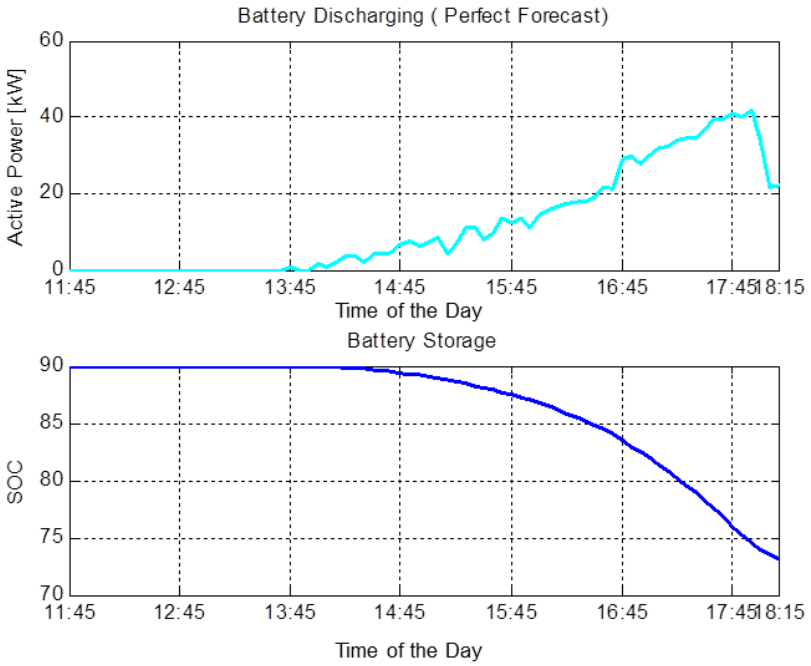

Figure 4-2 Battery Operation and Storage Simulation Under Ideal Forecast

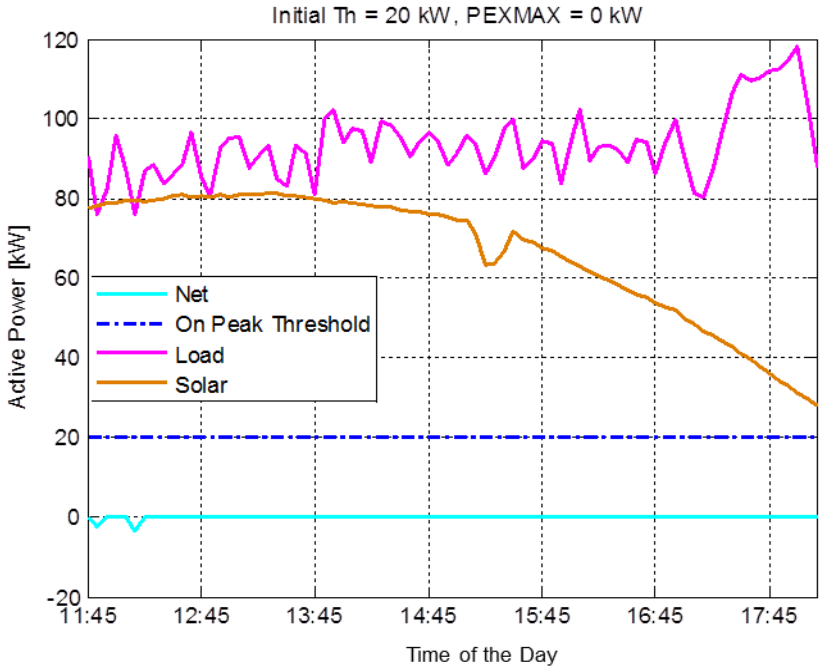

Figure 4-3 Net Load Simulation Under Normal Days

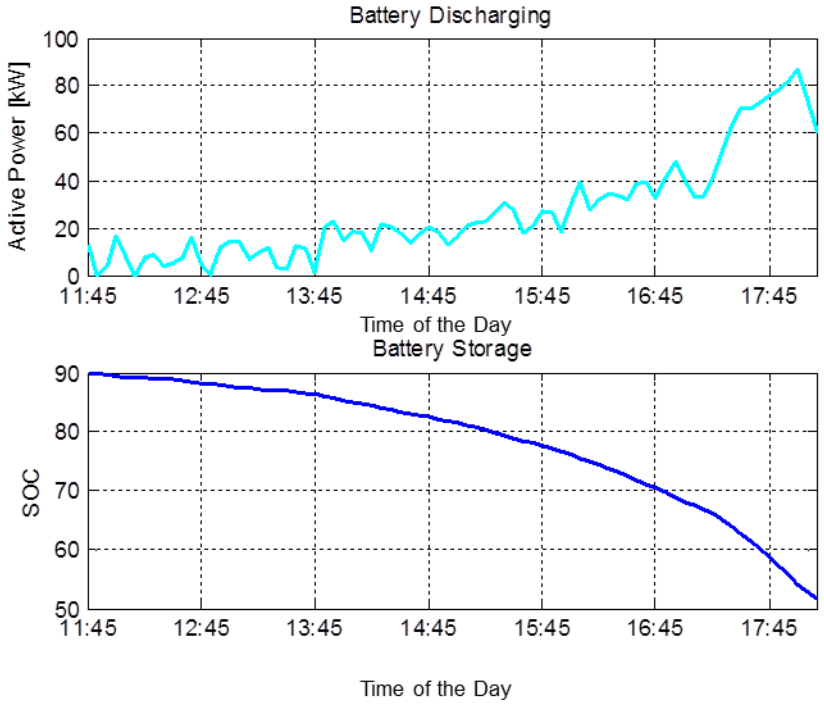

Figure 4-4 Battery Operation and Storage Simulation Under Normal Days

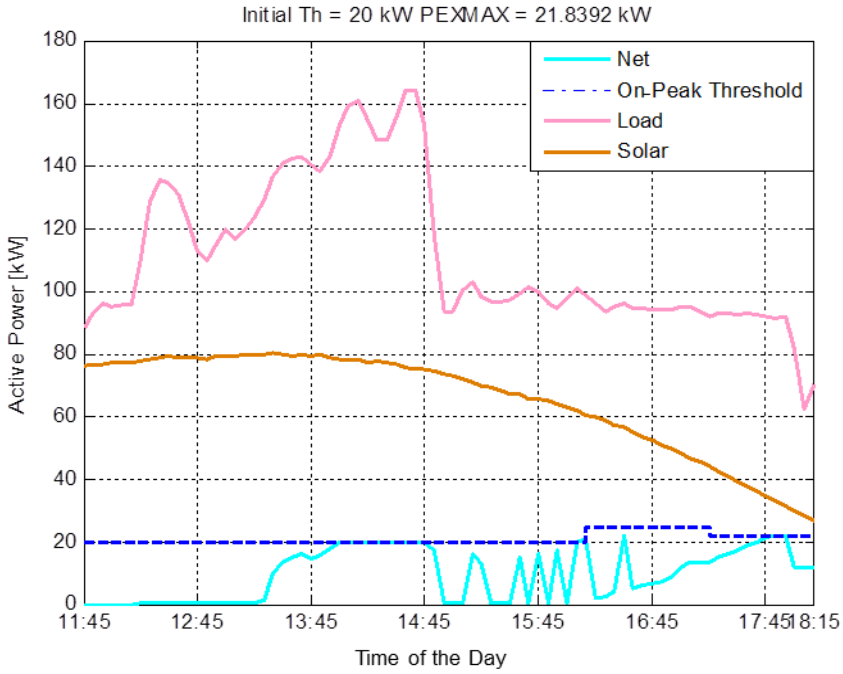

Figure 4-5 Net Load Simulation Under Period High Load

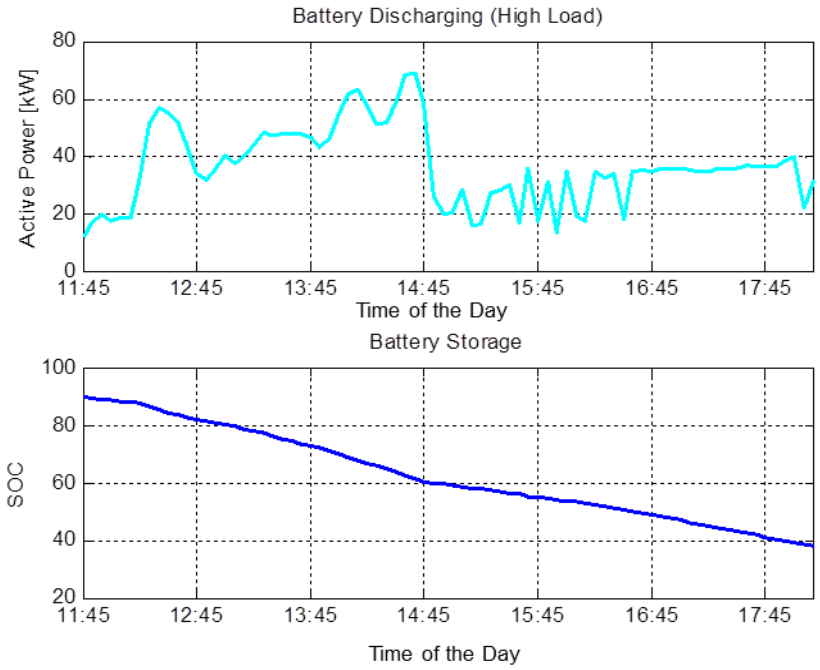

Figure 4-6 Battery Operation and Storage Simulation Under Period High Load

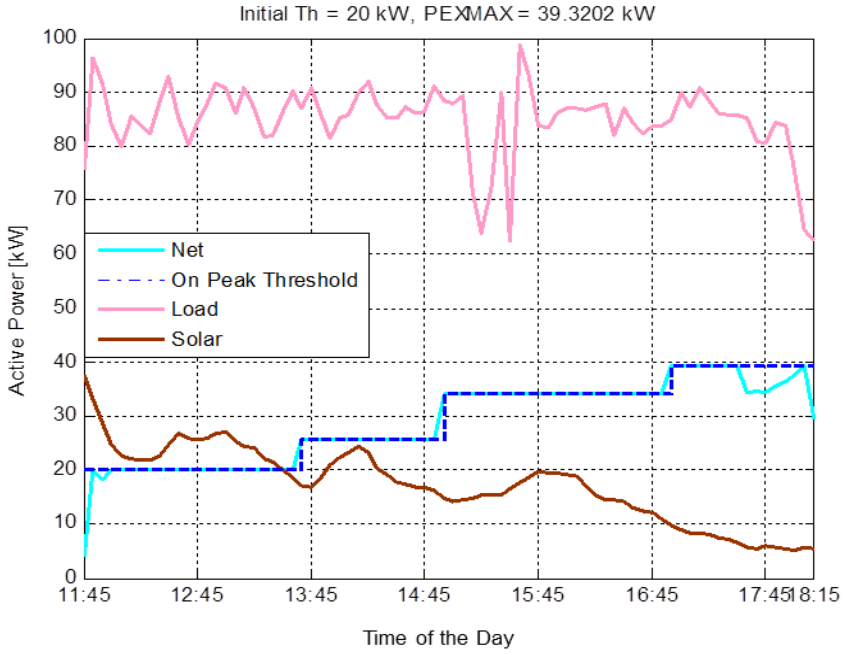

Figure 4-7 Net Load Simulation Under Cloudy Day

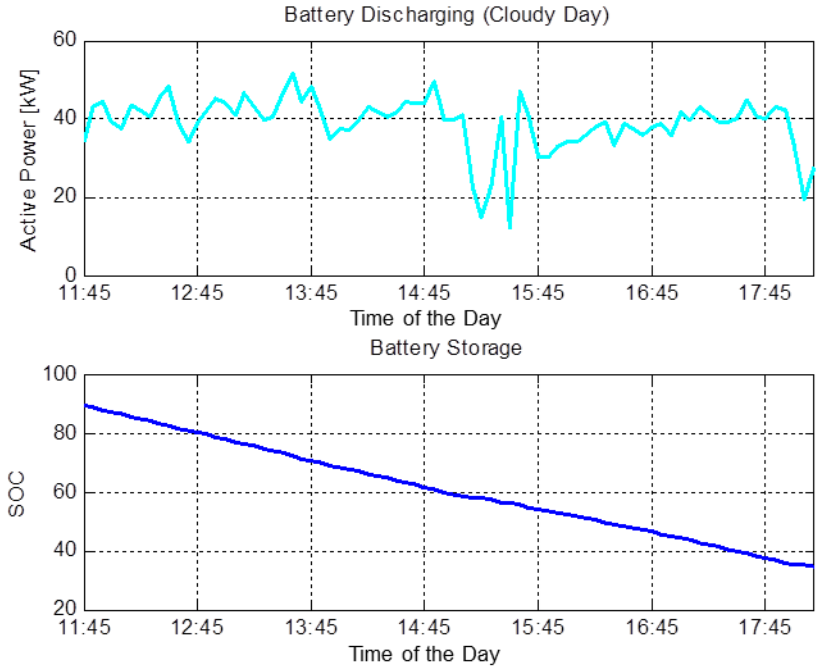

Figure 4-8 Battery Operation and Storage Simulation Under Cloudy Day

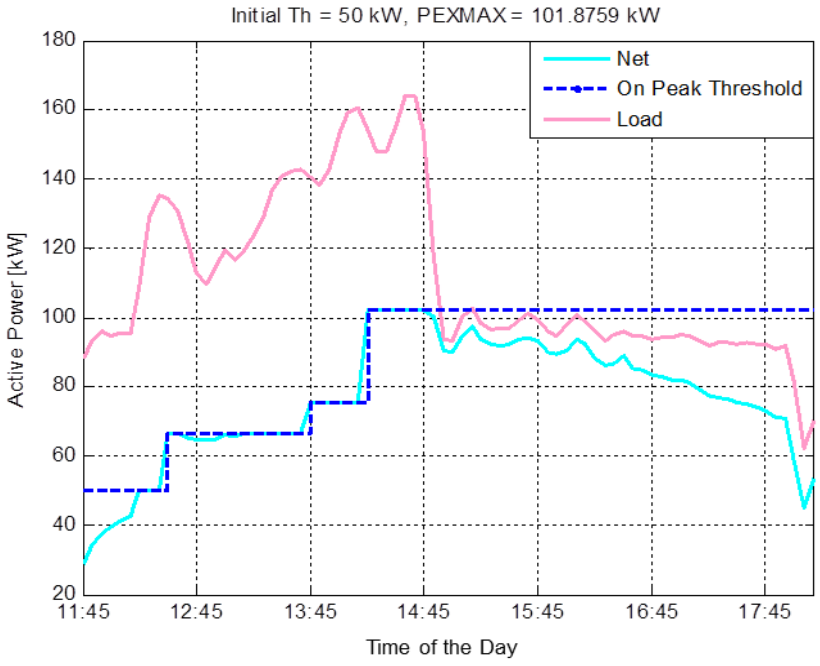

Figure 4-9 Net Load Simulation Under Period High Load W/O Solar Generation

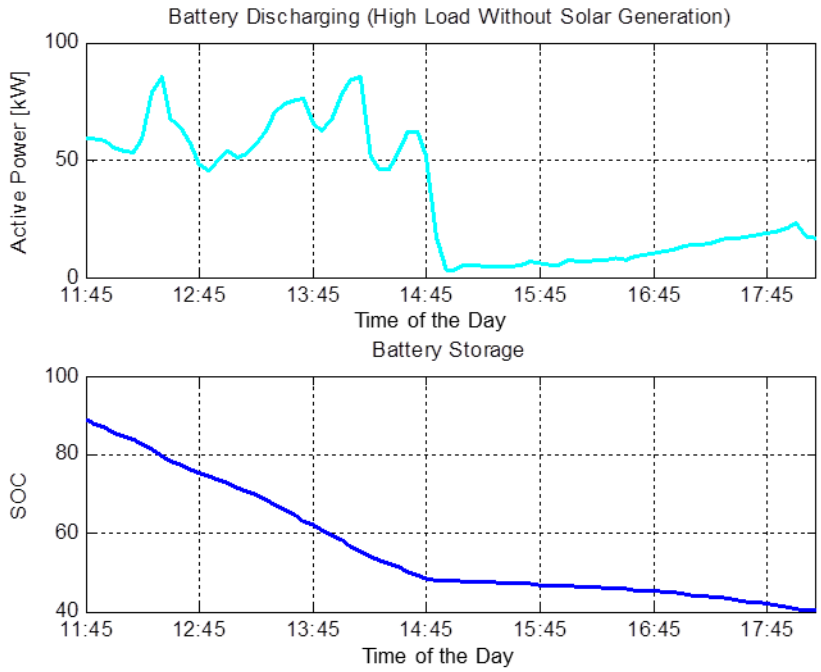

Figure 4-10 Battery Operation and Storage Simulation Under High Load W/O Solar Generation

The prediction models use the profiles of solar generation and building load shown in Figure 4-1. The ε in Formula (4-2) is equal to -2 and $onPeakini = 20\,\text{kW}$. The Figures from 4-1 to 4-10 are the simulations for different loads or solar generation conditions. In Figures 4-1 and 4-2, the prediction model is chosen by the actual building load and solar generation profile. Under an ideal forecast prediction situation as in Figure 4-1, the net load can be maintained at zero net. During the first two hours, solar generation is always larger than the building load. So in these two hours $\Delta SOC > 0$ and net is negative. In the next 4 hours because of the remaining battery capacity, when solar generation is decreasing the net load can be minimized. During the entire rate period, the threshold stays at *onPeakini*, resulting from the sufficient solar generation. From Figure

4-2, it is clear to see the discharging power (active power) increasing with decreasing solar generation. Because of sufficient solar generation on this typical summer day, there is excess battery capacity remaining and this capacity can be used during the Mid-Peak rate period.

Figures 4-3 and 4-4 show simulations based on a normal day operation in B1200. The solar generation and load data is from the actual data on 6/17/15. In summer time, there is sufficient solar generation during most days of the month in Southern California. In a day the solar generation is sometimes affected by clouds. So in Figure 4-3， there is a decrease of solar generation between 14:45 and 15:45. The load profile of this day behaves randomly (increasing and decreasing throughout), but the building load is maintained at about 90 kW during most of the On-Peak rate period. From the load prediction graph in Figure 4-1, the building load on this day is higher than the prediction load profile. This is a common situation in real world experiments. The simulated net load in this situation can still be maintained near zero so the energy consumption from external grid is zero during the On-Peak rate period. In Figure 4-4 the battery is discharged according to the actual load and solar information. Due to the sufficient solar generation during this day, there is more than 10% SOC left for the Mid-Peak rate period. The demand threshold does not change in this situation.

Figures 4-5 and 4-6 show another real world load profile. The data is based on 7/15/15 for B1200. In Figure 4-5, there is a very large building load around 12:45 AM that lasts for about 2 hours. This figure shows another common situation in an actual building where very high loads happen intermittently, and are very difficult to predict. In this condition, the simulated net goes up till near the threshold value and cannot be maintained near 0. There are two changes of the demand threshold: first occurs at $i = 53$ and the time is 16:15, and the second is at $i = 66$ at 17:15. When $i = 53$, the constraints of the optimization problem cannot be met and $node = 1,\ \Delta SOC_{i=53} = -3.88$. And based on Formula (4-3), *onPeak* increases to $onPeak = 20 - \frac{\Delta SOC_{53} \cdot 5}{(53-0) \cdot \Delta t} \approx 24.39$ kW. When $i = 66$, $flag > 12$ is met so *onPeak* is changed based on Formula (4-4). Since the previous maximum net load was 21.84 kW, $onPeak = 21.84$ kW is the updated value used for the new On-Peak threshold. From Figure 4-6, the battery is discharged at a much higher rate during the high load time and the SOC goes down to 37.97%. From these two graphs, it is clear to see that without a BESS, the peak demand for this day could reach 82.63 kW. With the help of the BESS the peak demand is decreased by 60.79kW.

Figures 4-7 and 4-8 are generated under a cloudy weather condition. The solar and building load data for these two graphs are from 6/9/15. The solar generation during this day is very low but the building load is at a high level compared to the forecast load profile in Figure 4-1. In this condition, the battery should provide more energy to

maintain a low On-Peak demand value. From Figure 4-7, the On-Peak threshold increases sequentially three times, from 20 kW to 39.32 kW at $i = 23,\ i = 38,\ i = 62$. These increases are due to insufficient results from the optimization problem:

when $i = 23,\ \Delta\mathrm{SOC}_i = -2.15$, $onPeak = 20 - \dfrac{\Delta SOC_{23} \cdot 5}{(23-0)\cdot \Delta t} \approx 25.6\ \mathrm{kW}$;

when $i = 38,\ \Delta SOC_i = -2.1$, $onPeak = 25.6 - \dfrac{\Delta SOC_{23} \cdot 5}{(38-23)\cdot \Delta t} \approx 34\ \mathrm{kW}$;

when $i = 62,\ \Delta SOC = -2.13$, $onPeak = 34 - \dfrac{\Delta SOC_{23} \cdot 5}{(62-38)\cdot \Delta t} \approx 39.32\ \mathrm{kW}$.

In Figure 4-8, the battery is discharged to 34.44% SOC which is still within the safety 20% SOC. Without the BESS, the maximum net load would have reached an On-Peak demand value of 82.44 kW. With the help of the BESS contribution, the demand is decreased by 43.12 kW.

Figures 4-9 and 4-10 show a simulation of a system with no PV generation. The building load in Figure 4-9 is the same as Figure 4-5, which is much larger than the prediction model. Under this scenario, all the energy saving operation available should be deployed by the battery storage system. In Figure 4-9, the initial On-Peak threshold was chosen at 50 kW. Three adjustments create a final threshold of 101.88 kW. From Figure 4-10, it can be seen that the battery is discharged at a higher rate during the high load time period and the rate is reduced as the load decreases in the last three hours. The peak

net load occurs between 13:45 to 14:45; after the peak net load the algorithm reduces the discharging rate (battery power) to steadily maintain the SOC within 40%.

4.2.2 Scenario 2: Different Choice of ε

From the constraint (4-2) ε is a key factor for the time and range of the deviation to change *onPeak*. In this section, the influence of the parameter ε to *onPeak* will be fully discussed.

The solar generation and building load profiles are based on actual data from 6/9/15 which is also shown in Figure 4-7. It is a cloudy day and as expected solar generation is much lower than in sunny days. The prediction profiles are the same as Scenario 1 with $onPeakini = 30\,\text{kW}$.

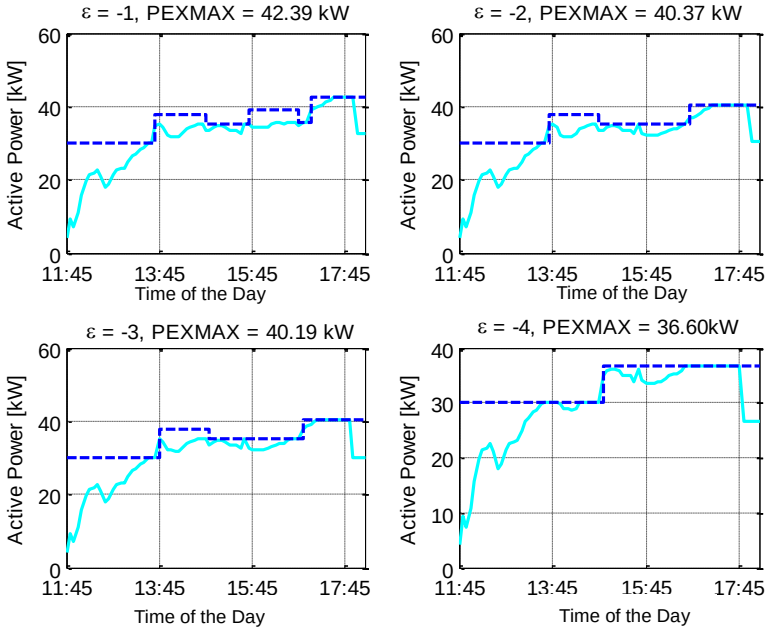

Figure 4-11 Net Load and Threshold Comparison Between Different ε

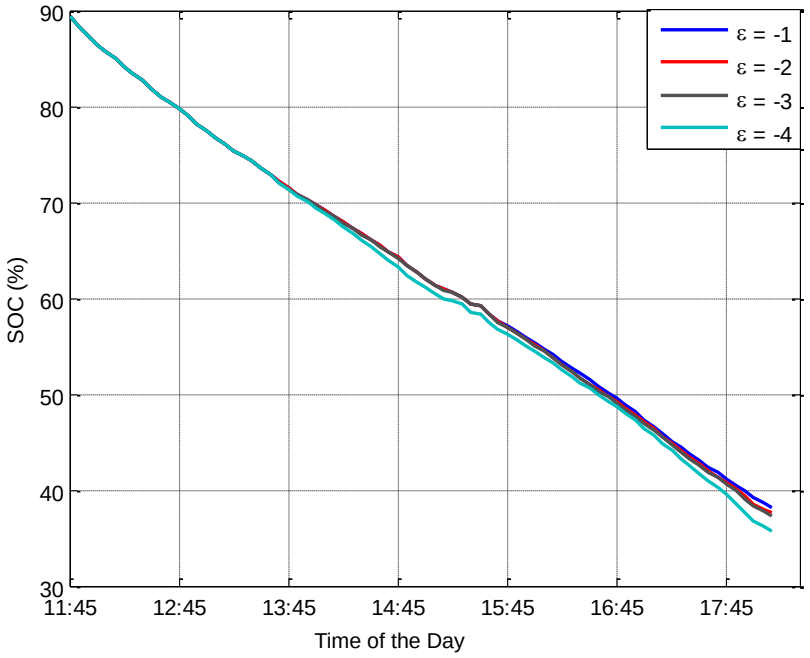

Figure 4-12 Remaining SOC Comparison Between Different ε

Figure 4-11 compares simulated net load and threshold between different ΔSOC. In these four graphs peak net demand is reduced by more than 40 kW when comparing to a non-battery storage system with the On-Peak demand of 82.44 kW. From these four graphs it is clear to see smaller $|\varepsilon|$ responds more rapidly to change of $onPeak$. If $|\varepsilon|$ is smaller, the algorithm reacts to system dynamics changes more quickly and vice versa. A shorter response time, caused by a small value of $|\varepsilon|$, influences the accuracy of adjusting threshold. Meanwhile a large $|\varepsilon|$ value increases the time to adjust to a new threshold which uses more battery capacity to maintain the previous low load. In Figure 4-12 the SOC left by $\varepsilon = -4$ is the lowest, among the four specified values, and $\varepsilon = -1$ is the highest. While $\varepsilon = -2$ or -3, yield similar results in the simulation. There is no

simulation for $|\varepsilon| \geq 5$ because from Formula (4-3) the threshold changes once it reaches $\Delta SOC_k \leq -5$. The net demand under the four conditions is increasing as $|\varepsilon|$ decreases. So the tradeoff is between the system's sensitivity and battery storage.

4.2.3 Scenario 3: Different Choice of Initial Threshold *onPeakini*

The other key factor of how and when to change *onPeak* is the initial demand value *onPeakini*. In this section, different *onPeakini* will be chosen to simulate its effect, while maintaining in solar generation and building load profiles the same. The influence of the parameter *onPeakini* on *onPeak* is fully discussed in this section.

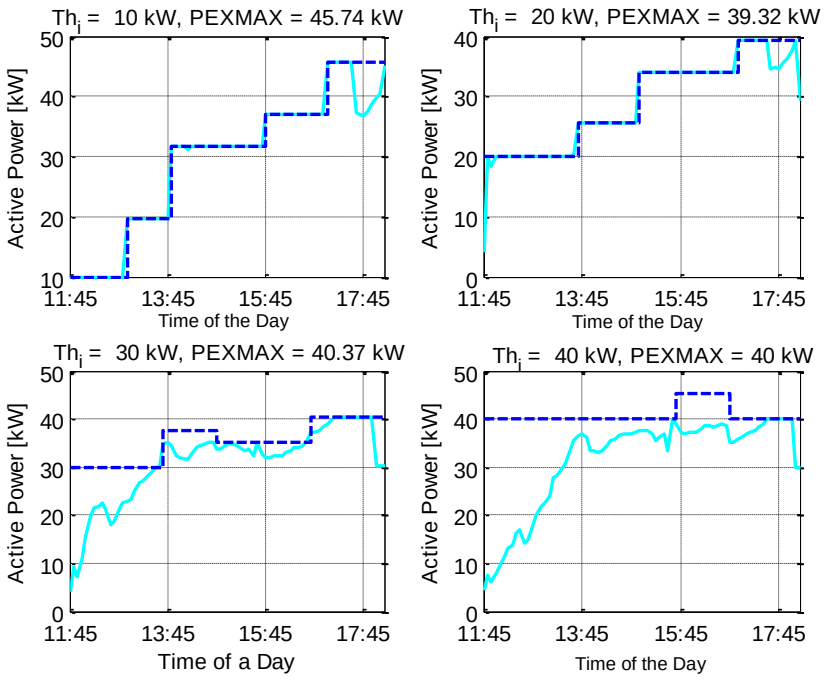

Figure 4-13 Net Load and Threshold Comparison Between Different Initial Thresholds

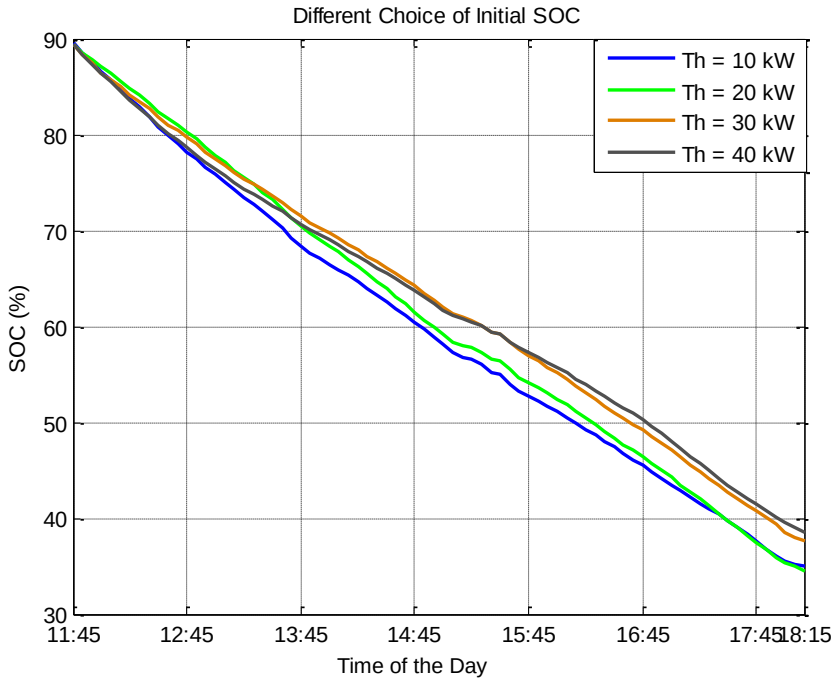

Figure 4-14 Remaining SOC Comparison Between Different Initial Thresholds

The actual solar generation and building load profiles are the same as in Figure 4-7, and the prediction profiles are the same as Scenario 1 with $\varepsilon = -2$. In Figure 4-13, the solid line represents the simulated net load and the dashed line represents the adjusting threshold trend. The On-Peak thresholds in Figures 4-13 increase from 10 kW to 40 kW. An initial threshold $Th_i = 10$ kW combined with low solar generation causes the threshold to rise quickly in the first few hours and eventually reaches 45.74 kW. When $Th_i = 10$ kW the net load is kept within the On-Peak threshold instead of zero net load due to the limited solar generation of the day. When $Th_i = 20$ kW, the threshold adjusts 1 hour later than when $Th_i = 10$ kW and eventually adjusts to 39.32 kW. When $Th_i = 30$

kW the threshold adjusts three times during the rate period and eventually adjusts to 40.37 kW. The first increase of the threshold line is caused by constraint (4-2) and the second decrease is by the constraint of (4-3) and the last is also caused by constraint (4-2). The net load is tightly maintained near the threshold. The fourth graph shows that when $Th_i = 40$ kW the net load can be maintained below 40 kW. Only one adjustment of threshold occurs before 15:45, and then re-adjusts to a new threshold according to Formula (4-3). The threshold for $Th_i = 40$ is maintained at 40 kW.

In Figure 4-14, when $Th_i = 10$ kW and $Th_i = 20$ kW in both the remaining battery capacity decreased to nearly the same values and the largest battery capacity is used. When $Th_i = 40$ kW the least battery capacity is used. All of scenarios are maintained the remaining capacity above 20% SOC. Compared to a system without a battery storage system, the net demand of On-Peak rate period decreases to about 40 kW from 82.44kW.

With the comparison of different initial thresholds the final threshold can always be adjusted to an optimum value. If the initial threshold is too small for a system the adjustment operates quickly but the battery storage will be used more due to the small initial threshold. If the initial threshold is chosen properly from the start, the system will behave better with less adjustments during one cycle. The experiments above shows that although different Th_i were selected all achieve the goals of cost saving and maintaining SOC over 20%.

From Section 4.2.2 and 4.2.3, both ε and Th_i will affect the threshold adjustment during the time period resulting in small variations to SOC. Therefore, even in a system without comprehensive information about renewable energy generation and building load profile, or a system with unpredictable and uncommon situation for loads or energy generation, the adjustment of On-Peak threshold can always maintain the relatively minimal energy consumption and net demand. In this thesis, the proper choice for $Th_i = 30\,\text{kW}$, $\varepsilon = -2$ and they are used in week-long simulations.

4.2.4 Weekly Simulations

In this section, the ADT-MPC will be implemented under different scenarios of actual solar generation and building load profiles.

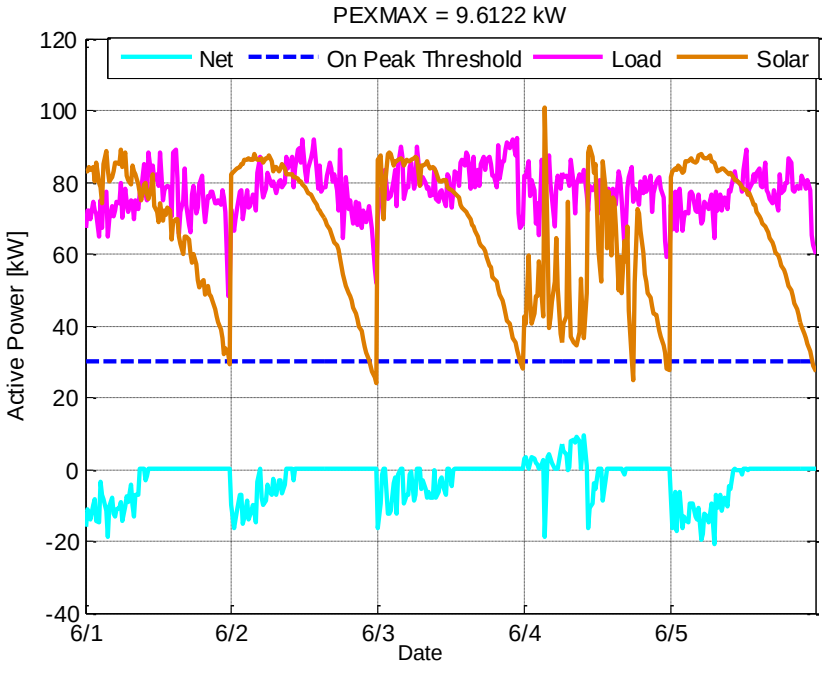

Figure 4-15 Net Load and Threshold Adjustment Under ADT - MPC Algorithm in Week 1 of June

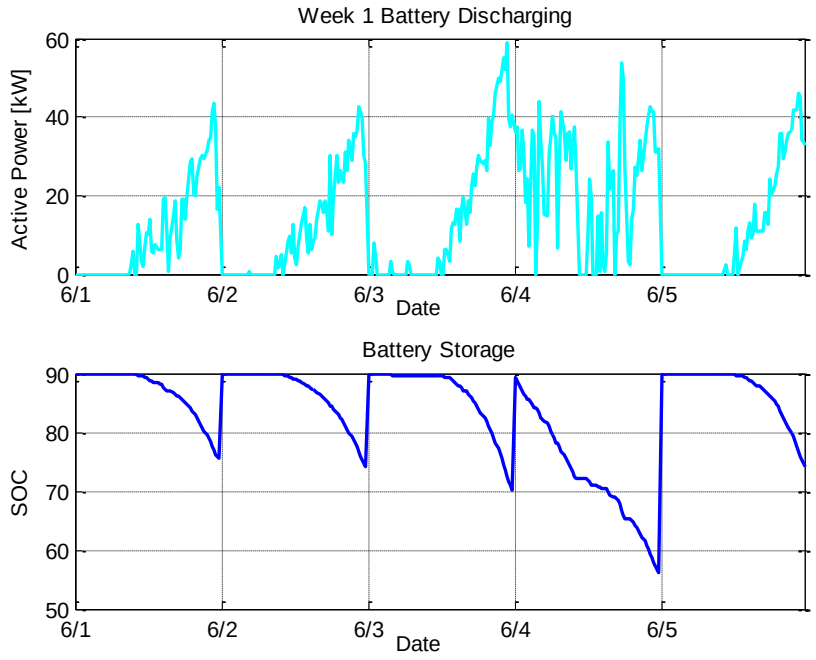

Figure 4-16 Battery Operation and Storage Under ADT - MPC Algorithm in Week 1 of June

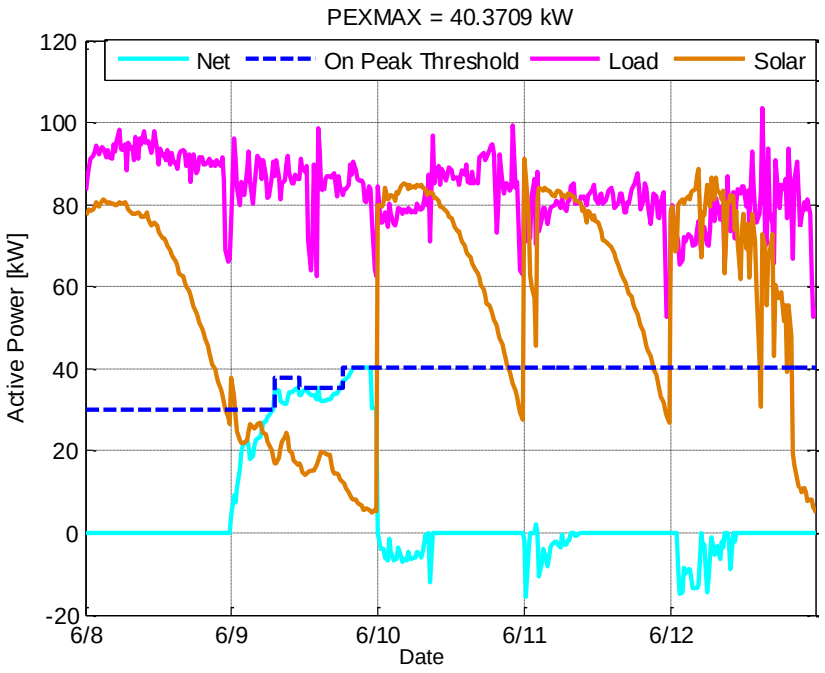

Figure 4-17 Net Load and Threshold Adjustment Under ADT - MPC Algorithm in Week 2 of June

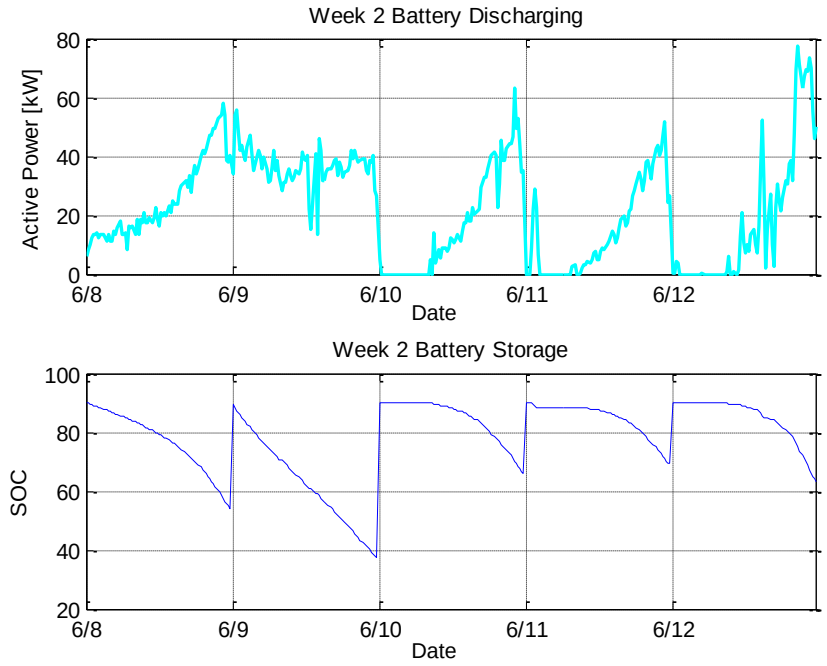

Figure 4-18 Battery Operation and Storage Under ADT - MPC Algorithm in Week 2 of June

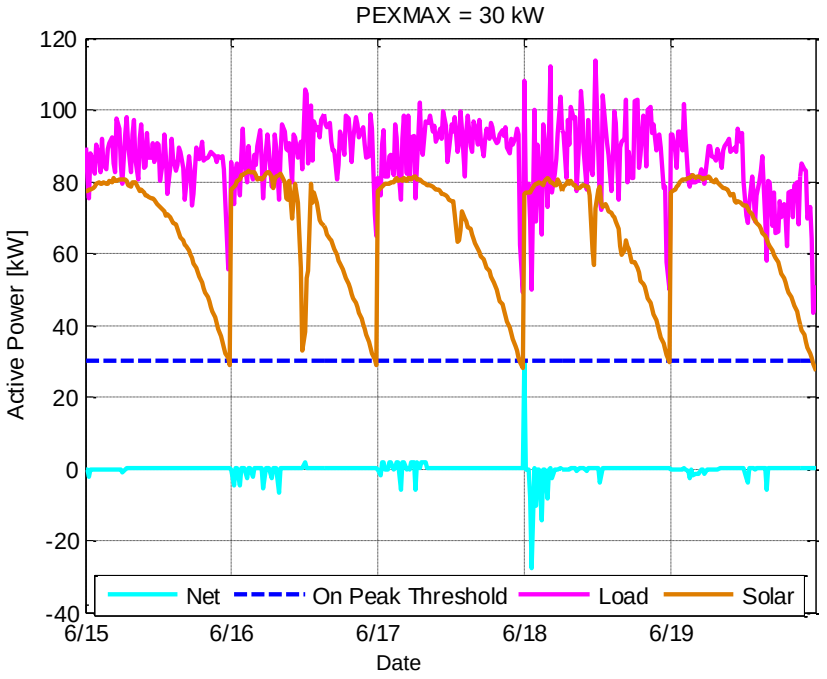

Figure 4-19 Net Load and Threshold Adjustment Under ADT - MPC Algorithm in Week 3 of June

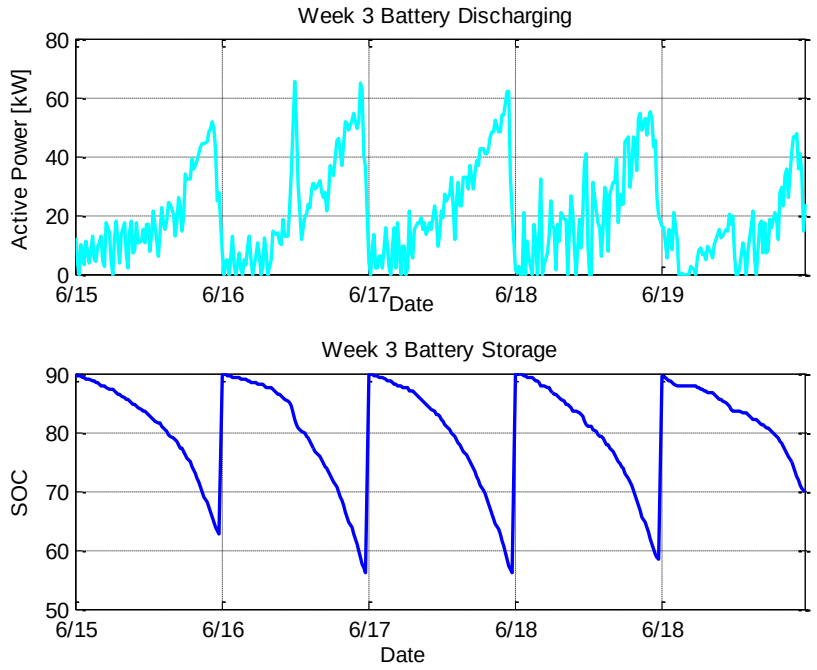

Figure 4-20 Battery Operation and Storage Under ADT - MPC Algorithm in Week 3 of June

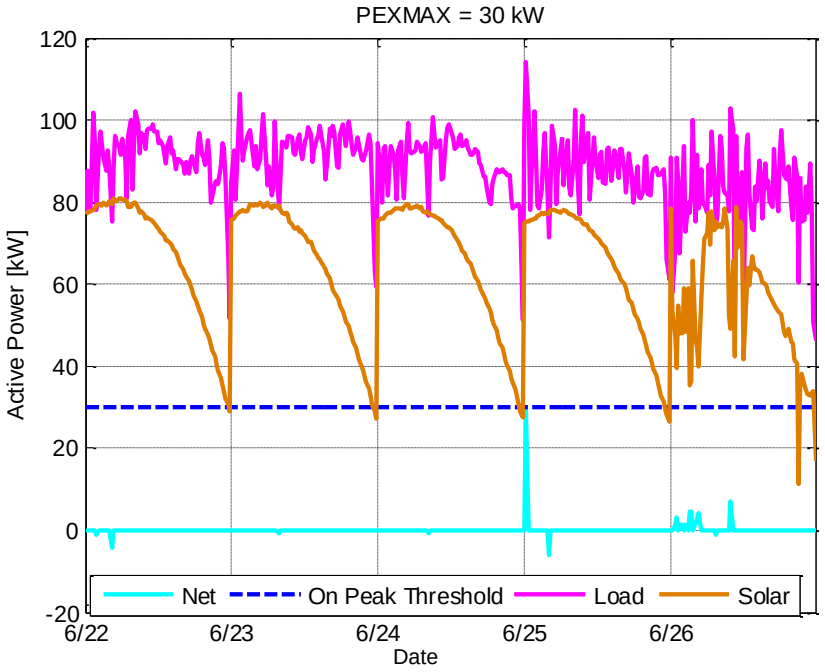

Figure 4-21 Net Load and Threshold Adjustment Under ADT - MPC Algorithm in Week 4 of June

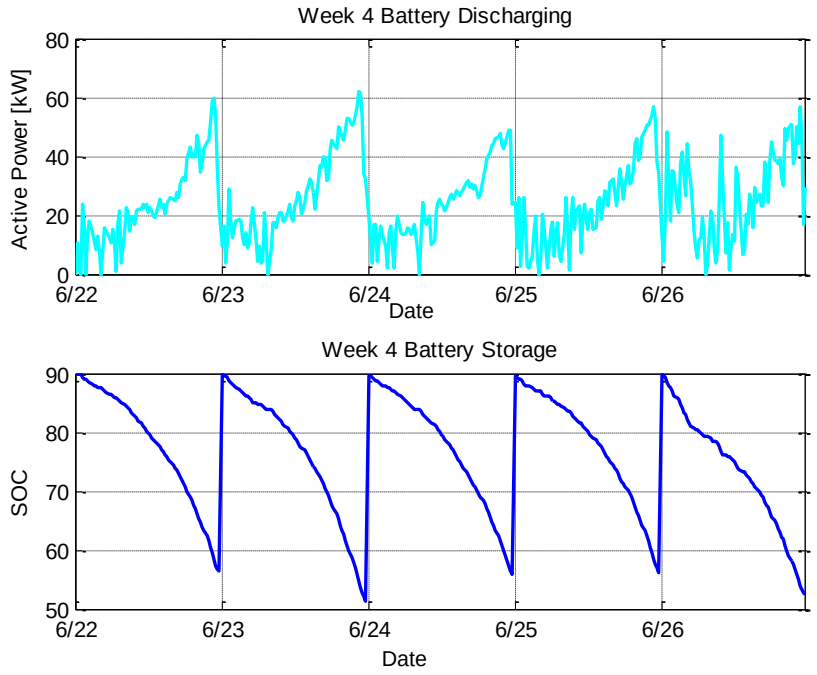

Figure 4-22 Battery Operation and Storage Under ADT - MPC Algorithm in Week 4 of June

Figure 4-15 through Figure 4-22 are the simulations for all the weekdays over a full month's period. The prediction model for these simulations is the same as Scenario 1. From these graphs, the solar generation in most days is large enough so that at the end of On-Peak rate period, the remaining SOC is larger than 40%. The remaining battery capacity left is used during the Mid-Peak control algorithm discussed in Chapter 5. The initial threshold $Th_i = 30$ kW is large enough for most of the days therefore in these days the net load can be maintained near 0 kW. In Figure 4-17 and Figure 4-18 the adjustment happens on 6/9 and the peak demand for this day is 40.37 kW. The occurrence of one high peak early in the week results in the On-Peak threshold staying at 40.37 kW.

In these figures, with simulations under different situations of solar generation and building load, the ADT-MPC algorithm has been validated to work properly.

4.2.5 Validation of ADT-MPC Algorithm

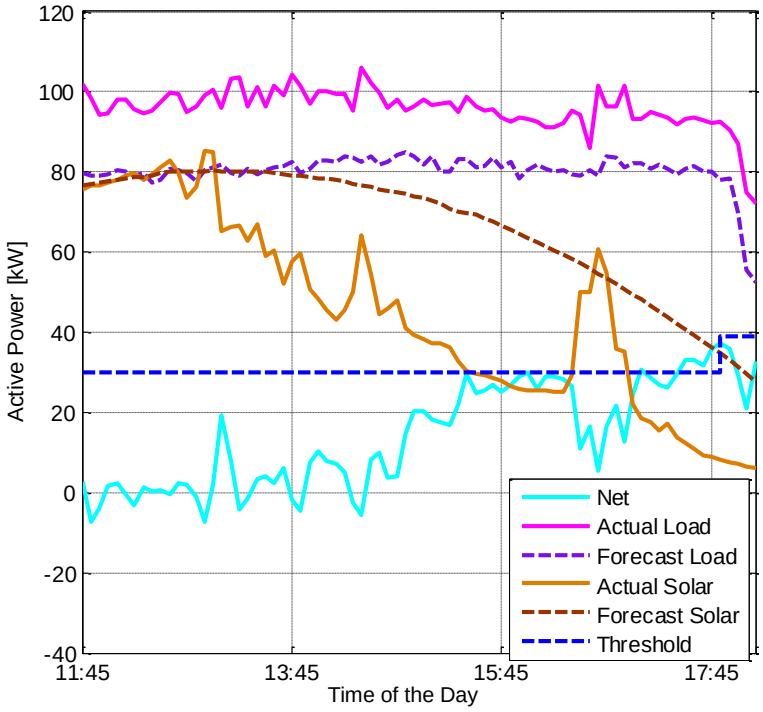

Figure 4-23 Experiment of ADT-MPC Algorithm Operated on 7/31/15

Figures 4-23 and 4-24 show the experimental results from the actual operation on 7/31/15. In Figure 4-23, the prediction for solar and building load combined with the real time solar and building load is shown. It is obvious from the graph that the building load forecast is smaller than the actual building load, while the actual solar generation is smaller than the predicted solar generation. The initial $onPeakini = 30$ kW is eventually adjusted to 38.88 kW.

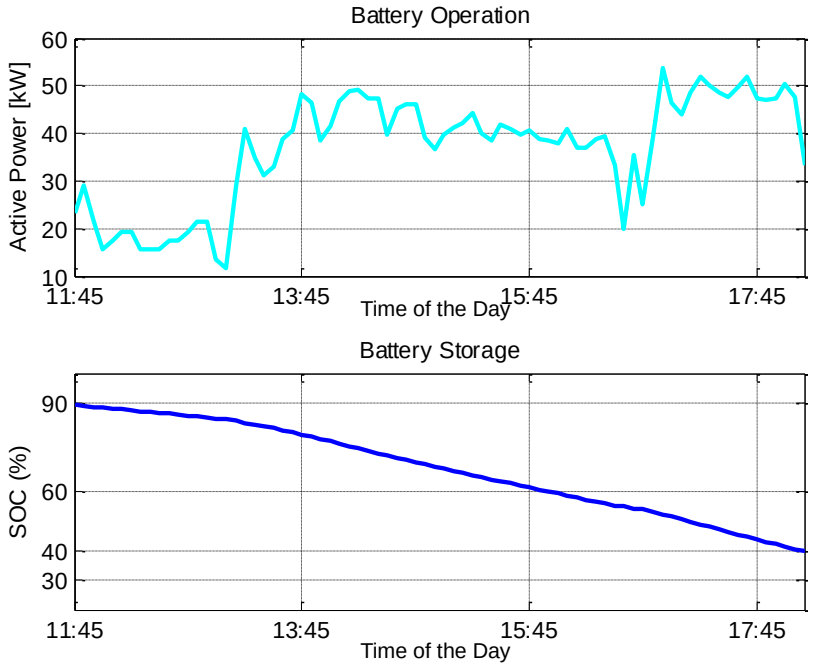

Figure 4-24 Battery Operation and Storage Under Experiment of 7/31/15

From Figure 4-24, with the large need for battery operation, the remaining SOC was still kept near 40% through the end of On-Peak rate period. In this experiment the ADT-MPC algorithm works properly adjusting the threshold to a suitable value dynamically and effectively minimizes the net load throughout the On-Peak rate period.

4.3 Comparison between ADT-MPC Algorithm and CT-MPC Algorithm

In this section, two different scenarios are simulated for comparing the ADT-MPC and CT-MPC algorithms. One scenario is a cloudy day with a reduced solar generation; the second scenario is a day with a large building load.

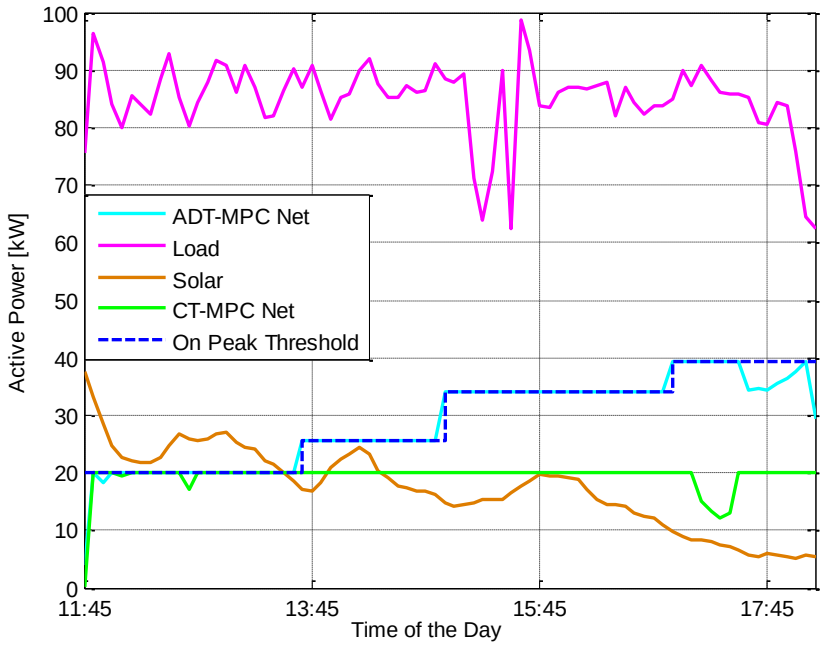

Figure 4-25 Net Load Comparison on a Cloudy Day

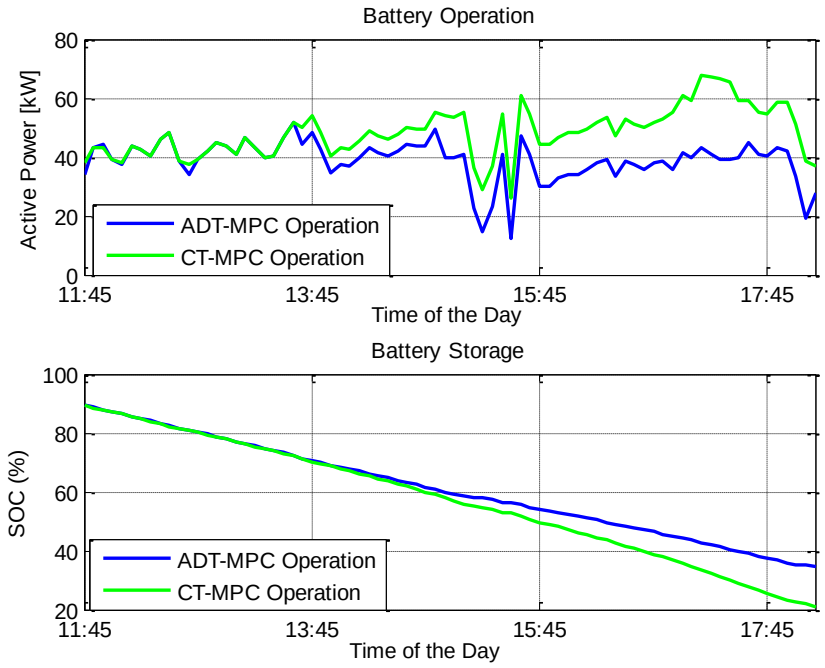

Figure 4-26 Battery Operation and Storage Comparison on a Cloudy Day

Figure 4-25 is the net load comparison between ADT-MPC algorithm and CT-MPC algorithm. The prediction model used to simulate is the same as Figure 4-1 and the initial threshold is 20 kW. In the graph, the net load threshold has been adjusted to 39.32 kW under ADT-MPC operation while it is kept below 20 kW under CT-MPC operation.

From Figure 4-26, the first two hours of the battery operations are similar due to similar demand threshold. Subsequently, the threshold in ADT-MPC algorithm is adjusted to a higher level due to low solar generation. Eventually the remaining SOC for ADT-MPC is 34.44% while it drops to the lowest level 20% in CT-MPC algorithm.

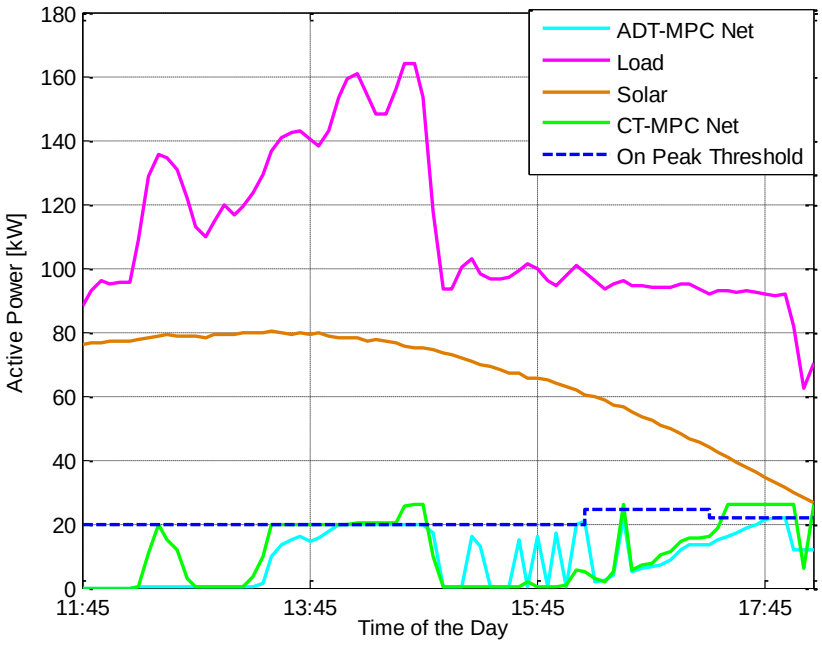

Figure 4-27 Net Load Comparison on a Large Building Load Day

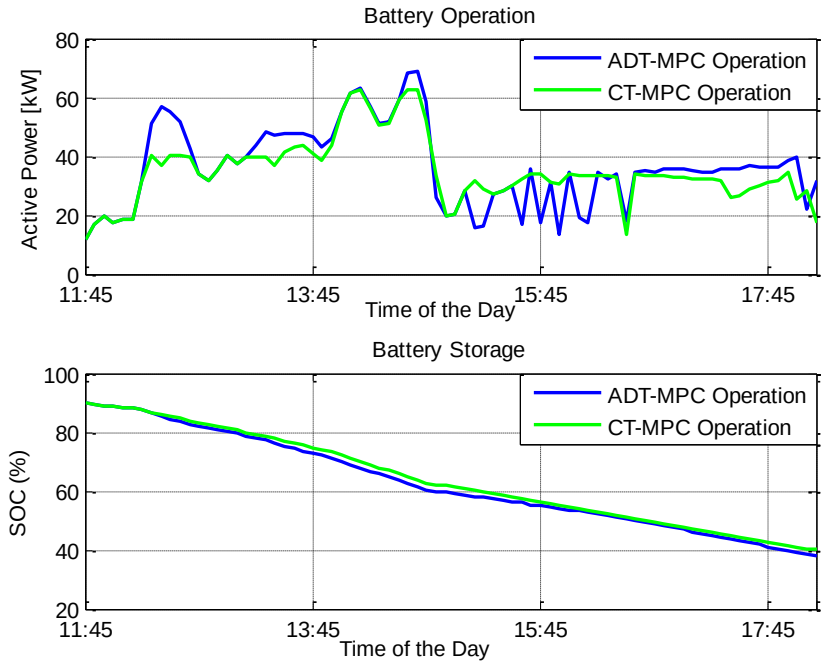

Figure 4-28 Battery Operation and Storage Comparison on a Large Building load day

Figures 4-27 and 4-28 show the simulation under an increased building load scenario. The prediction model used to simulate is the same as Figure 4-1 and the initial threshold is 20 kW. In Figure 4-27, the building load is very large for the first one and half hours. The maximum net load is 21.84 kW for ADT-MPC and 26.12 kW for CT-MPC operation. The changing threshold value in CT-MPC is due to the maximum discharging power based on Formula (3-17). If the load is larger than the load in Figure 4-27, a higher net demand will appear. In Figure 4-28, the final SOC for these two algorithms are similar to each other.

4.4 Conclusion

In this chapter, detailed ADT-MPC principles are discussed, and the ADT-MPC control algorithm is simulated under different scenarios on the days of the summer time.

With longer On-Peak time period and more fluctuating solar generation and building load than the winter time, the ADT-MPC algorithm can adjust the On-Peak threshold timely to maintain the lowest On-Peak demand and electricity consumption from the external grid.

After the full discussion of the On-Peak rate time control algorithm in Chapters 3 and 4, to fulfill the real-time battery control management, the control algorithms for the Off-Peak and Mid-Peak rate time control algorithms are needed. Therefore, in Chapter 5, both of the algorithms are fully discussed.

Chapter 5 One-Day Control Algorithm and Cost Efficiency Analysis

5.1 Off-Peak Time Control Algorithm

During working days, the Off-Peak rate period is from 11 PM to 8 AM in the summer time, and from 10 PM to 8 AM in the winter time. Throughout the year, weekends and Holidays are in the Off-Peak rate period. During the Off-Peak rate period, the electricity rate is the lowest and electricity consumption in the building is also the lowest and relatively stable. During the Off-Peak rate period, the control algorithm is set to charge the battery to 90% SOC and maintain the Off-Peak demand below a certain value *offSch*. With the Schedule Operation in Tables 1 and 2, the BESS can be fully charged from 40% SOC to 90% SOC during the Off-Peak rate period in most days of the month. In some cases, the BESS will be used down to 20% SOC during On-Peak operation, or in some other cases the building load during Off-Peak time is much higher than normal. As a result, the BESS will not be able to fully charge during Off-Peak rate period. To resolve these issues, a new method is proposed in the thesis. By adjusting the *offSch* value, the battery is ensured to be fully charged during the Off-Peak rate period, while maintaining the Off-Peak demand as small as possible. The detailed algorithm and flowchart is shown in Figure 5-1. The Off-Peak rate period is divided into M_{off} slots

and each slot is a 5 minutes interval. The charging process starts 15 minutes after the start of the Off-Peak rate period and 15 minutes before the end of the period.

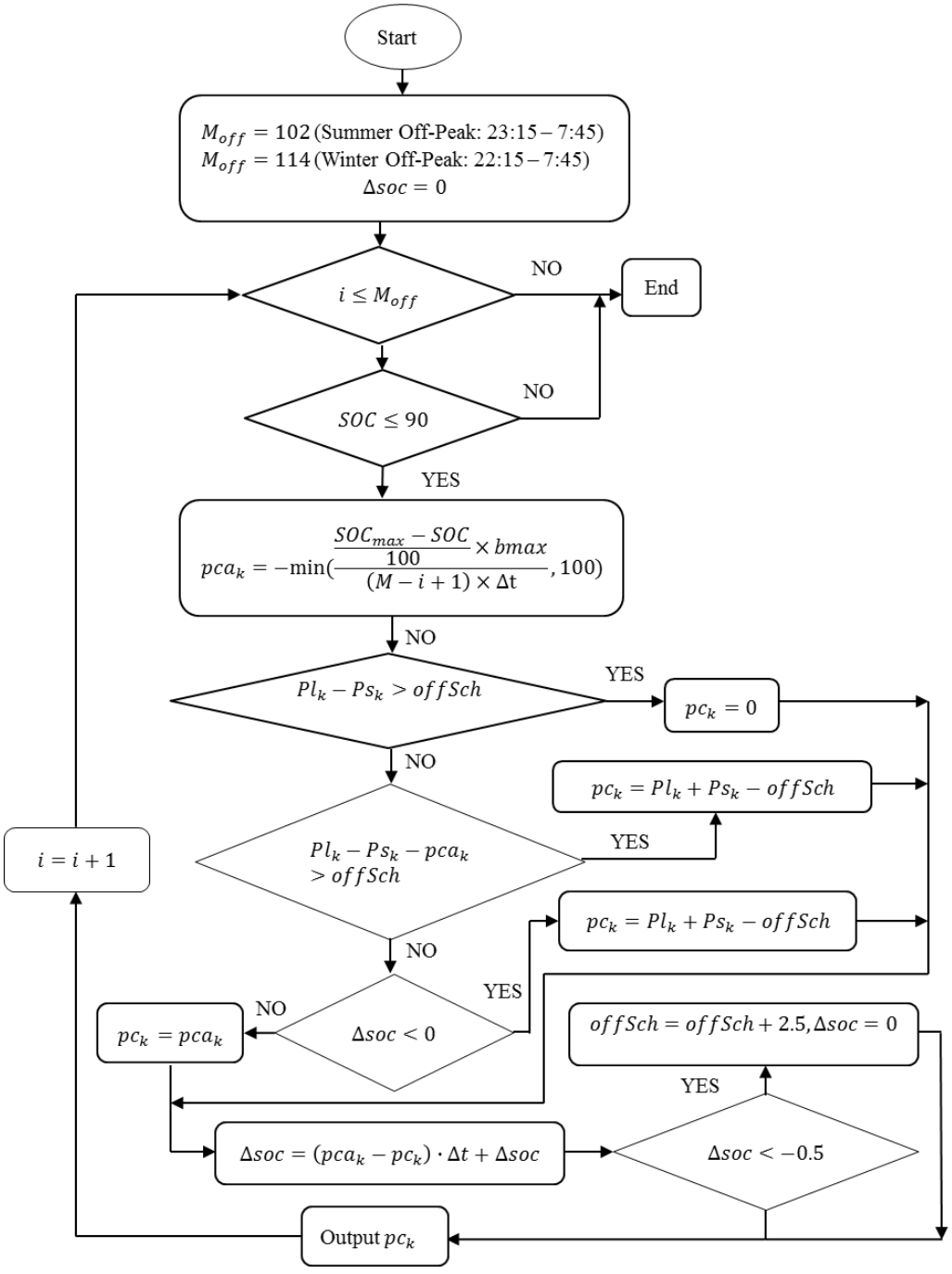

Figure 5-1 Off-Peak Control Flowchart

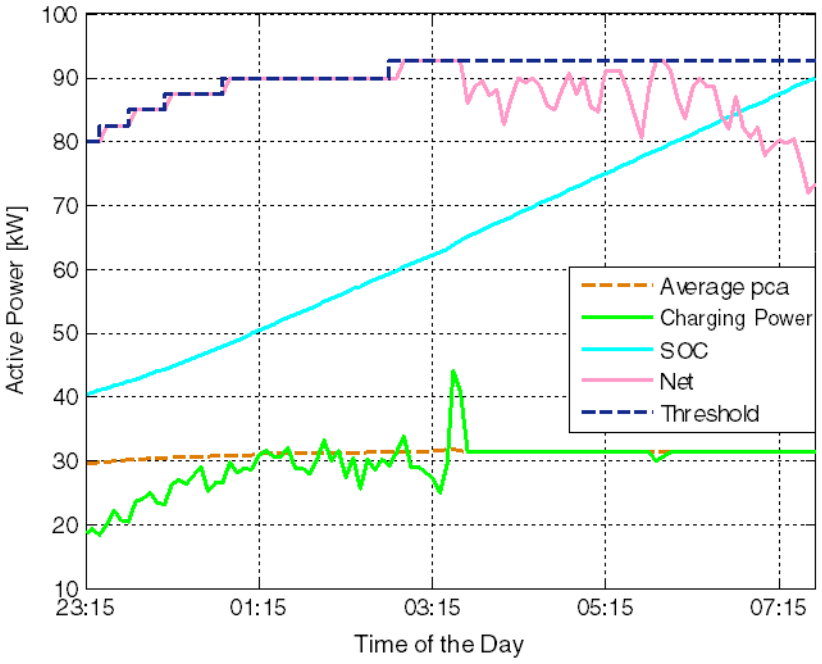

Figure 5-2 Adjusting *OffSch* Simulation Under high Off-Peak Load Situation

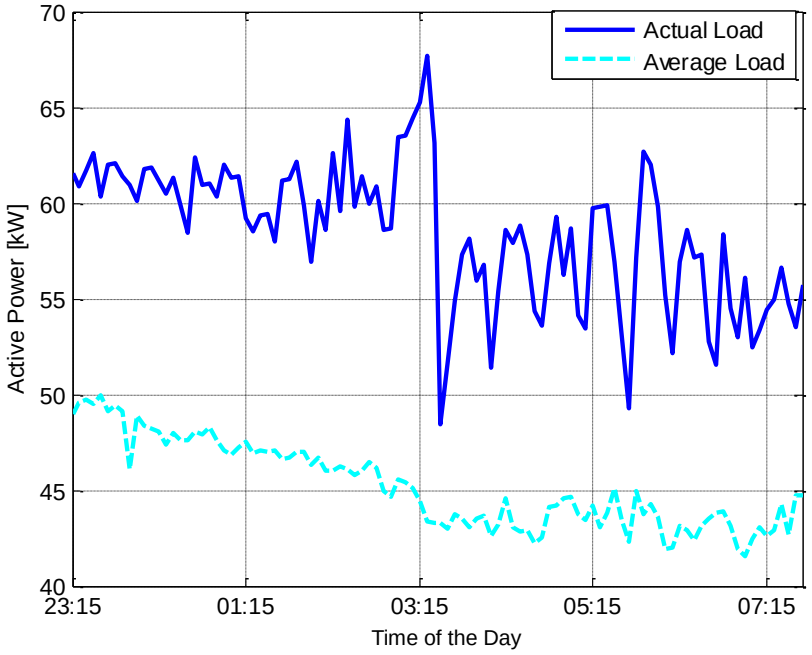

Figure 5-3 Actual Load vs. Average Load

Figures 5-2 and 5-3 show a simulation for the algorithm adjusting *offSch*. The actual building load in Figure 5-3 is based on the actual building load profile from B1200 on 6/8/15--- 6/9/15. The average load curve, averages all of June's workdays' Off-Peak building load values. It is obvious that the building load is much higher than the monthly average Off-Peak building load. In Figure 5-2, Charging power refers to $|pc_k|$ and Average pca refers to $|pca_k|$; $pc_k \le 0$ *and* $pca_k \le 0$. During the first hour, $|pc_k| < |pca_k|$, *offSch* increases rapidly. Over the next few hours, the battery is charged relatively stable near $|pca_k|$. At last $off_{AT} = 92.25\,\text{kW}$; if there's no adjusting method and the battery is only charged with Schedule Control, eventually $off_{SCH} = 97.7\,\text{kW}$.

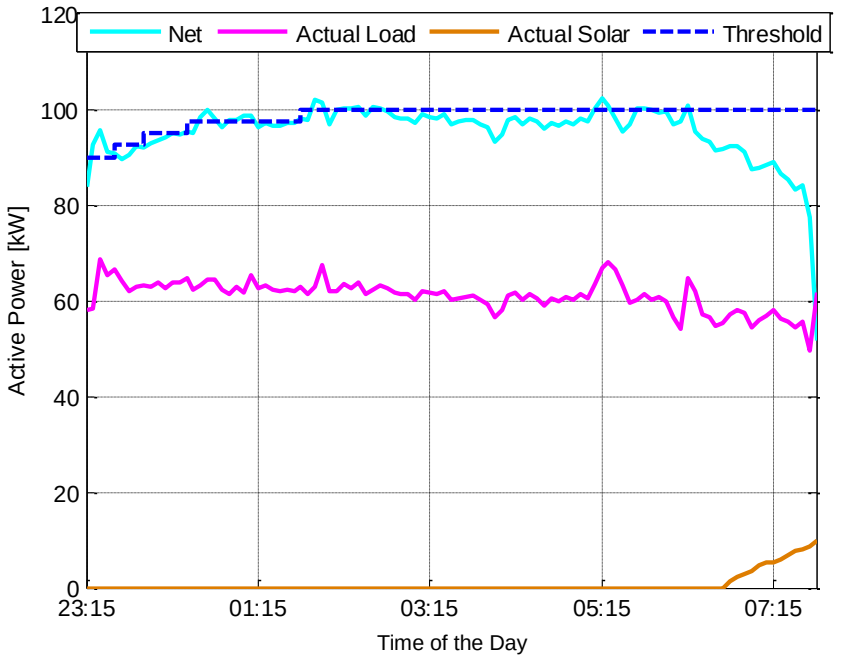

Figure 5-4 Adjusting *OffSch* Experiment on 7/20/15 --- 7/21/15

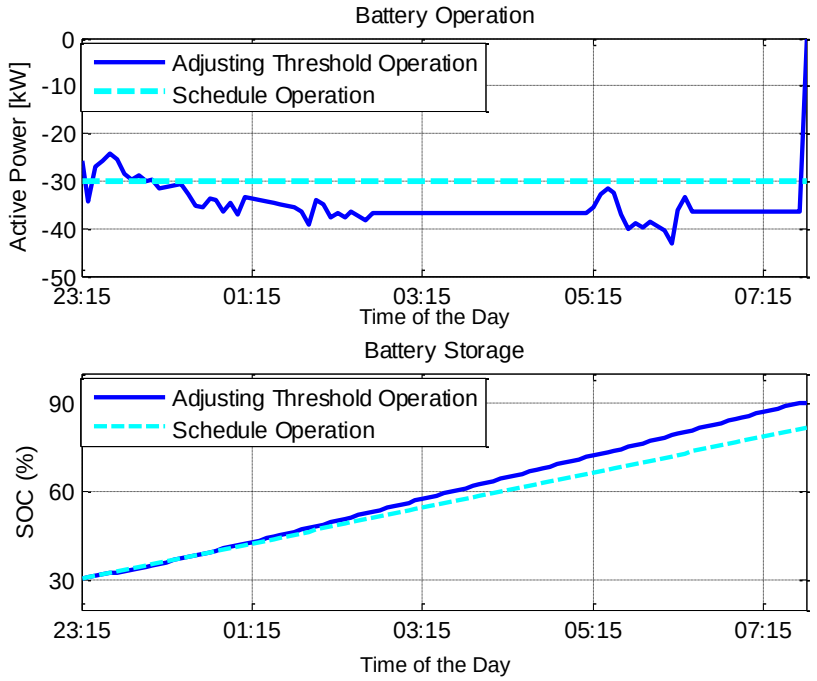

Figure 5-5 MPC Operation vs. Schedule Operation Comparison

Figure 5-4 and 5-5 is one experiment operated during the Off-Peak rate period on 7/20—7/21. The entire data shown in the graphs is based on the actual measurements taken during the experiment. The initial SOC was 30%. From Figure 5-4, the Off-Peak threshold adjusted from an initial value of 90 kW to a final value of 100 kW. The net load was larger than the building load due to the battery charging process. From the comparison between the two operations in Figure 5-5, the battery was fully charged to 90% SOC under Adjusting Threshold Operation while only up to 81.5% SOC by the Schedule Operation. Meanwhile, the maximum net load $off_{SCH} = 98.55$ kW under Schedule Operation and $off_{AT} = 102.35$ kW under Adjusting Threshold Operation with 5 minute average. If the net load is chosen by a 15-minutes moving average, the difference

between off_{SCH} and off_{AT} will be smaller. Therefore while maintaining a similar Off-Peak demand, Adjusting Threshold Operation can also ensure a battery charging status and make the battery fully charged during Off-Peak time.

5.2 Mid-Peak Time Control Algorithm

In the winter time Mid-Peak is from 08:00 to 17:00, and in the summer time Mid-Peak rate period is from 08:00 to 12:00 and 18:00 to 23:00. In the winter time, the Mid-Peak time is during working hours and much of the solar generation can be used to support the building's electricity consumption. Additionally, the BESS can be fully used during On-Peak period so during Mid-Peak time in winter there's no specific control algorithm. In the summer time, one concise control algorithm is proposed as following: for the first Mid-Peak period from 08:00 to noon, 10% SOC (from 90% to 80%) of the battery capacity is allowed to be discharged during this time for avoiding high Mid-Peak demand. For the second period, the remaining battery capacity left from the On-Peak rate period, is uniformly distributed over this period. When there's high building load, the algorithm decides larger discharge rate to maintain the scheduled Mid-Peak demand. In the second Mid-Peak period, the battery is allowed to discharge down to 20% SOC.

The detailed control algorithms are demonstrated in Figures 5-6 and 5-7.

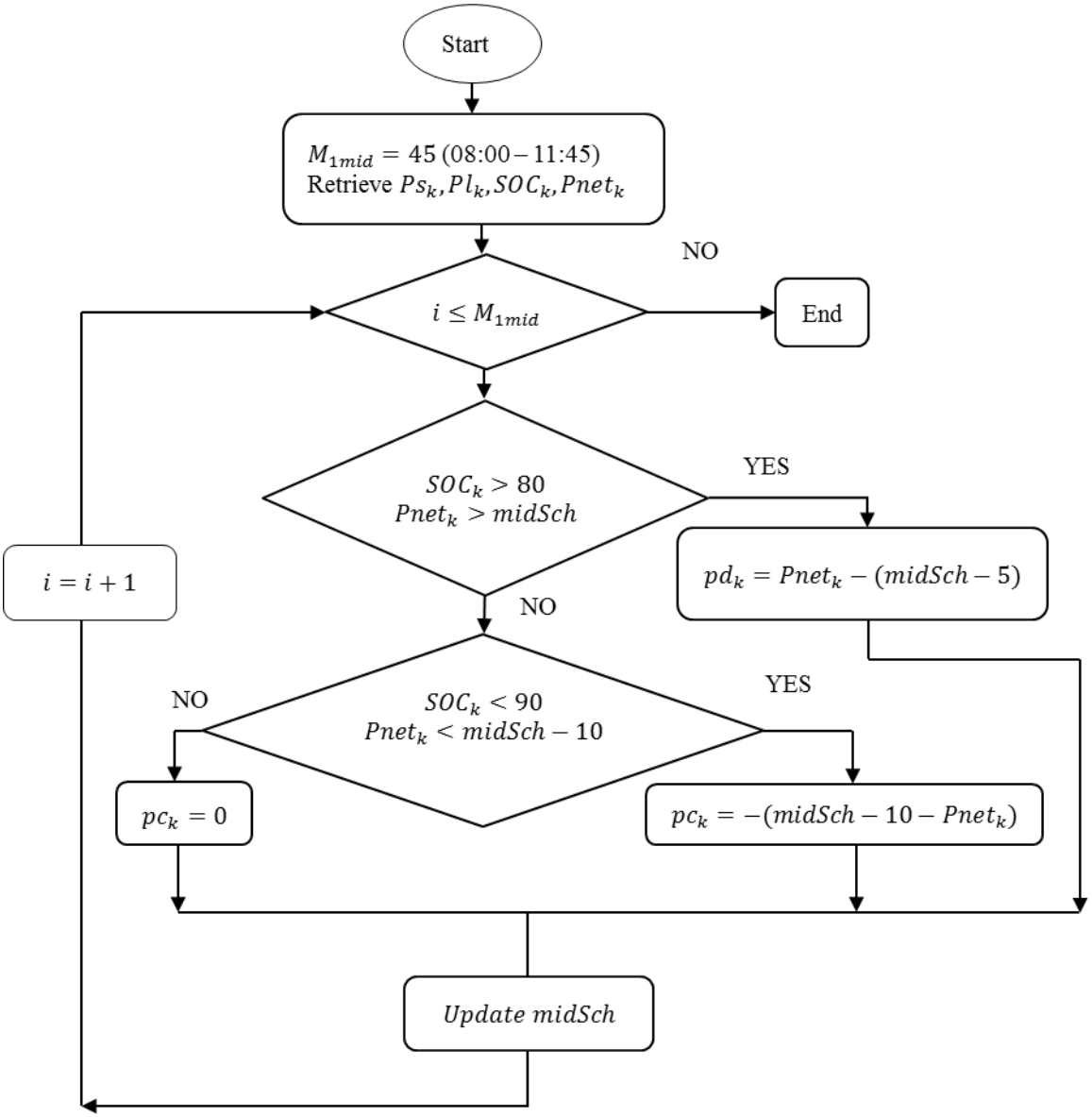

Figure 5-6 First Mid-Peak Period Control Algorithm Flowchart

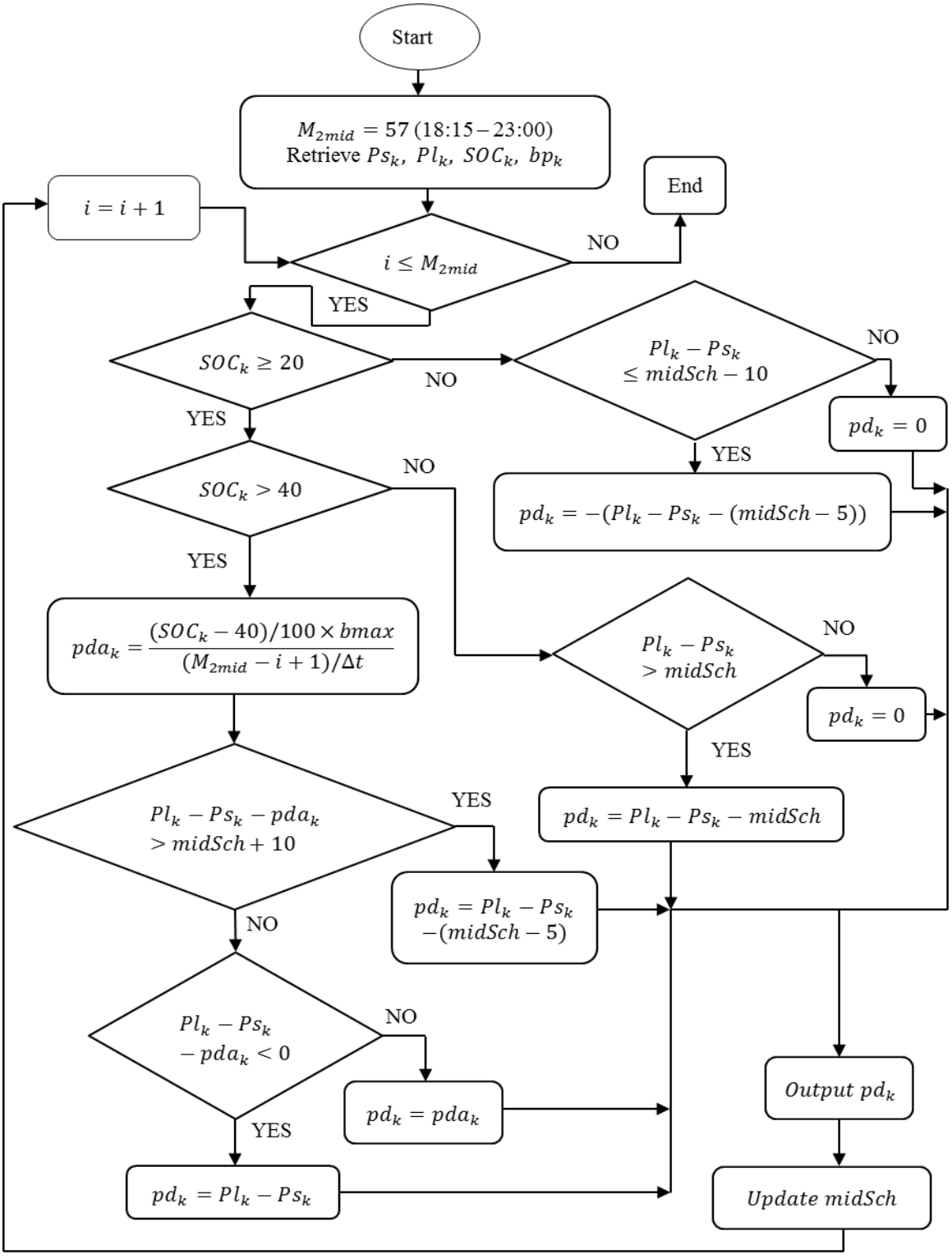

Figure 5-7 Second Mid-Peak Period Control Algorithm Flowchart

5.3 One-Day Experiment with Three Different Time Periods Control Algorithm

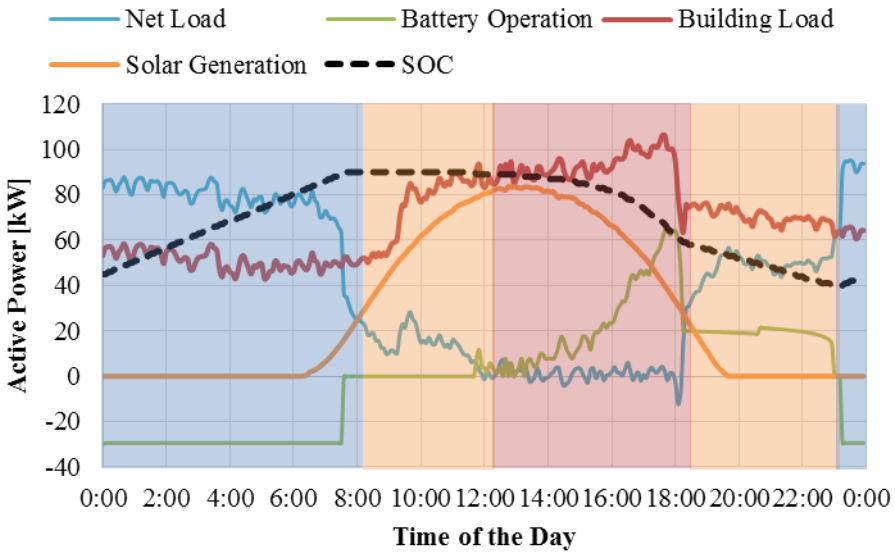

Figure 5-8 Battery One-Day Operation on 7/28/15

Figure 5-8 shows the result of a full-day experiment conducted on 7/28/15. The three different shaded areas show the three different rate periods during a 24-hour period. The experiment was carried out on a regular working Tuesday. The solar generation and building load are relatively similar to the average prediction model. The demand for this day is $offSch = 90\,\text{kW}$, $midSch = 60\,\text{kW}$ and $onPeakini = 30\,\text{kW}$. From the graph it is clear to see that the battery was charged during the Off-Peak rate period and then discharged during the On-Peak and the second Mid-Peak rate periods. Due to the sufficient solar generation the SOC was around 60% in the end of On-Peak rate period and the net load during the entire On-Peak rate period is near 0 kW with the lowest electricity

consumption from the external grid. For each rate period the net demand is tightly kept below the scheduled demand values.

5.4 Cost Efficiency

5.4.1 Comparison Between Different System

In this chapter the electricity cost is calculated for different systems arrangements: B1200 without solar PV generation or BESS; B1200 only with solar PV generation; B1200 with solar generation and a BESS, both with the thesis proposed controller system, and with a schedule controller system. The schedule controller is based on Tables 1 and 2. Two months electricity cost are chosen for both the winter season and the summer season.

System Comparison	Energy kWh Savings($)	Load Demand Savings($)			Total ($)
		On-Peak	Mid-Peak	Off-Peak	
Real vs. Schedule	209.65	105.92	17.24	6.19	339.00
Real vs. No Battery	104.38	381.12	17.24	-33.10	469.64
Real vs. No PV or Battery	1182.82	584.56	126.26	-27.21	1866.43

Table 5 June 2015 Electricity Cost Comparison for Different System Architectures

Table 5 is the electricity cost comparison based on the actual data for workdays in June (summer season). In the table, the term ‘real’ refers to the one-day control algorithm proposed in the thesis, and it is based on the real world data obtaining from the one-day control algorithm. All the data excludes the day when the system worked improperly (no control). Due to the large solar generation in the summer time, the energy (kWh) usage under schedule control is larger than the system without BESS, because the large battery

storage is sent back to the external grid during the On-Peak rate period, while the charging process is still undergoing. This is the reason why the savings for schedule control is larger than the system without BESS. In the Load Demand Savings section, with one-day control algorithm, savings are achieved in all three different rate periods compared to the schedule operation. Compared to the no-battery situation, the largest saving is in the On-Peak demand saving. And with the operation of charging during Off-Peak rate period and discharging during On-Peak and Mid-Peak rate period the shift of energy consumption saves a lot of money. The biggest cost difference is between the real and a system without solar PV and BESS. Enough electrical energy is produced by PV modules and most of the savings comes from the solar generation. The other important saving comes from demand decreasing. The On-Peak demand saving is approaching 1/3 of total saving.

Different Situation	Energy kWh Savings($)	Load Demand Savings($)			Total ($)
		On-Peak	Mid-Peak	Off-Peak	
Real vs. Schedule	84.26	59.5	0	14.6	158.36
Real vs. No Battery	97.44	472.3	24.84	-24.7	594.58
Real vs. No PV or Battery	953.7	585.65	115.44	-24.7	1630.09

Table 6 May 2015 Electricity Cost Comparison for Different System Architectures

Table 6 is the electricity cost comparison based on the real data for workdays in May (winter season). During this season, the CT-MPC control algorithm was applied. Comparing with the Schedule Control in the summer season, because there's less solar generation and the relatively stable load profile during the On-Peak rate period, Schedule Control can achieve better performance. Therefore the cost difference between real and

schedule is smaller than in Table 5. As mentioned before, in the winter season no specific control algorithm was used during the Mid-Peak rate period. This results in the difference between the Mid-Peak demand costs savings equal to 0. When comparing with the no-battery system, the On-Peak demand savings is the greatest because during the On-Peak time the solar generation decreases as the time goes on. Most of the energy comes from the battery storage system. When comparing to the system without PV and battery storage system, most energy (kWh) saving is from solar generation and the On-Peak demand saving is about 1/3 of total saving.

With the controller proposed in the thesis the electricity cost saving is significant comparing to other systems architectures.

5.4.2 Actual On-Peak Demand on Monthly Electrical Bill

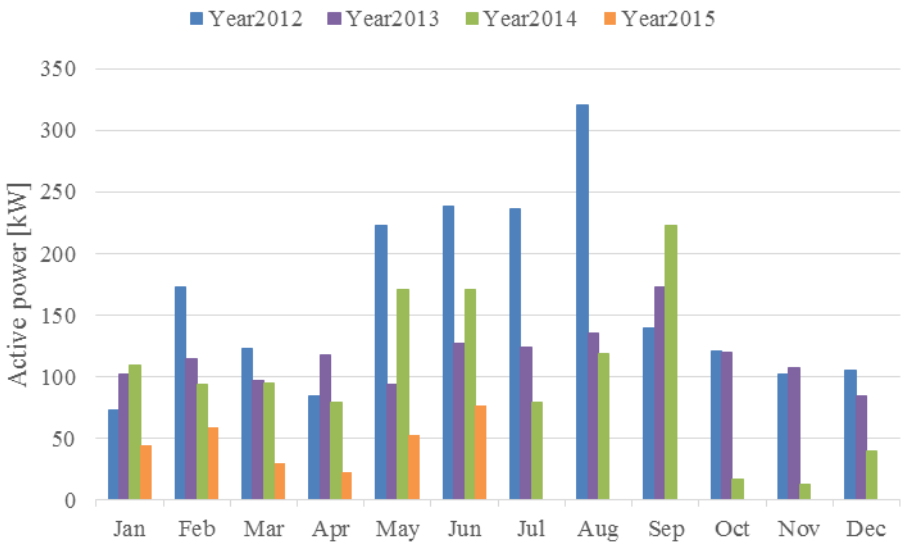

Figure 5-9 2012−2015 B1200 On-Peak Demand in Electrical Bill

Figure 5-9 shows the On-Peak demand in the electrical bills over four years. The battery storage system was implemented in October 2014. The battery was operated manually in the first two months and controlled automatically by the Schedule Operation from December to March and from April till now it is operated by the two proposed MPC algorithms. The manual operation was done by the students at CE-CERT. They kept monitoring the system and manually changed the values of discharging power during On-Peak time. The Schedule Operation is based on Table 1 and the BESS was automatically controlled by the LabVIEW program. It is clearly seen that in the first two months the net load was the lowest and later on the net load was higher than the net load in the first two months because during automate control operation sometimes the system undertook the communication failure between the Arduino and the Princeton inverter/LabVIEW program or the LabVIEW program was not working. All these issues will lead to the control system temporarily losing efficacy. The May's On-Peak demand happened on a day when the LabVIEW program closed and the June's On-Peak Demand happened on a day when the control system had a communication issue between the Arduino and the Princeton inverter. But in comparison with the last two to three years, the On-Peak demand has been decreased with the help of the battery storage system.

5.5 Conclusion

In this chapter, the Off-Peak and Mid-Peak rate period control algorithms are fully discussed and tested. With the combination of three different rate time control algorithms, a one-day control strategy is developed and implemented in the actual system. Based on the real-time solar generation and building load, the real-time control (one-day) strategy can achieve satisfactory performance compared to three different situations, such as the normal building without solar generation or BESS, B1200 only with solar generation and B1200 under Schedule Control in different seasons. At a glance of the four-year On-Peak demand in the electrical bill, the reduction of the On-Peak demand is apparent for each month. Therefore with the help of the BESS under the real-time control algorithm, the electricity cost can reduce significantly for each month.

Chapter 6 Conclusions and Future Work

6.1 Conclusions

In this thesis, the real-time battery control management for a Microgrid is developed by combining the Off-Peak, Mid-Peak and On-Peak control algorithms. Different simulations and experiments were performed under various scenarios of solar generation and building load profiles.

In Chapter 1, an introduction of a Microgrid system is discussed. Three key factors in the Microgrid system are generators, electrical energy storage system (ESS) and controlled loads.

In Chapter 2, the hardware infrastructure and the communication architecture of the SIGI Microgrid testbed are fully introduced. For the B1200, the Microgrid system is mainly comprised of 100 kW of solar PV generation, 500 kWh of stationary battery energy storage and the real-time battery control strategy developed in the thesis. Within the battery control system, different types of data communicate with each other through one of three communication protocols: Modbus, CAN bus and Ethernet.

In Chapter 3, detailed principles of the MPC algorithm and its application to SIGI's battery control system during On-Peak rate period are discussed. In the control system, there are three main components in the MPC problem, which are the battery system

model, the predictive model of the solar generation and the building load for B1200, and the optimization model. With the combination of these three models, constant threshold MPC (CT-MPC) algorithm is developed. The CT-MPC algorithm can maintain the On-Peak demand below a constant threshold and minimize the electricity usage from the external grid in a situation with relative stable solar generation and building load, such as in the winter time when the On-Peak time is from 5 PM to 9 PM.

In Chapter 4, the adjusting demand threshold MPC (ADT-MPC) algorithm is developed and demonstrated. In the summer time, the On-Peak rate period changes to 12 AM to 6 PM (overlapping with regular working hours). The solar generation and the building load profiles fluctuate significantly more than in the winter time. Under these situations, the On-Peak demand threshold will adjust to the optimum value during the entire On-Peak rate periods based on the ADT-MPC algorithm. The ADT-MPC control algorithm has the advantage of the motility to any system even the ones without comprehensive historical energy generation or building load profiles.

In Chapter 5, the control algorithms for the Off-Peak and Mid-Peak rate periods are discussed. During the Off-Peak rate period, the two tasks for the Off-Peak algorithm are to fully charge the BESS and maintain low Off-Peak demand. Two different control algorithms are developed for each of the two different Mid-Peak rate periods. The tasks for these two algorithms are to maintain the Mid-Peak demand below the scheduled value

and utilize the remaining available battery energy capacity (down to 40% SOC). After the analysis of the cost savings comparing different system architectures and the last four-year electrical bills, the electricity cost is reduced significantly with the implementation of the BESS and the real-time control strategy.

6.2 Future work

As discussed in Section 2.1, one 500 kWh mobile BESS is also available as part of the SIGI architecture. The functionality of the mobile BESS system is the same as the stationary BESS, except for the communication protocols which allow the mobile BESS to communicate over a wireless network. Therefore, the real-time control system can utilize these two BESSs as a coherent system in the future battery operation.

As discussed in Section 2.2.2, the OPTO 22 system can control AH system in B1200 intelligently and maintain the net load below a certain threshold. Right now, the proposed algorithm can only control the battery system to supplement certain power to the grid. In the ADT-MPC and Off-Peak control algorithms, the thresholds adjust over the rate period. The new threshold could be sent to the OPTO 22 system in the future to further reduce the demand for different rate periods.

As discussed in Chapter 3 and 4, the CT-MPC and ADT-MPC algorithms are not fully dependent on the accuracy of the prediction model. In Figures 3-12 and 4-1, it is easy to see that better performance can be achieved with more accurate predictions. In the

future, more attention should be paid to building a more sophisticated predictive model for renewable energy generation and building load.

As discussed in Sections 5.1 and 5.2, the Off-Peak and Mid-Peak control algorithms are developed in a straightforward manner, especially the Mid-Peak control algorithm. In the future work, elaborated control algorithms can be developed for both rate periods.

As discussed in Section 5.4.2, the control system experience failure instances, such as communication issues between the Arduino microcontroller and the LabVIEW software. This kind of failure has negative impact on the demand control within one month. Right now one standing issue is when the battery is discharged to 20% SOC, the Arduino sends a command to turn off the inverter; the inverter stays shutdown until it is manually reset. The command from the Arduino does not control the inverter at all. The only method to re-start communication between the two is to turn on the inverter manually. Therefore, within an automated system, a powerful alert function should be developed in the future to allow users to become readily aware of the break in communication and can manually solve the issues.

Citations

[1] REN21. 2014. Renewables 2014 Global Status Report.

[2][6] n.d.. Solar Industry Data---Solar Industry Breaks 20 GW Barrier - Grows 34% Over 2013. Retrieve from: http://www.seia.org/research-resources/solar-industry-data

[3]Hayden, E., (2013). INTRODUCTION TO MICROGRID. Retrieved from https://www.securicon.com/sites/default/files/Introduction%20to%20Microgrids%20-%20Securicon%20-%202013_1.pdf.

[4] Ellabban, O., Abu-Rub, H., & Blaabjerg, F. (n.d.). Renewable energy resources: Current status, future prospects and their enabling technology. Renewable and Sustainable Energy Reviews, p. 748-764.

[5] n.d.. Photovoltaic (Solar Electric) Retrieved from: http://www.seia.org/policy/solar-technology/photovoltaic-solar-electric

[7] Chen, H., Cong, T., Yang, W., Tan, C., Li, Y., & Ding, Y. (n.d.). Progress In Electrical Energy Storage System: A Critical Review. Progress in Natural Science, p. 291-312.

[8] Díaz-González, F., Sumper, A., Gomis-Bellmunt, O., & Villafáfila-Robles, R. (n.d.). A review of energy storage technologies for wind power applications. Renewable and Sustainable Energy Reviews, p. 2154-2171.

[9] The Authoritative Dictionary of IEEE Standards Terms. (2000). In IEEE 100: The authoritative dictionary of IEEE standards terms. (7th ed., p. 588). New York: Standards Information Network, IEEE Press.

[10] Kjaer, S., Pedersen, J., & Blaabjerg, F. (n.d.). Power inverter topologies for photovoltaic modules-a review. Conference Record of the 2002 IEEE Industry Applications Conference. 37th IAS Annual Meeting (Cat. No.02CH37344).

[11]Appert, S., Mukdad, W., & Malashenko, E. (2013, January 18). Advanced Inverter Technologies Report GRID PLANNING AND RELIABILITY ENERGY DIVISION. Retrieved from http://www.cpuc.ca.gov/NR/rdonlyres/6B8A077D-ABA8-449B-8DD4-CA5E3428D459/0/CPUCAdvancedInverterReport2013FINAL.pdf

[12] n.d.. Research Towards a Sustainable Future: Integrating solar electricity generation, smart distribution, commercial-scale energy storage, and electric transportation. Retrieved from http://www.cert.ucr.edu/newgrid/

[13] Obvius AcquiSuite official website: http://obvius.com/

[14] Princeton Inverter official website: http://www.princetonpower.com/products.html

[15] Shark Meter official website: http://electroind.com/

[16] Arduino official website: https://www.arduino.cc/

[17] Orion BMS official website: http://www.orionbms.com/

[18] Pulse Meter official website: http://www.autonics.com/products/products_2.php?big=02&mid=02/05

[19] Deck official website: http://www.deckmonitoring.com/

[20] Advanced Energy. (2014). AE 100TX COMMERCIAL INVERTERS. Retrieved from http://solarenergy.advanced-energy.com/upload/File/AE_Data_Sheets/ENG-AE100TX-250-01.pdf

[21]Advanced Energy. (2014). AE 250TX and AE 260TX. Retrieved from http://solarenergy.advanced-energy.com/upload/File/AE_Data_Sheets/ENG-AE250TX-260TX-250-08_Web.pdf

[22] LabVIEW. (n. d.). Retrieved August 25, 2015 from Wiki: https://en.wikipedia.org/wiki/LabVIEW

[23] MATLAB. (n. d.) In Wikipedia online. Retrieved from https://en.wikipedia.org/wiki/MATLAB

[24] OPTO 22 controller website: http://www.opto-engineering.com/

[25] RS485 & Modbus Protocol Guide tyco Electronics Energy Division

[26] CAN bus. (n. d.). Retrieved August 25, 2015 from Wiki: http://en.wikipedia.org/wiki/CAN_bus

[27] Corrigan, S. (2008, July). Introduction to the Controller Area Network (CAN). Retrieved from http://www.ti.com/lit/an/sloa101a/sloa101a.pdf

[28] n.d.. Orion BMS Operation Manual Rev 2.1. Retrieved from http://www.orionbms.com/manuals/pdf/operational_manual.pdf

[29] Model predictive control. (n. d.). Retreved from August 25, 2015 from Wiki: http://en.wikipedia.org/wiki/Model_predictive_control

[30] Findeisen, R. (2007). Assessment and future directions of nonlinear model predictive control (Vol. 358, 2007, pp. 1). Berlin: Springer.

[31] Ruscio, D. D. (2001). MODEL PREDICTIVE CONTROL and optimization [PDF documents]; Retrieved from Lecture Notes: http://home.hit.no/~hansha/documents/control/theory/mpc.pdf

[32] Seron, M. M. (2004). Receding Horizon Control [PDF document]. Retrieved from http://www.eng.newcastle.edu.au/eecs/cdsc/books/cce/Slides/RecedingHorizonControl.pdf

[33] Boyd, S., & Vandenberghe, L. (2004). Convex optimization . Cambridge, UK: Cambridge University Press: p.21, p.127.

[34] Winton Battery.WB-LYP1000AHC. Retrieved from http://en.winston-battery.com/index.php/products/power-battery/item/wb-lyp1000ahc?category_id=176

[35] SAM official website: https://sam.nrel.gov/

[36] n.d.. System Advisor Model (SAM)'s Help System, version 2015.6.30 Retrieved from https://sam.nrel.gov/sites/sam.nrel.gov/files/content/help/sam-help-2015-5-30.pdf

[37] Sustineo Corporation. (2013). SPVPS – UC Riverside Bourns Facility Commissioning Report. Riverside, CA: n.d..